5-2022

Fabrication of MOF Films of UiO or PCN Type Through Layer-by-Layer Molecular Deposition as well as Bulk Deposition for Catalytic Applications

John Ozdemir
University of Arkansas, Fayetteville

Fabrication of MOF Films of UiO or PCN Type Through Layer-by-Layer Molecular Deposition as well as Bulk Deposition for Catalytic Applications

A dissertation submitted in partial fulfillment
of the requirements for the degree of
Doctor of Philosophy in Chemistry

by

John Aytekin Ozdemir
University of Arkansas
Bachelor of Science Chemistry, 2016

May 2022
University of Arkansas

This dissertation approved for recommendation to the Graduate Council.

_____
Matthias C. McIntosh, PhD
Dissertation Director

_____
Robert Henry Coridan, PhD
Committee Member

_____
Peter Pulay, PhD
Committee Member

_____
Jackson Lay Jr., PhD
Committee Member

_____
Nan Zheng, PhD
Committee Member

ABSTRACT

Metal-organic frameworks (MOFs) are crystalline, porous materials comprised of symmetric organic linkers coordinated to positively charged metal atoms or metal oxide nodes. This dissertation uses strategies in crystal engineering to advance the study of functional MOFs with emphasis on thin film deposition. The first chapter of this dissertation will introduce the field of reticular chemistry to the reader and describe synthetic efforts to develop useful building blocks for MOF materials: namely porphyrin macrocycles and carboxylate capped zirconium-oxo and hafnium-oxo clusters. The building blocks for MOFs developed in the first chapter will be employed in the second and third chapters through incorporation into MOF thin films through molecular deposition and bulk deposition respectively. New methods for the molecular deposition of Hf-based MOF films are described which will expand the available MOF types which are known to be deposited in a molecular layer-by-layer fashion. A key methodology is the use of Hf-oxo clusters capped by carboxylate ligands to be used as a potential Hf source for molecular layer-by-layer Hf-MOF deposition. Using an automated epitaxial workstation, films of UiO-66 (Hf) are fabricated for the first time and porphyrinic Hf-based MOFs are developed for catalytic applications. Following these efforts, experiments regarding the bulk-deposition of UiO-66 and UiO-66 (Hf) films are laid out. The UiO-66 (Hf) bulk deposited films are shown to be a promising catalyst for CO_2 fixation to epoxides for cyclic carbonate synthesis.

ACKNOWLEDGEMENTS

I want to thank my beautiful wife Yoshie Sakamaki who I was so lucky to meet during graduate school. Thanks, Yoshie for standing by me and putting up with the tumultuous times we faced during graduate school. I look forward to starting the next journey of our life together and starting every journey from here on out together. I also want to thank my family, Burcu, Aytekin and Levent, thank so much for being the support network I needed so much during these past 4 years.

I also owe great thanks to my committee, especially Dr. Peter Pulay who encouraged me to return to the University after my undergraduate studies. I owe a big thanks to my committee chair Dr. Matt McIntosh who's leadership in guiding my dissertation to the finish line was essential to my success. I am grateful for Dr. Robert Coridan for his role as an excellent educator who's expertise was essential in growing my own knowledge base as a scientist. I appreciate the role played by Dr. Nan Zheng and by Dr. Jackson Lay Jr. for always supporting my research inquiries and taking part in my committee.

Lastly I would like to thank the University of Arkansas and the city of Fayetteville, AR for being a wonderful environment for my studies and a beautiful home for the past 10 years.

TABLE OF CONTENTS

A. Introduction

Reticular chemistry is an emerging field of science defined as the study of porous coordination polymers with intricate, net-like molecular structures which give the field its name.[1,2] Synthetic efforts in reticular chemistry consists primarily of solvothermal reactions which result it the formation of crystalline powders for study.[3,4] Within reticular chemistry the largest class of materials discovered thus far are metal-organic frameworks (MOFs).[5] MOFs are hybrid coordination polymers comprised of organic linkers coordinated to either metal ions or metal-oxo ionic clusters. To be classified as a MOF a material should display crystallinity, porosity and hybrid organic-inorganic structural composition. These defining characteristics have also made MOFs relevant in applications such as catalysis[6,7], gas storage,[8,9] water capture[10,11] and electronics.[12,13] Reticular materials similar to MOFs include metal-organic polymers;[14,15] which will share the hybrid structural composition and perhaps porosity, but lack crystallinity. Another burgeoning class of reticular materials are covalent organic frameworks (COFs)[4,16], which are also crystalline but are formed through covalent bonds between organic linkers.

MOFs offer chemists a unique opportunity to develop crystal structures tailored to a particular function. Careful consideration of a crystal's structure as it relates to the function of a material is a cornerstone of crystal engineering.[17,18] Different families of MOFs can often be categorized by topologies,[19,20] and two distinct MOFs may have the same topology but with different dimensions.[21,22] For instance: the MOF UiO-66[23] is comprised of terephthalate molecules coordinated to zirconium-oxo clusters to form an extended crystal lattice; with each terephthalate coordinated to two clusters, giving the molecular formula of $C_{48}H_{24}O_{30}Zr_6$. Replacing the terephthalate with the longer 4,4'-Biphenyldicarboxylic acid gives the MOF UiO-67[24] with the same topology but with a longer distance between zirconium-oxo clusters (Figure

1.1). This example shows the reticular nature of MOF synthesis where complex topologies can be expanded or retracted to influence characteristics like pore size and internal surface area. The symmetry of the organic linker and the coordination environment of the inorganic node will determine the topology of a MOF.[25] Careful selection of the two components provides boundless potential architectures, and finding synthetic conditions which result in the formation of a crystal lattice between the organic and inorganic moieties is a major hurdle in preparing a new MOF.

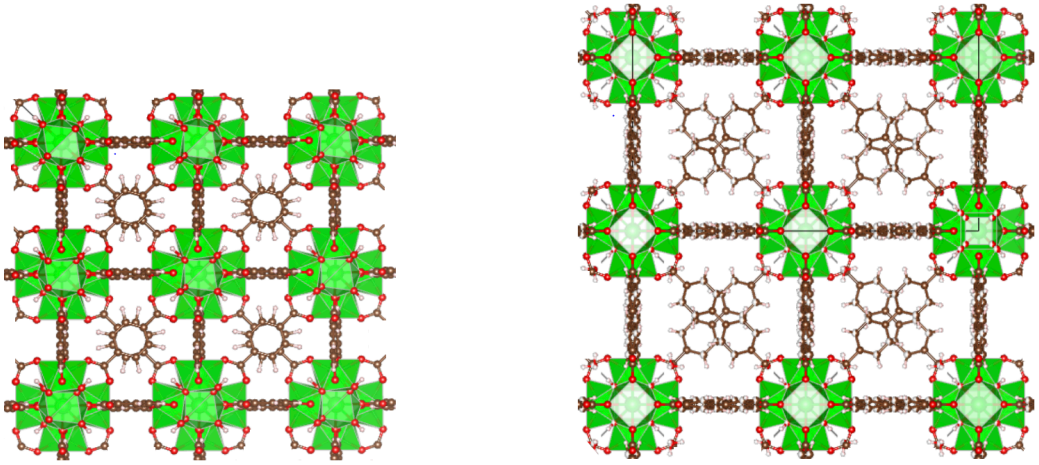

Figure 1.1: Depiction of MOF UiO-66 and UiO-67, an example of two isostructural MOFs with identical topology but with organic linkers of different length.

The hybrid structure of MOFs provides a platform to explore the interplay between organic and inorganic centers while also testing which combinations best suite a desired application. The organic linkers and inorganic nodes of a MOF are the chemist's building blocks when envisioning a potential MOF to synthesize, while discovering the exact synthetic conditions that result in the formation of a crystalline material is the main challenge. So far, the most common method for MOF synthesis is solvothermal synthesis in a sealed reaction vessel, heated in an autoclave. Theoretically the chemist seeks to obtain the more thermodynamically stable crystalline product by overcoming energetic boundaries that would lead to the kinetically

favored amorphous products.[26] To develop crystallinity from these kinetically favored amorphous structures requires very specific chemical equilibriums between the organic linker and metal nodes, and so in solvothermal MOF synthesis the selection of solvent, temperatures and even reaction vessel size will all require optimization to produce the desired crystals in sufficient yields.

Two of the first MOFs described included examples such as MOF-5[27] ($Zn_4O(bdc)_3$, bdc = benzene dicarboxylate) and HKUST-1[28] ($Cu_3(btc)_2$, btc = 1,3,5-benzene tricarboxylate). Both of these initial examples feature benzene-based organic linkers which serve only to link the inorganic nodes; leading to crystallinity and porosity, but otherwise totally inactive. In the following years MOF-74[29] Zn_2(dhbdc), dhbdc = 2,5-dihydroxy-1,4-benzenedicarboxylate, was described and with the addition of two phenolic functional groups to the benzene backbone MOF-74 displayed greater hydrophilicity within the pore structure and a greater affinity to adsorption of polar molecules, initiating a simple proof-of-concept for how functionalizing organic-linkers might influence MOF applications. In 2009; the synthesis of Mg-MOF-74[30] was described, which was isostructural to MOF-74 but contains the Mg metal cation instead of Zn. Mg-MOF-74 has received much interest for its high physioadsorption isotherm for CO_2 at low pressure (35.2 wt% at 1 atm). Interestingly Mg-MOF-74 outperformed 3 other metal isostrucutural MOFs (Ni, Co and Zn metal variants) and makes a prime example of how the interplay of the metal SBUs and organic linkers of a MOF framework are crucial for optimizing functionality.

Future perspectives in the field of MOF chemistry include a wide range of applications from drug delivery[31] to advanced catalytic[32] applications. Effective research protocols for the development of MOF materials requires the synthesis of novel organic linkers that can be

synthesized in scale adequate to test a large number of synthetic conditions. Looking forward, new efforts in MOF synthesis should include methodologies focused on size-controlled MOF nanoparticle synthesis[33] and MOF thin film[18,34,35] deposition; doing so would greatly expand the potential use cases for MOFs.

B. Chapter 1: Synthesis of Carboxylate Capped Group-IV (Zr and Hf) Metal-oxo Clusters and Porphyrin Macrocycles to Serve as Building Blocks for the Synthesis of MOF Materials

I. Introduction to Group-IV Metal MOFs

1. Increased Stability of Zirconium Based MOFs

The stability of a MOF material is dependent greatly on the strength of the ionic interaction between the carboxylate linkers and the inorganic metal centers. The reversible equilibrium that leads to MOF crystal formation becomes a hindrance to MOF stability as the reactions involved in forming the material are themselves reversible. Other factors that influence the stability of MOFs are the pK_a of the ligands[36] and the oxidation state of the metals in the inorganic nodes.[37] Structural factors such as the metal-ligand coordination geometry[38] also have effects on MOF stability as does the hydrophobicity of the pores.[39] Many MOFs lack the stability required for uses in practical applications.[40]

In 2008 Cavka et al discovered the synthesis of zirconium-based MOFs formed by the interlinkage of Zr-oxo clusters each containing 6 Zr atoms linked together by terepthalate organic linkers.[41] The so named UiO-66 was a major breakthrough in reticular chemistry as displayed a level of stability; especially resistance to water, that was totally unprecedented at the time. The stability of UiO-66[42] is largely due to the $Zr_6(O)_4(OH)_4$ clusters, which differs from the metal centers of other MOFs in that it is a discreet metal-oxo cluster, whereas only metal ions

had been reported prior. Crystallographic data on the Zr_6 oxo nodes had been previously reported by Kickelbick and coworkers[43] but until the synthesis of UiO-66 these metal-oxo clusters had never been incorporated into a MOF.

Since the discovery of UiO-66 the field of Zr based MOFs expanded quickly as new organic linkers with different symmetries were utilized. Due in great part to their stability Zr-base MOFs have been the subject of impactful publications in applications such as catalysis[44], gas adsorption[45] and chemical sensing.[46,47] Group IV metal ions such as Zr^{4+} have a high charge density leading to the interactions between the Zr atoms of the to create strong interactions with the O atoms in the organic ligands. As a result, Zr MOFs can withstand boiling aqueous conditions, heating up to 500C and pH ranges from 2-11.[37] One remaining challenge is that Zr MOFs are less tolerant to alkaline conditions compared to acidic due to the chemistry of the Zr_6O_8 clusters as the Zr^{4+} ions show a strong affinity to the OH^- ion so in alkaline conditions will promote disassociation of the Zr^{4+} ions with their linkers.[37,46]

2. Hafnium Based MOFs

Hafnium is the second group-IV element and is known to form MOFs isostructural to the Zr counterparts. While isostructural; the $Hf_6(O)_4(OH)_4$ clusters found in Hf-based MOFs are known have stronger Brønsted acid activity than the Zr-clusters.[48] This stronger Brønsted acidity is rationalized by the higher oxophilicity of the Hf atom when compared to the Zr atom made evident by the different dissociation enthalpies of Hf-O and Zr-O bonds (802 vs 776 kJ mol^{-1}).[49] This idea was first made evident in studies regarding the fixation of CO_2 to epoxide for the synthesis of cyclic carbonates by Hf-NU-1000,[50] the Hf-isostructural analog of the previously discovered NU-1000. Since this initial study of Hf MOFs as a Brønsted acid catalyst follow-up

studies have confirmed that Hf-based MOFs display higher Brønsted acid catalytic activity than their Zr counterparts notably for the Solketal synthesis from glycerol acetylation.[51]

3. Current Challenges in Zr and Hf MOF Thin Film Fabrication

The metal-oxo clusters which provide group-IV MOFs with increased stability also add a structural complexity to the MOFs because the inorganic nodes are large metal-oxo clusters instead of discreet metal ions. During a solvothermal synthesis the metal source for a MOF synthesis is the metal salt, so the metal-oxo clusters are not present from the start of the reaction and will instead be formed during the MOF synthesis. The added complexity of both the reaction dynamics and structural complexity of group IV-metal based MOFs decreases their lability and makes obtaining large crystals difficult.[52] This causes issues in MOF fabrication for any application where a large crystal domain is needed. This problem is well-observed by MOF chemists because structural elucidation of Zr and Hf MOFs by single crystal X-ray diffraction is known to be difficult due to the small size of the sample crystals, often < 10 um scale.[53] One synthetic advent that has allowed for some progress in obtaining Zr/Hf-based MOF single crystals is the use of acidic modulators in MOF synthesis.[54] In cases where obtaining single crystals is not possible structural investigations of Zr and Hf MOFs often take place by comparing powder diffraction data to collected data, either from a computational model[55] or isostructural MOFs.[56]

The need to form discrete metal-oxo clusters makes the thin film deposition of group-IV MOFs more synthetically involved when compared to the deposition of MOFs with simpler inorganic nodes. Whereas the deposition of most classes of MOF would entail just the use of a metal salt solution; for a group-IV metal MOFs, it is required to use the discreet metal-oxo clusters capped by carboxylates. The synthesis of these standalone carboxylate-substituted metal

oxo clusters has been thoroughly described by Schubert and Kickelbick in a number of papers.[43,57–59] Incorporating these clusters into a MOF synthesis should be possible because of the dynamic nature of the carboxylate substituents on the surface of the clusters,[60] and ligand exchange in Zr clusters has been observed but is not well understood. Specifically, the $Zr_6O_4(OH)_4(OMc)_{12}$ (OMc = methacrylate), which has a metal-oxo cluster isostructural to the metal-oxo cluster of UiO-66, displays a stability enough to undergo ligand exchange.[58]

In 2019 Semrau et al developed a novel route for growing films of UiO-66 through molecular layer-by-layer deposition through use of the $Zr_6O_4(OH)_4(OMc)_{12}$ clusters, initiating ligand exchange through use of modulating acid and water content in the Zr_6 oxo cluster solutions.[61] The methacrylate ligand on the Zr_6 oxo clusters were successfully exchanged with the terephthalic acid linker of UiO-66 as evidenced by X-ray diffraction studies of the resultant film. This same technique would be used again in 2021 to develop films of UiO-66-NH_2,[62] an isostructural MOF to UiO-66. Noting these two papers, and working in parallel to these researchers, synthetic efforts to derive metal-oxo clusters suitable for MOF thin film synthesis began.

II. Porphyrinic MOFs

One of the most ubiquitous selections for an organic linker in modern MOF synthesis is the porphyrin macrocycle. The porphyrin backbone consists of an [18π]-electron heteroaromatic ring system comprised of 4 conjugated pyrrole rings, the porphyrin macrocycle is a basis for several important biomolecules such as chlorophyll, hemin and cytochrome p450. Porphyrin chemistry is made rich by the litany of functional groups that can be added to the meso positions of the porphyrin ring that can change the polarity and electronics of the molecule without loss of aromaticity. Porphyrin macrocycles are also able to coordinate metal ions at the heteroatomic

center which further expands the range of porphyrin applications. Porphyrin makes an optimal organic linker for MOF synthesis for two major reasons: firstly, the macrocycle can have bitopic, tritopic, tetratopic and octatopic topicities depending on functionalization at the meso positions and secondly, the rigid planar aromatic ring allows for the formation of crystallin MOFs that a less rigid, more labial linker could not afford. Overall, what porphyrin chemistry has brought to MOF synthesis is the ability to reliably incorporate a wide range of functional organic linkers into a MOF crystal framework. Researchers have been able to use the porphyrin linkers to impart therapeutic and catalytic activity to MOFs. Porphyrin containing MOFs have also been notable for applications in fluorescence, chromatography and even quantum computing.

Initial efforts to incorporate porphyrin linkers into a MOF framework took place before the discovery of group IV metal-based MOFs like UiO-66, and so these initial efforts utilized Zn(II) or Cu(II) inorganic nodes. In 1994 Roberson and coworkers reported a porous coordination polymer made from cyanophenyl substituted porphyrin linkers and Cu ions; however, the polymers lost porosity and crystallinity after solvent evacuation from the pores. By using tetrakis(4-carboxyphenyl)porphyrin (TCPP) as the organic linker and Co-based inorganic nodes Suslick, et al. were able to develop the porous and crystallin material, PIZA-1 (porphyrinic Illinois zeolite analogue). PIZA-1 was the first porphyrin containing MOF used for catalytic applications and cemented the TCPP molecule as reliable linker for porphyrinic MOF synthesis. The development of stable porphyrin-linked MOF crystals saw a major breakthrough when porphyrin linkers were combined with group-IV metal-oxo clusters to form highly stable porphyrinic MOFs.

The organic linkers that coordinate between the inorganic nodes of MOF crystals are crucial in determining not only pore size and topology, but also the chemical and physical

properties of a MOF. A MOF linker must meet certain criteria to be incorporated into a hybrid organic-inorganic crystal structure. First and foremost, the organic linker must have the appropriate functional groups to coordinate to the metal cations, and secondly the linker must have a symmetry appropriate to be incorporated into a repeating crystal structure.[63] To coordinate to the metal cations the vast majority of discovered MOFs use carboxylate functional groups however N-donor ligands are also widely used as MOF linkers.[64] In reticular chemistry one way to categorize and describe MOF linkers is by referencing topicity. Topicity refers to the number coordination sites present on the molecule and MOF linkers to date are categorized as ditopic, tritopic, tetratopic, hexatopic or octatopic.[65]

1. PCN Type MOFs with Tetratopic Porphyrin Linkers

The first major breakthrough in the development of stable group-IV based MOFs was the discovery of PCN-222(Fe) (PCN = porous coordination network) by the Zhou group in 2012. PCN-222 consisted of Fe-TCPP (the TCPP molecule with an Fe(II) coordinated to the center heteroatoms) coordinated to Zr_6 clusters, with each Zr_6 cluster coordinated to eight TCPP ligands. PCN-222 was applied a catalyst with activity biomimetic to enzymatic peroxidases. In terms of stability, PCN-222(Fe) was at the time discovered to be one of the most stable MOFs known, maintaining crystallinity even after exposure to concentrated HCl for 24 hours. Another notable feature of the PCN-222 family of MOFs is that a litany of different metalloporphyrins can successfully be incorporated into isostructural MOFs.

Since the initial study on PCN-224 the combination of TCPP and zirconium nodes has been used to develop several new PCN MOFs with various topologies. Differences in topologies between the MOFs arises based on the connectivity of Zr-oxo nodes. Examples include PCN-

223,[66] PCN-224,[67] PCN-225,[68] PCN-226[69] and PCN-133.[70] The wide range of applications explored for PCN MOFs has made them a mainstay in MOF literature.

2. UiO-type MOFs with Ditopic Porphyrin Linkers

Unlike their tetratopic counterparts, ditopic MOF linkers are more synthetically involved and this a likely reason that there are fewer reports of ditopic porphyrins in MOF synthesis. In 2014 Lu et al. were the first to report the synthesis of MOF featuring a ditopic porphyrin linker, using 5,15-di(*p*-benzoato)porphyrin (DBP) to synthesize a MOF of formula $Hf_6(\mu_3\text{-}O)_4(\mu_3\text{-}OH)_4(DBP)_6$, consisting of 12-connected Hf_6 oxo clusters linked by the ditopic porphyrin molecules so named DBP-UiO. This MOF used the porphyrin linker as a photosensitizer (PS) to carry out photodynamic therapy (PDT) on cancer cells of the neck and head.

III. Synthesis of Metal-oxo Building Blocks for Group-IV Metal Based MOFs

To begin investigations on utilizing carboxylate-substituted metal oxo clusters as precursors form MOF materials; especially thin film fabrication, first a reliable method for the synthesis of the desired clusters should be developed. The synthetic route selected should produce metal oxo clusters in sufficient quantity for repeated experimentation. To enhance catalytic applications of the resultant MOFs the synthetic protocols should be applicable to the formation of Hf-oxo clusters, not just Zr. Finding a suitable Hf precursor for Hf-oxo cluster synthesis is difficult as the hafnium(IV) butoxide source found in literature is prohibitively expensive. Instead the hafnium(IV) isopropoxide should be used as a hafnium source. For use in ligand exchange reactions for MOF formation the different capping ligands may serve to be more amiable to exchange than others based on pKa of the carboxylic acid. Known capping ligands for group-IV metal-oxo clusters include methacrylate, acrylate, buntanoate and benzoate.[58]

1. Synthesis of $Zr_6O_4(OH)_4(OBz)_{12}$ (OBz = Benzoate) and the Isostructural Hafnium analog $Hf_6O_4(OH)_4(OBz)_{12}$

Challenges associated with the synthesis of carboxylate-substituted metal oxo clusters include long reaction times, expensive precursors and difficulty in characterization. For initial investigations in the synthesis of carboxylate-substituted metal oxo clusters as MOF precursors the $Zr_6(OH)_4O_4(OBz)_{12}$ (**1.1**), and $Hf_6(OH)_4O_4(OBz)_{12}$ (**1.2**) were selected as target compounds for synthesis. For the synthesis of zirconium cluster **1.1** the known route developed by Kickelbick et al.[58] was used but a new synthetic route for hafnium cluster **1.2** was devised. To assure that the isostructural Hf product had been formed, comparison of powder diffraction patterns for **1.1** and **1.2** was carried out and the two patterns confirm the similarity in structure (Figure 1.2). Unambiguous structural determination of **1.2** was then carried out by single crystal x-ray diffraction and confirmed the suspected structure. Structural information gathered from the single crystal diffraction of **1.2** allows for the calculation of the powder diffraction pattern trivially with Mercury software. Checking the diffraction pattern of new batches and comparing them to the calculated diffraction pattern is a reliable method to determine a successful synthesis

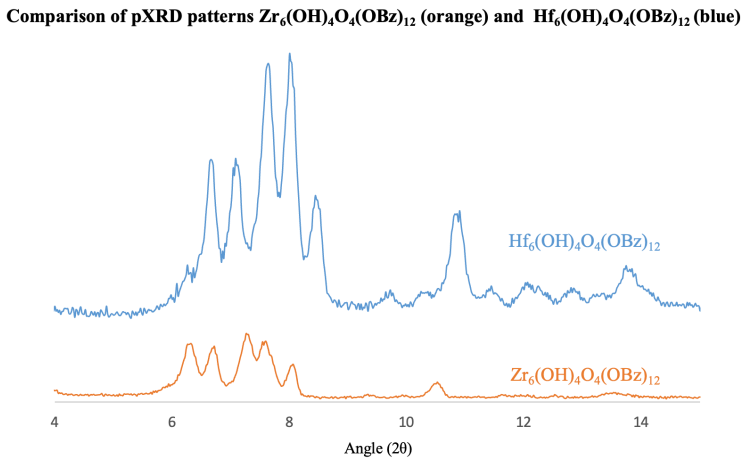

Figure 1.2: The collected diffraction pattern for compound Zr-oxo cluster **1.1** synthesized via methods described by Kickelbick et al can be seen in orange compared to the diffraction pattern for Hf-oxo cluster **1.2**.

(Figure 1.3).The reliable synthesis of benzoate-substituted Zr/Hf oxo clusters is a necessary step in developing a toolbox of MOF building blocks for layer-by-layer thin film deposition.

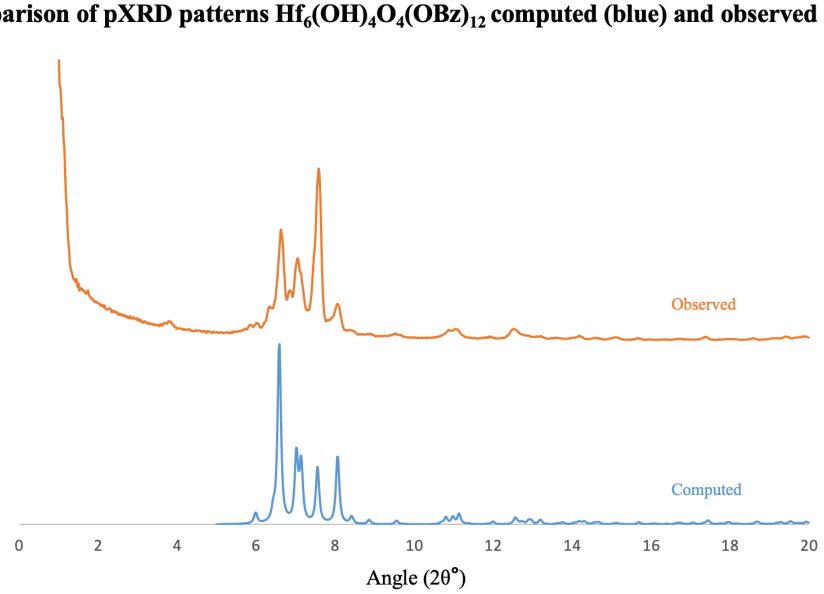

Figure 1.3: The computed diffraction pattern of $Hf_6(OH)_4O_4(OBz)_{12}$ as determined by single crystal diffraction data obtained in 2018 in blue compared to the observed powder diffraction pattern of the crystalline solid obtained from synthesis a year later, showcasing how the computed diffraction can be used to confirm successful synthesis of $Hf_6(OH)_4O_4(OBz)_{12}$.

The potential for ligand exchange between the monodentate carboxylate ligand and a more symmetric carboxylate is promising, but the long synthesis time and dilute reaction conditions do pose setbacks for use of the benzoate-capped clusters as MOF building blocks in layer-by-layer molecular deposition. The x-ray characterization of these clusters however, provide a meaningful pathway to the rapid characterization of these materials. Recently, advances made by Farha and coworkers show that methacrylate-substituted metal oxo clusters are readily synthesized in timescales of a single using reflux temperatures instead of the slow crystallization process traditionally utilized for metal-oxo clusters.[71] Motivated by these reports the rapid synthesis of the cluster **1.2** was attempted. The synthesis was initiated by refluxing 0.5 g of hafnium isopropoxide adduct into 10 mL of 1-propanol with 2.75 g of benzoic acid added to

the solution which was stirred for 24 hours under reflux with N_2 protection. After the solution returned to room temperature a 280 mg of a white powder crashed from solution which was collected via filtration and rinsed with chilled 1-propanol. After drying under vacuum the powder was analyzed with x-ray diffraction giving a diffraction pattern closely adhering to the computed diffraction pattern of cluster **1.2**; although seemingly less crystalline as the same materials synthesized over 7 days at room temperature (Figure 1.4).

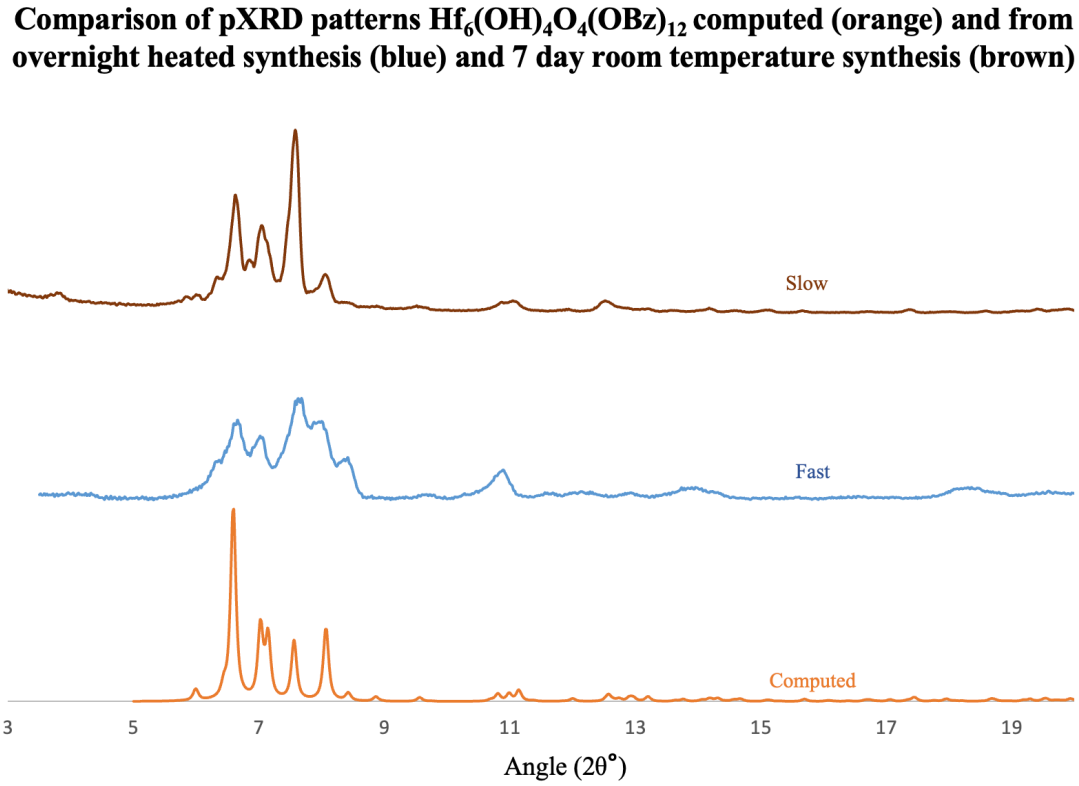

Figure 1.4: Comparing the diffraction patterns of $Hf_6O_4(OH)_4(OBz)_{12}$ as computed from single crystal data (orange) to powder diffraction patterns of samples synthesized with heat overnight (blue) or over 7 days at room temperature (brown).

2. Synthesis of $Zr_6O_4(OH)_4(OMc)_{12}$ (OMc = methacrylate) and the Isostructural Hafnium Analog $Hf_6O_4(OH)_4(OMc)_{12}$

Continuing with the synthesis of carboxylate-substituted metal oxo clusters towards the goal of attaining building blocks for MOF synthesis, methacrylate was selected as a promising

capping ligand. The methacrylate ligand provides an alternative to the aromatic benzoate ligand and the differing pKa between the mother acids of these two carboxylates will make different the dynamic kinetics of these respective ligands. Developing a set of clusters with different surface ligands will expand the toolbox of MOF building blocks available for experimentation in pursuit of group-IV MOF molecular layer-by-layer thin film deposition.

Using hafnium butoxide, the author was not able to produce samples of the methacrylate-capped Hf_6-oxo cluster suitable for single crystal x-ray diffraction. Structural elucidation of crystals generated with hafnium butoxide using x-ray diffraction determined clusters of structure $Hf_4O_2(OMc)_{12}$ (**1.3**). In order to carry on with investigations the synthesis of the isostructural Zr analog would be carried out as described by Kickelbick et al., with the intention of gaining a crystal structure for computing powder diffraction patterns. With the computed diffraction pattern of the $Zr_6O_4(OH)_4(OMc)_{12}$ **(1.4)** one could then optimize reaction parameters for the Hf analog and perform pXRD on the resultant powders attempting to find conditions which yield crystalline material with diffraction patterns matching the isostructural Zr analog.

Crystals of zirconium cluster **1.4** were synthesized via a slow crystallization process in the glovebox and single crystal x-ray diffraction used to determine the structure and compute a powder diffraction pattern. With this information synthetic efforts towards $Hf_6O_4(OH)_4(OMc)_{12}$ (**1.5**) were reinitiated and reaction parameters screened with the powder products being analyzed with simple pXRD to check for success. By mixing 1.0 g of the hafnium isopropoxide into a solution of 1 mL propanol and 1.7 mL methacrylic acid and allowing to solution to sit for 4 days in the glovebox a white crystalline solid **1.5** was obtained with a diffraction pattern matching the computed pattern of $Zr_6O_4(OH)_4(OMc)_{12}$. As was observed with the benzoate capped Zr_6/Hf_6-oxo analogs, it can be confidently assessed that the matching powder patterns indicates strong

structural similarity to the point that we can assess the two materials are isostructural analogs of each other (Figure 1.5).

Comparison of pXRD patterns, computed $Zr_6(OH)_4O_4(OMc)_{12}$ (blue) and the observed pattern of $Hf_6(OH)_4O_4(OMc)_{12}$

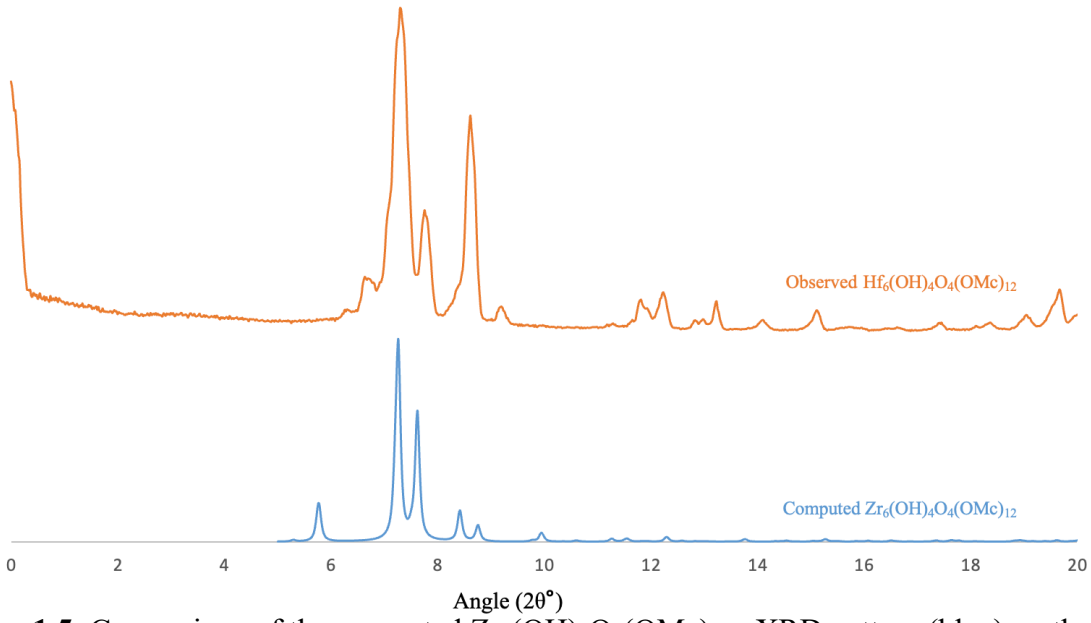

Figure 1.5: Comparison of the computed $Zr_6(OH)_4O_4(OMc)_{12}$ pXRD pattern (blue) on the bottom and the observed diffraction pattern for $Hf_6(OH)_4O_4(OMc)_{12}$ (orange) on the top.

3. Using the $Hf_2O_4(OMc)_{12}$ Cluster as a Precursor for the Synthesis of UiO-66 (Hf)

While the clusters **1.2** and **1.5** could easily be incorporated into a fabrication method for Hf-based MOFs, it was less clear that the smaller Hf cluster **1.3** would be suitable as a MOF precursor. To date, no MOF which utilized an Hf_2O_4 cluster as the inorganic node is known. In an attempt to develop a MOF which is based on the Hf_2O_4 cluster, a series of attempted synthesis were carried out which featured dissolving cluster **1.3** into solutions of DMF with an acetic acid modulator and three distinct linkers, terephthalic acid, trimesic acid and 1,4-phenylenediacetic acid. Only the use of terephthalic acid resulted in the formation of a crystalline solid. In an interesting development, the solid which was produced from solution was not a novel MOF, but in fact matched the diffraction pattern of UiO-66. Considering the starting material was the

Hafnium cluster **1.3** the resultant MOF is the isostructural hafnium UiO-66 analog, UiO-66 (Hf). The structure of the highly crystallin UiO-66 (Hf) was confirmed by comparing the observed diffraction pattern to the computed UiO-66 diffraction pattern (Figure 1.6). This result not only provides an application of the Hf cluster **1.3** but is also a very surprising result. The synthesis of UiO-66 (Hf) in this example was carried out at room temperature which is a relevant at the synthesis will usually require long solvothermal synthesis in an autoclave. Moreover, it is interesting using the cluster **1.3** with a Hf_2O_4 center can someone result in a MOF based on the Hf_6O_8 cluster.

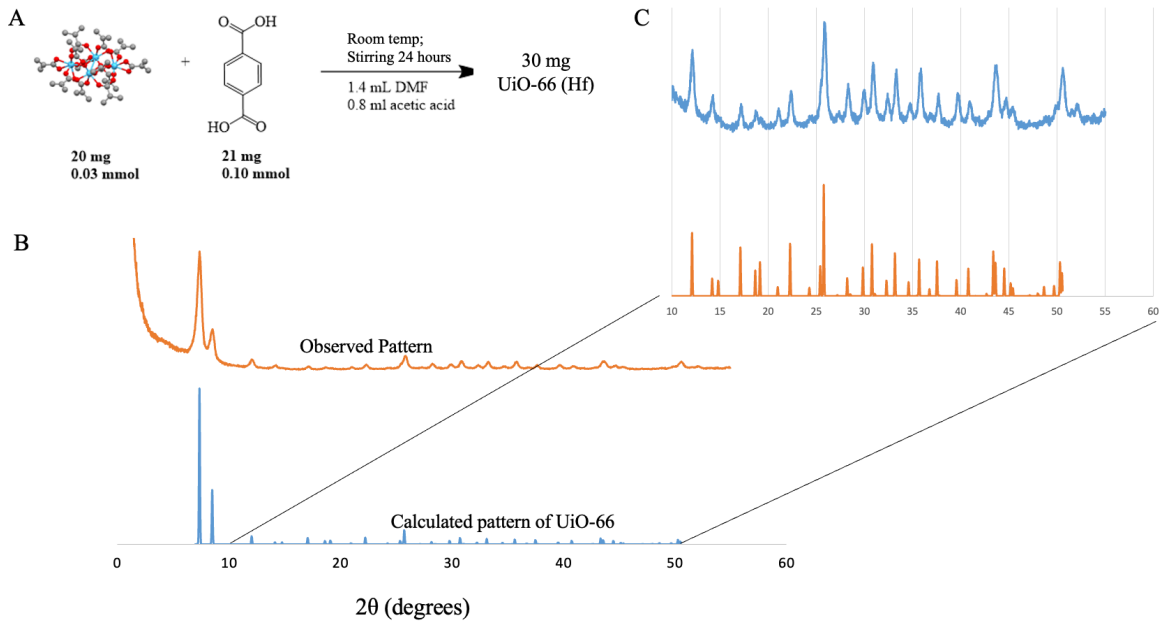

Figure 1.6: Synthesis and analysis of UiO-66 (Hf) synthesized from the $Hf_2O_4(OMc)_{12}$ cluster. A) The synthetic conditions of the UiO-66 (Hf) synthesis. B) Diffraction pattern of the synthesized UiO-66 (Hf) powder (in orange) compared to the calculated pattern of UiO-66 (in blue). C) Inset of observed and computed diffraction patterns from 10-55° 2θ zoomed in for greater clarity.

IV. Developing a Library of Porphyrin Linkers for MOF Synthesis

Towards the goal of developing functional nanoparticles and thin films, and inspired by the great success of past utilizations, the porphyrin macrocycle was selected as the optimal MOF organic linker for experimental explorations. In order to facilitate a further study into the construction of functional MOF a library of porphyrin linkers was prepared (Figure 1.7). The porphyrin linker synthesized were either tetratopic or ditopic in the hopes of synthesizing MOF particles of either PCN or UiO topology. For the ditopic linkers variations in the 5 and 15 meso positions of the porphyrin macrocycles allows for probing the effect steric and electronic variations of the porphyrin linker will have on the synthesis of MOF-based materials and the final applications.

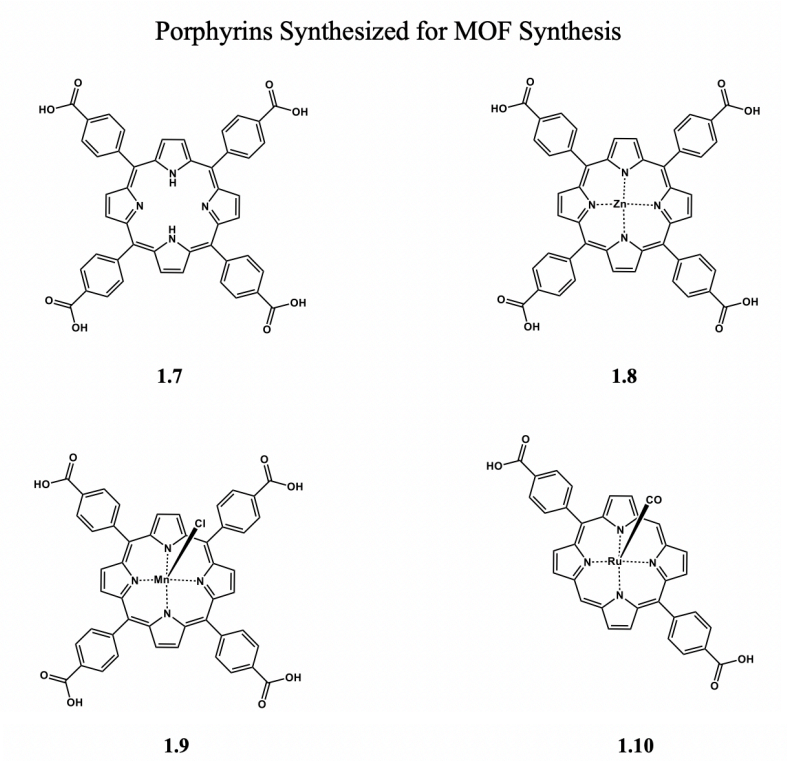

Figure 1.7: Chemical structures of the porphyrins in the synthesized linker library.

The preparation of porphyrin MOF linkers for future studies into functional MOFs began with the synthesis of TCPP. This tetratopic MOF linker is highly symmetric and so can be synthesized readily from pyrrole and monomethyl terephthalate by refluxing of the two reactants in propionic acid to form the methyl-ester porphyrin, subsequent de-methylation afforded TCPP (1.7). The synthesis of TCPP proceeded routinely and the porphyrin macrocycle could be metalated in straightforward manner with Zn and RuCO to afford Zn-TCPP (**1.8**) and Mn-TCPP Cl (**1.9**) respectively. TCPP is one of the most ubiquitous linkers in MOF chemistry because it can be tailored to many applications by metalation and is easy to synthesize. Linkers **1.7-1.9** are tetratopic linkers for the attempted synthesis of PCN-type MOF thing films which will be discussed in Chapter 2. Through ligand exchange with the monodenate capping ligands of the Hf-oxo cluster $Hf_6(OH)_4O_4(OMc)_{12}$ **1.5** these linkers will be used for the layer-by-layer molecular deposition of MOF thin films.

The synthesis of ditopic MOF linkers would allow us to synthesize MOFs with the UiO topology but is a more involved synthetic process due to the reduced symmetry of the ditopic porphyrin macrocycles. Synthesis of the ditopic porphyrin macrocycles requires preparation of the dipyrrole methane precursors, making the synthesis more involved and requiring purification often by column chromatography. Porphyrin **1.10** was synthesized as a potential linker for a novel MOF with UiO topology. Molecule **1.10** was selected because the ruthenium(II) carbonyl porphyrins show potential for catalysis in oxidation reactions[72] and for carbene insertions into N-H bonds.[73] The development of a synthesis for a Hf-based MOF comprised of **1.10** in a UiO topology would represent a stable platform for useful catalytic applications.

1. RuCO DBP-UiO (Hf)

While the tetratopic linkers will later be employed in Chapter 2 for thin film synthesis the

ditopic porphyrin linker **1.10** was able to be incorporated into a novel Hf-based MOF with potential catalytic applications. Screening of various acids, times and temperatures led to the optimized condition which was able to produce crystals of a MOF which powder diffraction revealed held the UiO topology. X-ray diffraction of RuCO-DBP-UiO (Hf) provided a diffraction pattern which matched the diffraction pattern computed from Zn-DPDBP-UiO,[56] which is an isotructural MOF with UiO-type structure. The matching diffraction patterns confirm the UiO structure of the new MOF featuring the porphyrin linker **1.10** (Figure 1.8). To ensure that the resultant MOF still contained the RuCO moiety within the porphyrin macrocycles, both IR analysis and XPS analysis were used (Figure 1.9).

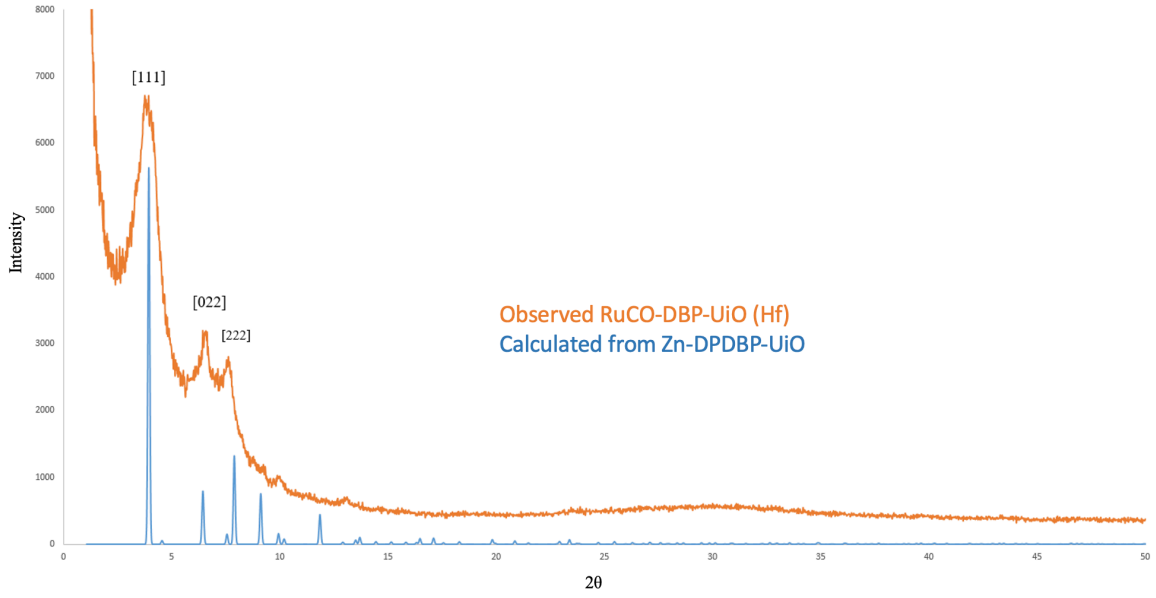

Figure 1.8: Comparison of the observed diffraction pattern of RuCO-DBP-UiO (Hf) to the calculated diffraction pattern of Zn-DPDBP-UiO. The (111), (022) and (222) indices show a strong correlation to the computed pattern.

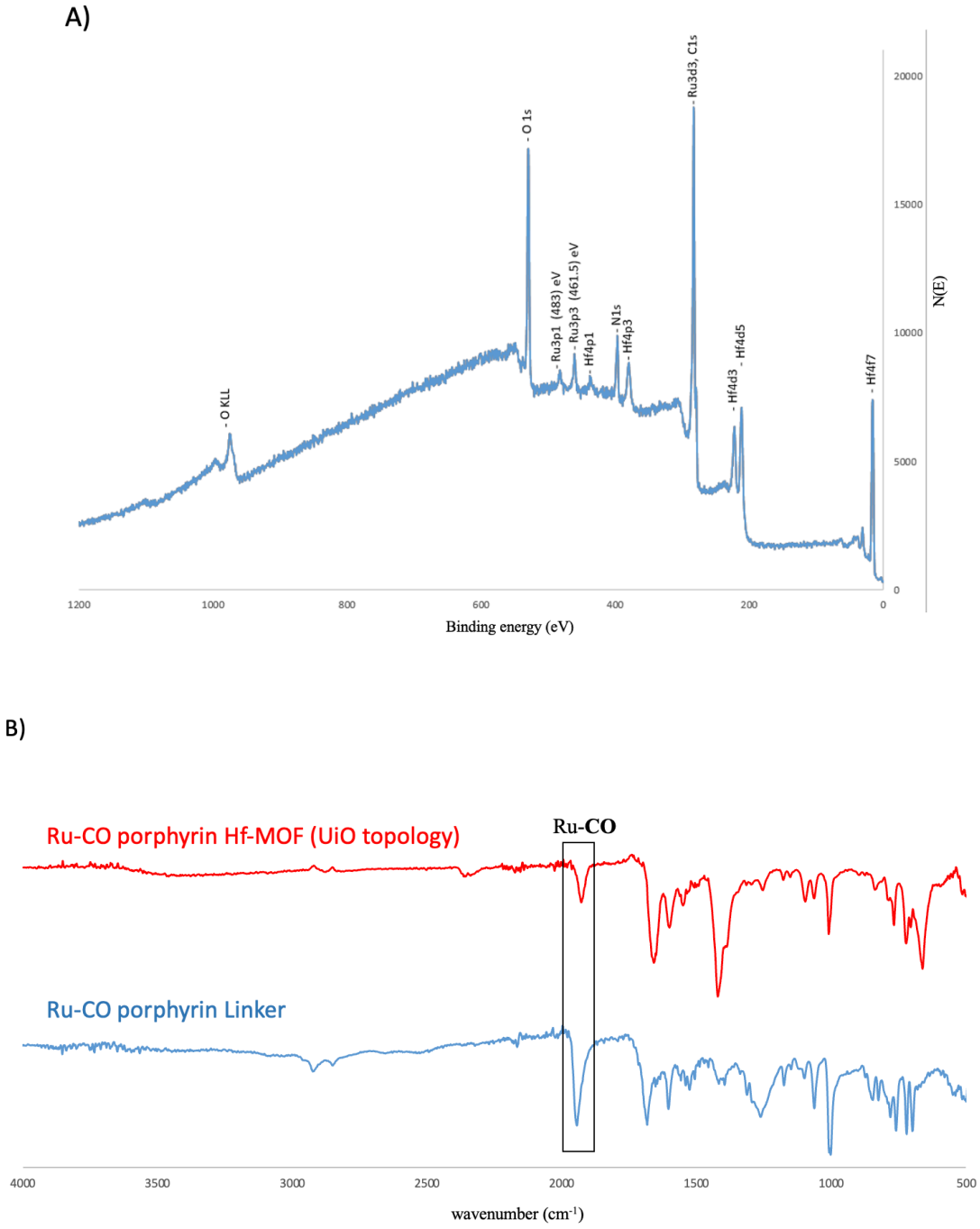

Figure 1.9: Characterization of RuCO-DBP-UiO (Hf). A) The XPS spectra of RuCO-DBP-UiO (Hf) which confirms Ru, Hf, C and N are all present in the MOF, binding energy of the Ru confirms the 2+ oxidation state. B) IR analysis of the RuCO-DBP-UiO (Hf) in red compared to the Ru-CO porphyrin linker **1.10** in blue, the carbonyl signal associated with the ruthenium carbonyl is present in both samples.

V. Experimental Section and Spectral Data

1. Synthesis of Carboxylate Substituted Metal-oxo Clusters

$Zr_6(OH)_4O_4(OBz)_{12}$ 1.1: Following the method of Kickelbick, in a 100 ml Schlenk vial 16 g of benzoic acid (32 mmol) was dissolved into 74 g of 1-propanol which requires sonication. The solution was degassed by 3 pump-thaw cycles and loaded into the glovebox. Then 1.0 mL of 70% Zr (IV) propoxide (1.6 mmol) was added to the solution and mixed. The Schlenk vial is left to sit in the glovebox without stirring and after 7 days for crystals of 1.1 started to fall from solution. The excess solution was decanted from the reaction vessel and the crystals were collected, rinsed with 1-propanol and stored in the glovebox after drying under vacuum.

$Hf_6(OH)_4O_4(OBz)_{12}$ 1.2: In a method adapted from Kickelbick et al., 16 g of benzoic acid (32 mmol) is dissolved in 74 g of 1-propanol in a 100 mL Schlenk tube with much sonication. The solution was degassed and brought into the glovebox where 0.930 g of hafnium isopropoxide (1.6 mmol) was dissolved added to the solution. The reaction mixture was left to sit in the glovebox for 7 days after which clear colorless crystals of 1.2 have fallen from solution. Crystals were collected and rinsed with 1-propanol, dried under a vacuum and were stored in the glovebox until use. Yield 0.255 g (48%)

$Hf_4O_2(OMc)_{12}$ 1.3: In the glovebox, 1.7 mL (35 mmol) of methacrylic acid, analytical grade, and 1.2 g of hafnium butoxide was mixed. The solution was left in the glovebox for 6 days after which crystals of 1.6 (0.4 mmol) had fallen from solution. The crystals were gently with 1-propanol and dried under vacuum. The crystals were stored in the glovebox until use. Yield 0.730 g (58%).

$Zr_6(OH)_4O_4(OMc)_{12}$ 1.4: Prepared using a method first described by Kickelbick et al. In the glovebox a 20 mL vial was charged with 1.0 mL of 70% Zr(IV) propoxide in propanol (2.23

mmol) and 1.7 mL of methacrylic acid (20 mmol), analytical grade, is added. The solution was left to sit in the glovebox without stirring for 11 days after which crystals of 1.3 formed from the solution. The crystals were collected and washed with 1-propanol, dried under vacuum and stored in the glovebox until use. Yield 1.151 mg (77%).

$Hf_6(OH)_4O_4(OMc)_{12}$ 1.5: In the glovebox a 20 mL vial was loaded with 1.0 g (2.38 mmol) of hafnium isopropoxide and 1.0 mL of 1-propanol was charged into the flask. The solution was stirred until the hafnium iospropoxide is brought to solution and then 1.7 mL (20 mmol) of methacrylic acid, analytical grade, was added to the solution and mixed to equilibrium. The reaction mixture was left to sit in the glovebox for four days with no stirring at room temp after which clear to colorless crystals of 1.5 fell from solution. The vial was removed from the glovebox and the liquid eluted from the crystals. The crystals were washed gently in 1-propanol, care should be given as the product is slightly soluble in the propanol. After rinsing the crystals were dried under vacuum and stored in the glovebox until use. Yield 0.698 g (79%).

2. Synthesis of Tetratopic Porphyrin MOF Linkers

Synthesis of 5,10,15,20-tetrakis(4-methoxycarbonylphenyl)porphyrin (TMeOCPP) (1.11): TMeOCPP was synthesized through a method modified from known procedures.[67] Into a 300 mL round bottom flask 150 mL of propionic acid was charged and 2.0 g of methyl-4 formyl benzoate (12.18 mmol) was dissolved followed by the addition of 0.817 g of distilled pyrrole (12.18 mmol). The solution was brought to reflux for 4 hours then allowed to cool to room temperature. The mixture was then placed in the fridge overnight and passed through a fritted funnel. The collected solid was rinsed with acetone and methanol until the filtrate was clear. After rinsing the collected solid was dried under vacuum to give 1.1g of 1.6 (10% yield).

Synthesis of 5,10,15,20-tetrakis(4-carboxyphenyl)porphyrin (TCPP) (1.7): 1.0 g of TMeOCPP was dissolved into a 60 mL in a 50/50 mixture of THF/MeOH. Then a solution of 500 mg KOH in 30 mL of water was added to the mixture and the stirred solution is brought to reflux at 80 C. After overnight reflux the solution was allowed to cool and the organic solvents were removed by rotary evaporation. The aqueous solution was placed in an ice bath and 1.0 M HCl is added dropwise to lower the pH to 1.0, at which the TCPP will fall out of solution as a purple powder. The powder is placed in a centrifuge tube and rinsed with water by centrifugation 3x. After drying in a vacuum oven overnight at 80 C at 100 mbar 812 mg of the TCPP powder is obtained (87% yield). The 1H NMR spectrum was recorded and matches reported spectra.[74]

Synthesis of Zinc(II) 5,10,15,20-tetrakis(4-methoxycarbonylphenyl)porphyrin (Zn-TMeOCPP) (1.11): 1.0 g of TMeOCPP dissolved into 100 mL of dimethylformamide (DMF) in a 200 mL round bottom flask and 1.0 g of $Zn(Oac)_2$ is added to the mixture and stirred to solution. The solution was stirred under reflux overnight then allowed to cool to room temperature. The reaction mixture was transferred to a beaker and 200g of ice was added. As the ice melts Zn-TMeOCPP falls from solution and can be collected by filtration as a pink powder. The solid was washed with water and dried in a vacuum oven. The 1H NMR was recorded and matches the spectra reported in literature.[75] ^{1}H NMR (400 MHz, $CDCl_3$) 4.12 (s, 12H), 8.31 (d, J=8.16 Hz, 8H), 8.45 (d, J=8.12 Hz, 8H), (s, J=8.92 Hz, 8H)

Synthesis of Zinc(II) 5,10,15,20-tetrakis(4-carboxyphenyl)porphyrin (Zn-TCPP) (1.8): 1.0 g of Zn-TMeOCPP was brought dissolved into 60 mL in a 50/50 by volume mixture of THF/MeOH. 500 mg of KOH was dissolved in 30 mL of water then added to the Zn-TMeOCPP solution. Stirring was initiated and the solution is brought to reflux. After reflux the reaction can be monitored by TLC. The organic solvents were removed through rotary evaporation, the

aqueous solution was placed in an ice bath and the 1.0 M HCl was added dropwise to bring the solution to 1.0 ph at which point Zn-TCPP will fall from solution as a pink solid. The solid was collected by filtration then placed in a centrifuge tube and washed with water 3x. The powder is dried in a vacuum oven at 80C at 100 mbar overnight to provide 739 mg of the final product (73% yield from TMeOCPP). UV-vis and 1H NMR spectra match previous reports.[75,76] ^{1}H NMR (400 MHz, DMSO-d_6) 8.31 (d, *J*=8.2 Hz, 8H), 8.37 (d, J=8.2 Hz, 8H), 8.80 (s, 8H)

Synthesis of Mn(III) 5,10,15,20-tetrakis(4-methoxycarbonylphenyl)porphyrin Chloride (Mn TMeOCPP Cl) (1.12): 1.0 g of **1.11** is dissolved into a 100 mL of DMF in a round bottom flask and 1.0 g of $Mn(Oac)_2$ was added to the mixture and brought to solution with stirring. The solution was brought to reflux at 140 C and allowed to reflux overnight. After allowing the reaction to cool to room temperature the solution was transferred to a round bottom flask and the reaction mixture flooded with 100 mL 1.0 M HCl solution and stirred for 3 hours after which the **1.12** had fallen out of solution as a brown powder. The metalloporphyrin was collected by centrifugation and the HCl solution decanted. The metalloporphyrin was rinsed with H_2O until the decanted H_2O after the rinses were neutral. The collected brown powder is dried in the vacuum oven at 80 C and 100 mbar overnight and was carried over to the next step as is.

Synthesis of Mn(III) 5,10,15,20-tetrakis(4-carboxyphenyl)porphyrin Chloride (Mn-TCPP Cl) (1.9): The collected **1.12** was placed into a 60 mL of a 50/50 by volume mixture of THF and MeOH. Then a solution of 500 mg of KOH in 30 mL of H_2O was added to the mixture and stirring was initiated. The solution was brough to reflux overnight and then allowed to cool to room temperature. The reaction mixture was moved to a beaker which was on ice and 1.0 M HCl was added dropwise until the pH of the solution reaches 1 after which **1.9** fell out of solution as a brown powder. The solid was collected by filtration after which it was transferred to

a centrifuge tube and rinsed 3x with H_2O. After rinsing the powder was dried in a vacuum oven at 80 C and 100 mbar overnight. 650 mgs (63% yield from the TMeOCPP) of the **1.9** was collected and characterized by UV-vis analysis which matches the spectra found in literature (Figure 1.10).[77]

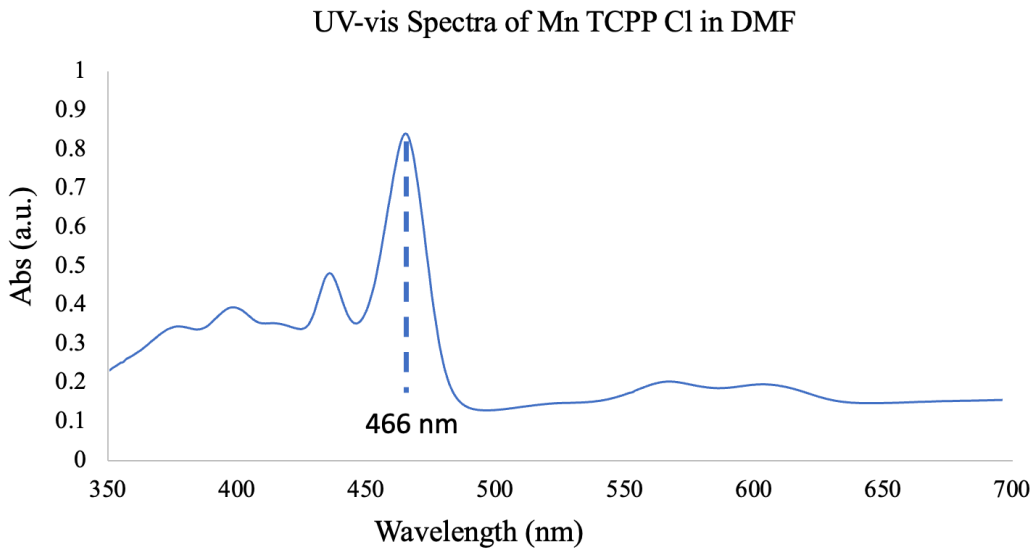

Figure 1.10: UV-vis spectra of the Mn TCPP Cl in DMF.

3. Synthesis of Ditopic Porphyrin MOF Linkers

Synthesis of dipyrrylmethane (1.13): Dipyrrylmethane was synthesized by a scaled down version of the procedure developed by Lu et al.[56] Into a 400 mL round bottom flask 250 mL of distilled pyrrole is charged followed by 0.87 g of paraformaldehyde. The mixture was heated to 80 C until all of the paraformaldehyde was dissolved then the solution is allowed to cool to room temperature. At room temperature a septum was placed over the flask and the solution was stirred under nitrogen with a balloon for 30 minutes. After 30 minutes of nitrogen purging, 0.215 mL of trifluoroacetic acid (TFA) was added dropwise to the solution through a septum. The mixture was stirred at room temperature overnight under a nitrogen balloon after which the reaction was monitored by TLC with elemental bromine used to stain the TLC plate, the dipyrrolemethane will stain pink upon exposure to bromine vapor. After TLC the septum was

removed and 406 mg of powdered NaOH was added to the mixture and stirred for one hour. The solution was then vacuum distilled to remove the excess pyrrole. The resultant brown solid was rinsed with water then methanol. The brown solid was purified through silica gel chromatography using and elutant of 20% Ethyl Acetate and 80% hexane. Fractions were monitored by staining on TLC plates with bromine and all fractions which stain pink were collected. After rotary evaporation 3.3 g of **1.13** was isolated (77% yield). The product matches the known 1H NMR.[56] ^{1}H NMR (400 MHz, $CDCl_3$) 3.99 (s, 2H), 6.06 (s, 2H), 6.17 (d, J=2.84 Hz, 2H), 6.68 (d, J=1.52 Hz, 2H), 7.83 (s, 2H)

Synthesis of 5, 15-di(p-methyl-benzoato)porphyrin (1.14): 5,15-di(p-methylbenzoato)porphyrin was synthesized by the method developed by Lu et al. to give 17% yield of compound **1.14** (Figure 1.11). 1H NMR was used to confirm the structure of the product.[56] ^{1}H NMR (500 MHz, $CDCl_3$) -3.11 (s, *2*H), 4.16 (s, 6H), 8.39 (d, *J*=8 MHz, 4H), 8.51 (d, *J*=8 MHz, 4H), 9.06 (d, *J*=4.5 MHz, 4H), 9.45 (d, *J*=4.5 MHz, 4H), 10.38 (s, 2H)

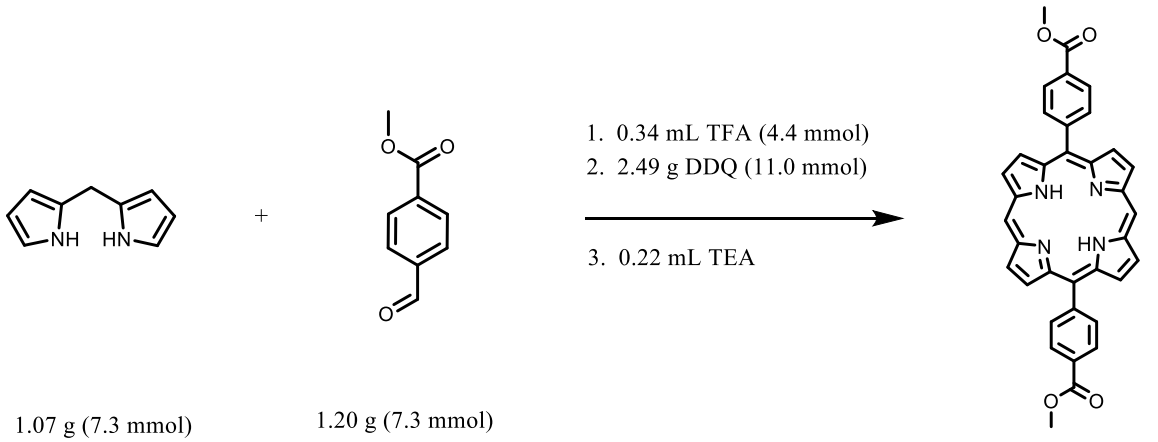

Figure 1.11: Reaction of dipyrrylmethane and (4-methoxycarbonyl)benzaldehyde to provide the 5, 15-di(p-methyl-benzoato)porphyrin in 17% yield.

Synthesis of 5, 15-di(p-methyl-benzoato)porphyrin Ruthenium(II) Carbonyl (1.15): The metalloporphyrin **1.15** was synthesized by mixing 50 mg of **1.14** into 50 mL of decaline then adding 50 mg of triruthenium dodecacarbonyl. The decaline was brought to reflux at 200 C and stirred overnight. After overnight reflux the reaction was allowed to cool to room temperature then the decaline was removed by vacuum distillation. After vacuum distillation a solid black residue was collected and the metalloporphyrin was purified by column chromatography using neutral alumina as the stationary phase and DCM and the mobile phase. **1.15** comes over the column as a bright red band which was collected. The solvent was removed through rotary evaporation to provide 45 mg of the metalloporphyrin **1.15** (75% yield). The product was confirmed through 1H NMR. ^{1}H NMR (500 MHz, $CDCl_3$) 4.15 (s, 6H), 8.29 (d, *J*=7.8 MHz, 2H), 8.38 (d, *J*=8.45 MHz, 2H), 8.46 (d, *J*=7.7 MHz, 2H), 8.48 (d, *J*=7.75 MHz, 2H), 8.83 (d, *J*=4.6 MHz, 4H), 9.20 (d, *J*=4.7 MHz, 4H), 10.07 (s, 2H)

Synthesis of 5, 15-di(p-benzoato)porphyrin Ruthenium(II) Carbonyl (1.10): 100 mg of the metalloporphyrin **1.15** was dissolved into 40 mL of a 50/50 mixture by volume of THF and methanol in a 100 mL round bottom flask. 300 mg of KOH was dissolved into 20 mL of water and the alkaline solution was added to the solution. Stirring was initiated and reflux at 80 C maintained overnight. The solution was allowed to cool to room temperature and the organic solvents were removed through rotary evaporation. The remaining aqueous mixture was placed in a beaker chilled over ice and 1.0 M HCl was added dropwise until the Ph of the solution lowered to 1.0 at which point **1.10** will fall from solution as a bright red powder. The product can be collected by centrifugation and rinsed 3x with water. The product was dried overnight in a vacuum oven at 80C and 100 mbar. High resolution mass spectrometry was used to confirm the presence of a compound having the expected elemental composition was present in prepared

samples, the mass of this detected compound correlates with structure 1.9. Samples for mass spectrometry were prepared by dissolving > 1mg of the product into HPLC grade acetonitrile. Using mass spectrometry the [M+1] peak is observed at 679.05 m/z and another peak a at 720.08 m/z arises from the acetonitrile adduct of the product (Figure 1.12). The [M+1] peak matches the calculate pattern (Figure 1.13).

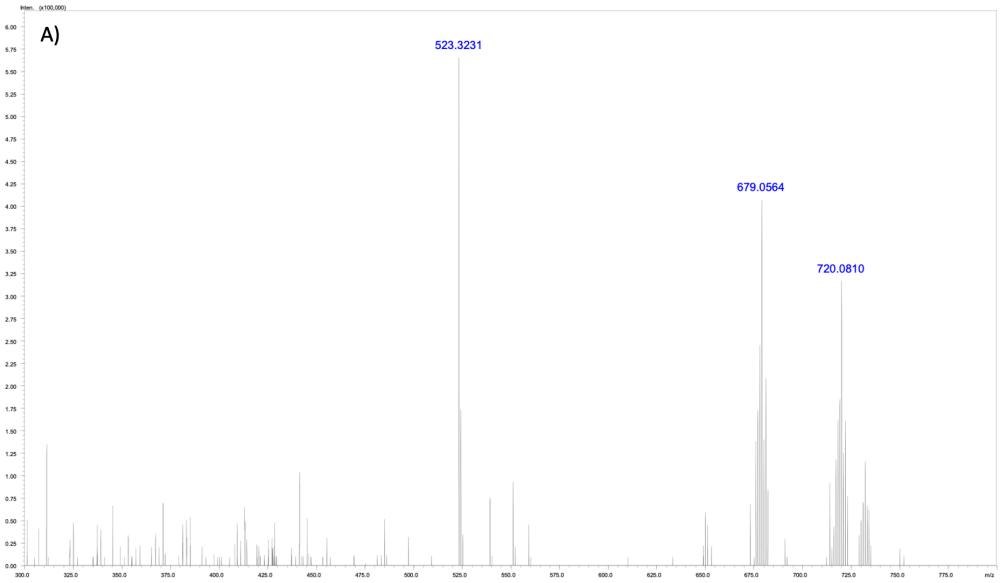

Figure 1.12: Mass spectrometry analysis of **1.10** with the [M+1] peak at 679.05 and the acetonitrile adduct of the **1.10** present at 720.08.

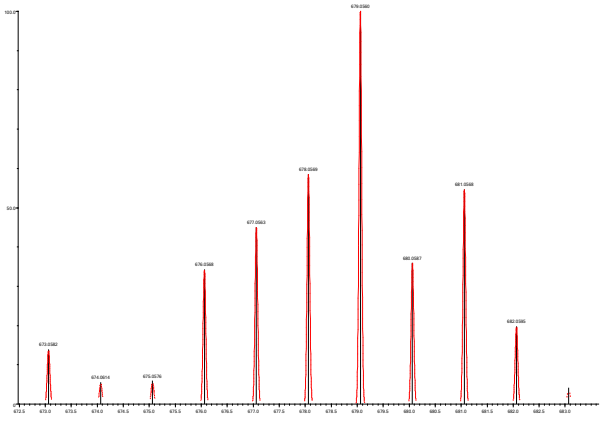

Figure 1.13: Observed mass spectrometry peaks in black compared to the computed m/z of **1.10** in red.

4. Synthesis of RuCO DBP-UiO (Hf)

The so named RuCO-DBP-UiO (Hf) was synthesized by dissolving 13 mg of **1.10** (0.019 mmol) and 6.1 mg of $HfCl_4$ (0.019) into 7 mL of DMF followed by the addition and of 1.0 uL of acetic acid, 68.7 mg of benzoic acid modulator was added and the mixture sonicated until all components are dissolved. The reaction mixture was sealed into a 20 mL glass screw-capped tube and placed into a 110 C autoclave for 48 hr after which crystal of RuCO-DBP-UiO (Hf) formed.

The excess solvent was eluted and the crystals collected. Crystals were washed in DMF 3x and acetone 3x after rinsing the porous crystals were purged of adsorbed solvent by placement in a vacuum oven at 120 C for 48 hours at 100 mbar pressure. The resultant red crystal were suitable for x-ray powder diffraction.

5. Crystallographic Information

Crystals of compounds **1.2**, **1.3**, and **1.4** were diffracted for unambiguous structural determination. The ORTEP crystal structures and the details of data collection can be seen in figures 1.14-1.16 respectively. The crystallographic information for compounds **1.2**, **1.3**, and **1.4** can be found in table 1.1.

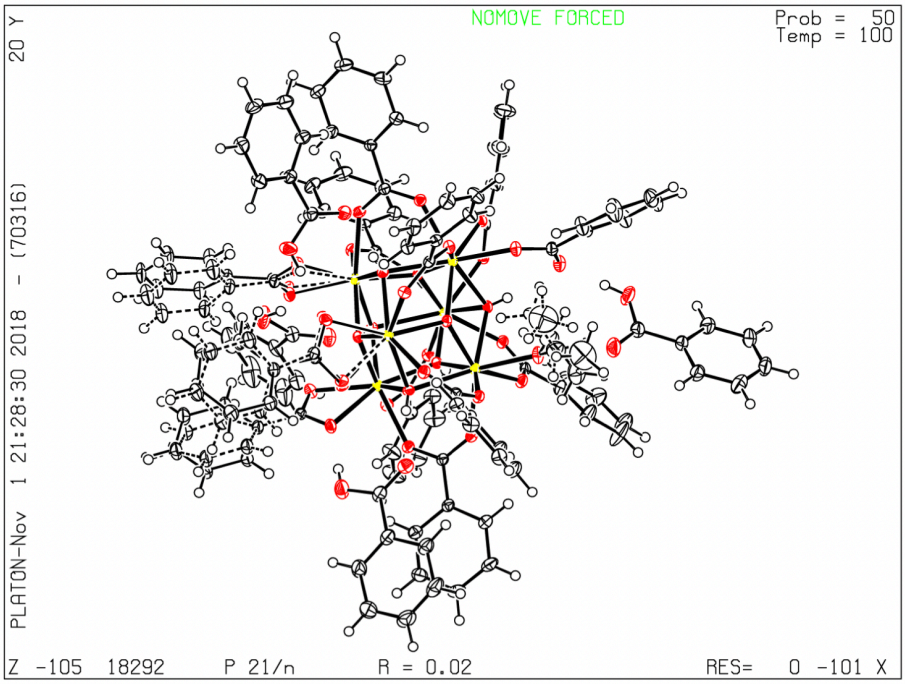

Bond precision: C-C = 0.0046 A Wavelength=0.71073

Cell: a=27.393(6) b=16.354(4) c=27.863(6)
alpha=90 beta=115.530(6) gamma=90

Temperature: 100 K

	Calculated	Reported
Volume	11263(4)	11263(4)
Space group	P 21/n	P 21/n
Hall group	: -P 2yn	-P 2yn
Moiety formula	C87 H72 Hf6 O33, 4(C7 H6 O2)	C87 H72 Hf6 O33, 4(C7 H6 O2)
Sum formula	C115 H96 Hf6 O41	C115 H96 Hf6 O41
Mr	3204.86	3204.85
Dx,g cm-3	1.890	1.890
Z	4	4
Mu (mm-1)	5.594	5.594
F000	6184.0	6184.0
F000'	6173.57	
h,k,lmax	39,23,39	39,23,39
Nref	34357	34304
Tmin,Tmax	0.396,0.827	0.268,0.406
Tmin'	0.314	

Correction method= # Reported T Limits: Tmin=0.268 Tmax=0.406
AbsCorr = MULTI-SCAN

Data completeness= 0.998 Theta(max)= 30.495

R(reflections)= 0.0217(30172) wR2(reflections)= 0.0556(34304)

S = 1.003 Npar= 1703

Figure 1.14: Crystal Structure of $Hf_6(OH)_4O_4(OBz)_{12}$ **1.2**

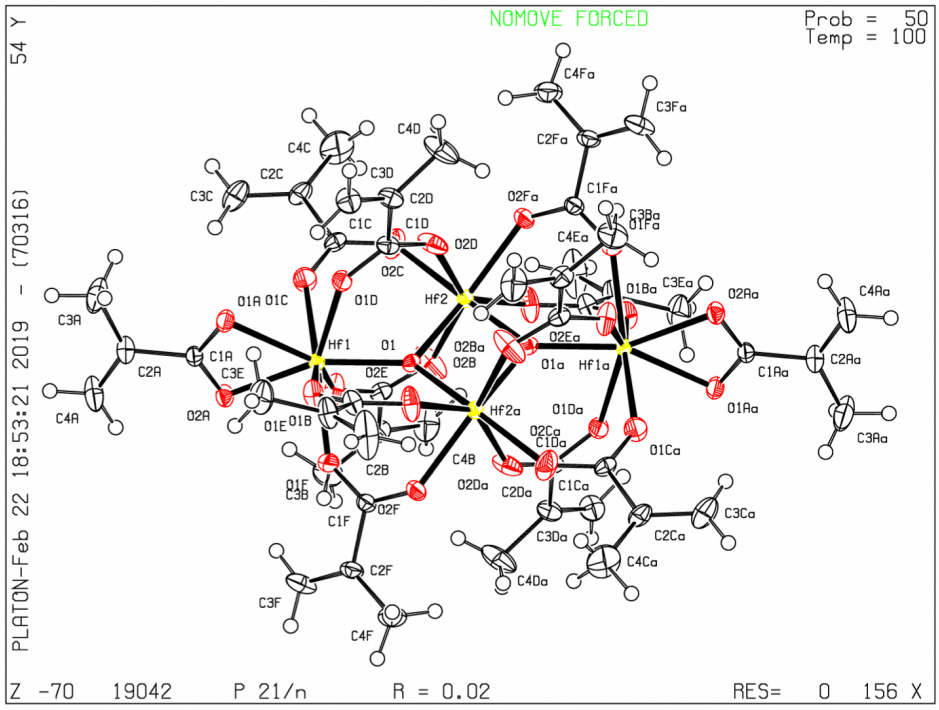


```
Bond precision:  C-C = 0.0036 A          Wavelength=0.71073

Cell:            a=13.1989(7)     b=16.7810(9)       c=13.6682(8)
                 alpha=90         beta=95.034(3)     gamma=90
Temperature:     100 K

                 Calculated                Reported
Volume           3015.7(3)                 3015.7(3)
Space group      P 21/n                    P 21/n
Hall group       -P 2yn                    -P 2yn
Moiety formula   C48 H60 Hf4 O26           C48 H60 Hf4 O26
Sum formula      C48 H60 Hf4 O26           C48 H60 Hf4 O26
Mr               1766.92                   1766.92
Dx,g cm-3        1.946                     1.946
Z                2                         2
Mu (mm-1)        6.939                     6.939
F000             1688.0                    1688.0
F000'            1684.49
h,k,lmax         20,26,21                  20,26,21
Nref             12087                     12079
Tmin,Tmax        0.286,0.460               0.332,0.496
Tmin'            0.265

Correction method= # Reported T Limits: Tmin=0.332 Tmax=0.496
AbsCorr = MULTI-SCAN

Data completeness= 0.999          Theta(max)= 33.764

R(reflections)= 0.0201( 11086)    wR2(reflections)= 0.0521( 12079)

S = 1.003                  Npar= 353
```

Figure 1.15: Crystal Structure $Hf_4O_2(OMc)_{12}$ **1.3**

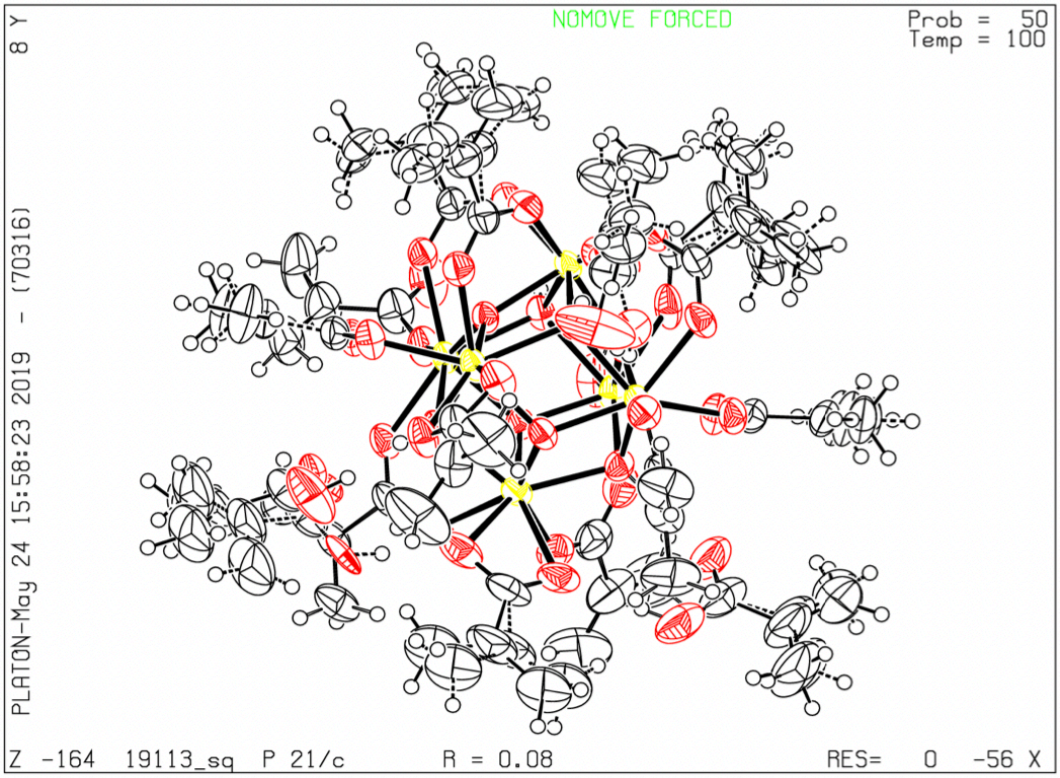

Bond precision: C-C = 0.0163 A Wavelength=0.71073

Cell: a=16.8917(12) b=17.7763(13) c=30.976(3)
alpha=90 beta=98.885(2) gamma=90

Temperature: 100 K

	Calculated	Reported
Volume	9189.6(13)	9189.6(13)
Space group	P 21/c	P 21/c
Hall group	-P 2ybc	-P 2ybc
Moiety formula	C48 H66 O33 Zr6, 3(C4 H6 O2) [+ solvent]	C48 H66 O33 Zr6, 3(C4 H6 O2)
Sum formula	C60 H84 O39 Zr6 [+ solvent]	C60 H84 O39 Zr6
Mr	1976.59	1976.59
Dx,g cm-3	1.429	1.429
Z	4	4
Mu (mm-1)	0.733	0.733
F000	3984.0	3984.0
F000'	3914.20	
h,k,lmax	19,20,35	19,20,35
Nref	14609	14714
Tmin,Tmax	0.864,0.874	0.438,0.491
Tmin'	0.864	

Correction method= # Reported T Limits: Tmin=0.438 Tmax=0.491
AbsCorr = MULTI-SCAN

Data completeness= 1.007 Theta(max)= 24.107

R(reflections)= 0.0821(13766) wR2(reflections)= 0.2530(14714)

S = 1.028 Npar= 1212

Figure 1.16: Crystal Structure of $Zr_6(OH)_4O_4(OMc)_{12}$ **1.4**

Table 1.1: Crystallographic information for 1.2-1.4

	1.2	1.3	1.4
Formula	$C_{115}H_{96}Hf_6O_{41}$	$C_{48}H_{60}Hf_4O_{26}$	$C_{60}H_{84}Zr_6O_{39}$
Formula Weight	3204.943 g/mole	1766.949 g/mole	1976.648 g/mole
Space Group	$P2_1/n$	$P2_1/n$	$P2_1/c$
a (Å)	27.393 Å	13.199 Å	16.892 Å
b (Å)	16.354 Å	16.781 Å	17.776 Å
c (Å)	27.863 Å	13.668 Å	30.976 Å
α (°)	90.00°	90.00°	90.00°
β (°)	115.153°	95.03°	98.88°
γ (°)	90.00°	90.00°	90.00°
Z	4	4	4
V (Å^3)	11263.44 Å^3	3015.70 Å^3	9189.75 Å^3
Density (g/cm^3)	1.890 g/cm^3	1.946 g/cm^3	1.429 g/cm^3
R(F)	0.02	0.02	0.08

VI. References

1. Yaghi, O. Reticular Chemistry—Construction, Properties, and Precision Reactions of Frameworks. *J. Am. Chem. Soc.* **138**, 15507–15509 (2016).

2. Jiang, H., Alezi, D. & Eddaoudi, M. A reticular chemistry guide for the design of periodic solids. *Nat. Rev. Mater.* **6**, 466–487 (2021).

3. Stock, N. & Biswas, S. Synthesis of Metal-Organic Frameworks (MOFs): Routes to Various MOF Topologies, Morphologies, and Composites. *Chem. Rev.* **112**, 933–969 (2012).

4. Geng, K. *et al.* Covalent Organic Frameworks: Design, Synthesis, and Functions. *Chem. Rev.* **120**, 8814–8933 (2020).

5. Zhou, H.-C., Long, J. R. & Yaghi, O. Introduction to Metal–Organic Frameworks. *Chem. Rev.* **112**, 673–674 (2012).

6. Yang, D. & Gates, B. C. Catalysis by Metal Organic Frameworks: Perspective and Suggestions for Future Research. *ACS Catal.* **9**, 1779–1798 (2019).

7. Bavykina, A. *et al.* Metal–Organic Frameworks in Heterogeneous Catalysis: Recent Progress, New Trends, and Future Perspectives. *Chem. Rev.* **120**, 8468–8535 (2020).

8. Qazvini, O. T., Babarao, R. & Telfer, S. G. Selective capture of carbon dioxide from hydrocarbons using a metal-organic framework. *Nat. Commun.* **12**, 197 (2021).

9. Kim, H. R. *et al.* Beyond pristine MOFs: carbon dioxide capture by metal–organic frameworks (MOFs)-derived porous carbon materials. *RSC Adv.* **7**, 1266–1270 (2017).

10. Xu, W. & Yaghi, O. M. Metal–Organic Frameworks for Water Harvesting from Air, Anywhere, Anytime. *ACS Cent. Sci.* **6**, 1348–1354 (2020).

11. Logan, M. W., Langevin, S. & Xia, Z. Reversible Atmospheric Water Harvesting Using Metal-Organic Frameworks. *Sci. Rep.* **10**, 1492 (2020).

12. Chidambaram, A. & Stylianou, K. C. Electronic metal–organic framework sensors. *Inorg. Chem. Front.* **5**, 979–998 (2018).

13. Zhang, L.-T., Zhou, Y. & Han, S.-T. The Role of Metal–Organic Frameworks in Electronic Sensors. *Angew. Chemie Int. Ed.* **60**, 15192–15212 (2021).

14. Wu, Z., Xie, J., Xu, Z. J., Zhang, S. & Zhang, Q. Recent progress in metal–organic polymers as promising electrodes for lithium/sodium rechargeable batteries. *J. Mater. Chem. A* **7**, 4259–4290 (2019).

15. Lv, Q. *et al.* Semiconducting Metal–Organic Polymer Nanosheets for a Photoinvolved Li–O2 Battery under Visible Light. *J. Am. Chem. Soc.* **143**, 1941–1947 (2021).

16. Abuzeid, H. R., EL-Mahdy, A. F. M. & Kuo, S.-W. Covalent organic frameworks: Design principles, synthetic strategies, and diverse applications. *Giant* **6**, 100054 (2021).

17. Wang, S. *et al.* Colloidal crystal engineering with metal–organic framework nanoparticles and DNA. *Nat. Commun.* **11**, 2495 (2020).

18. Babu, D. J., He, G., Villalobos, L. F. & Agrawal, K. V. Crystal Engineering of Metal–Organic Framework Thin Films for Gas Separations. *ACS Sustain. Chem. Eng.* **7**, 49–69 (2019).

19. Kim, D., Liu, X. & Lah, M. S. Topology analysis of metal–organic frameworks based on metal–organic polyhedra as secondary or tertiary building units. *Inorg. Chem. Front.* **2**, 336–360 (2015).

20. Li, M., Li, D., O'Keeffe, M. & Yaghi, O. M. Topological Analysis of Metal–Organic Frameworks with Polytopic Linkers and/or Multiple Building Units and the Minimal Transitivity Principle. *Chem. Rev.* **114**, 1343–1370 (2014).

21. Farha, O. K. *et al.* Metal–Organic Framework Materials with Ultrahigh Surface Areas: Is the Sky the Limit? *J. Am. Chem. Soc.* **134**, 15016–15021 (2012).

22. Al-Jadir, T. M. & Siperstein, F. R. The influence of the pore size in Metal−Organic Frameworks in adsorption and separation of hydrogen sulphide: A molecular simulation study. *Microporous Mesoporous Mater.* **271**, 160–168 (2018).

23. Winarta, J. *et al.* A Decade of UiO-66 Research: A Historic Review of Dynamic Structure, Synthesis Mechanisms, and Characterization Techniques of an Archetypal Metal–Organic Framework. *Cryst. Growth Des.* **20**, 1347–1362 (2020).

24. Kaur, G. *et al.* Controlling the Synthesis of Metal–Organic Framework UiO-67 by Tuning Its Kinetic Driving Force. *Cryst. Growth Des.* **19**, 4246–4251 (2019).

25. Zhao, D., Timmons, D. J., Yuan, D. & Zhou, H.-C. Tuning the Topology and Functionality of Metal−Organic Frameworks by Ligand Design. *Acc. Chem. Res.* **44**, 123–133 (2011).

26. Feng, L., Wang, K.-Y., Powell, J. & Zhou, H.-C. Controllable Synthesis of Metal-Organic Frameworks and Their Hierarchical Assemblies. *Matter* **1**, 801–824 (2019).

27. Li, J., Cheng, S., Zhao, Q., Long, P. & Dong, J. Synthesis and hydrogen-storage behavior of metal–organic framework MOF-5. *Int. J. Hydrogen Energy* **34**, 1377–1382 (2009).

28. Lin, K.-S., Adhikari, A. K., Ku, C.-N., Chiang, C.-L. & Kuo, H. Synthesis and

characterization of porous HKUST-1 metal organic frameworks for hydrogen storage. *Int. J. Hydrogen Energy* **37**, 13865–13871 (2012).

29. Calleja, G. *et al.* Copper-based MOF-74 material as effective acid catalyst in Friedel–Crafts acylation of anisole. *Catal. Today* **227**, 130–137 (2014).

30. Britt, D., Furukawa, H., Wang, B., Glover, T. G. & Yaghi, O. M. Highly efficient separation of carbon dioxide by a metal-organic framework replete with open metal sites. *Proc. Natl. Acad. Sci.* **106**, 20637 LP – 20640 (2009).

31. Lawson, H. D., Walton, S. P. & Chan, C. Metal–Organic Frameworks for Drug Delivery: A Design Perspective. *ACS Appl. Mater. Interfaces* **13**, 7004–7020 (2021).

32. Li, D., Xu, H.-Q., Jiao, L. & Jiang, H.-L. Metal-organic frameworks for catalysis: State of the art, challenges, and opportunities. *EnergyChem* **1**, 100005 (2019).

33. Marshall, C. R., Staudhammer, S. A. & Brozek, C. K. Size control over metal–organic framework porous nanocrystals. *Chem. Sci.* **10**, 9396–9408 (2019).

34. Bétard, A. & Fischer, R. A. Metal–Organic Framework Thin Films: From Fundamentals to Applications. *Chem. Rev.* **112**, 1055–1083 (2012).

35. Shekhah, O., Liu, J., Fischer, R. A. & Wöll, C. MOF thin films: existing and future applications. *Chem. Soc. Rev.* **40**, 1081–1106 (2011).

36. Lu, P. *et al.* What can pKa and NBO charges of the ligands tell us about the water and thermal stability of metal organic frameworks? *J. Mater. Chem. A* **2**, 16250–16267 (2014).

37. Yuan, S., Qin, J.-S., Lollar, C. T. & Zhou, H.-C. Stable Metal–Organic Frameworks with Group 4 Metals: Current Status and Trends. *ACS Cent. Sci.* **4**, 440–450 (2018).

38. Moosavi, S. M. *et al.* Understanding the diversity of the metal-organic framework ecosystem. *Nat. Commun.* **11**, 4068 (2020).

39. Wang, C., Liu, X., Keser Demir, N., Chen, J. P. & Li, K. Applications of water stable metal–organic frameworks. *Chem. Soc. Rev.* **45**, 5107–5134 (2016).

40. He, T., Kong, X.-J. & Li, J.-R. Chemically Stable Metal–Organic Frameworks: Rational Construction and Application Expansion. *Acc. Chem. Res.* **54**, 3083–3094 (2021).

41. Cavka, J. H. *et al.* A New Zirconium Inorganic Building Brick Forming Metal Organic Frameworks with Exceptional Stability. *J. Am. Chem. Soc.* **130**, 13850–13851 (2008).

42. Bůžek, D., Adamec, S., Lang, K. & Demel, J. Metal–organic frameworks vs. buffers: case study of UiO-66 stability. *Inorg. Chem. Front.* **8**, 720–734 (2021).

43. Kickelbick, G. & Schubert, U. Oxozirconium Methacrylate Clusters:

Zr6(OH)4O4(OMc)12 and Zr4O2(OMc)12 (OMc = Methacrylate). *Chem. Ber.* **130**, 473–478 (1997).

44. Rimoldi, M. *et al.* Catalytic Zirconium/Hafnium-Based Metal–Organic Frameworks. *ACS Catal.* **7**, 997–1014 (2017).

45. Yang, Q. *et al.* CH4 storage and CO2 capture in highly porous zirconium oxide based metal–organic frameworks. *Chem. Commun.* **48**, 9831–9833 (2012).

46. Zhang, H., Xiong, P., Li, G., Liao, C. & Jiang, G. Applications of multifunctional zirconium-based metal-organic frameworks in analytical chemistry: Overview and perspectives. *TrAC Trends Anal. Chem.* **131**, 116015 (2020).

47. DMello, M. E., Sundaram, N. G., Singh, A., Singh, A. K. & Kalidindi, S. B. An amine functionalized zirconium metal–organic framework as an effective chemiresistive sensor for acidic gases. *Chem. Commun.* **55**, 349–352 (2019).

48. Hu, Z., Wang, Y. & Zhao, D. The chemistry and applications of hafnium and cerium(iv) metal–organic frameworks. *Chem. Soc. Rev.* **50**, 4629–4683 (2021).

49. Kerr, J. A. *Handbook of Chemistry and Physics*. (CRC Press, 2000).

50. Beyzavi, M. H. *et al.* A Hafnium-Based Metal–Organic Framework as an Efficient and Multifunctional Catalyst for Facile CO2 Fixation and Regioselective and Enantioretentive Epoxide Activation. *J. Am. Chem. Soc.* **136**, 15861–15864 (2014).

51. Bakuru, V. R., Churipard, S. R., Maradur, S. P. & Kalidindi, S. B. Exploring the Brønsted acidity of UiO-66 (Zr, Ce, Hf) metal–organic frameworks for efficient solketal synthesis from glycerol acetalization. *Dalt. Trans.* **48**, 843–847 (2019).

52. Bosch, M., Zhang, M. & Zhou, H.-C. Increasing the Stability of Metal-Organic Frameworks. *Adv. Chem.* **2014**, 182327 (2014).

53. Øien, S. *et al.* Detailed Structure Analysis of Atomic Positions and Defects in Zirconium Metal–Organic Frameworks. *Cryst. Growth Des.* **14**, 5370–5372 (2014).

54. Schaate, A. *et al.* Modulated Synthesis of Zr-Based Metal–Organic Frameworks: From Nano to Single Crystals. *Chem. – A Eur. J.* **17**, 6643–6651 (2011).

55. Wahiduzzaman, M., Wang, S., Sikora, B. J., Serre, C. & Maurin, G. Computational structure determination of novel metal–organic frameworks. *Chem. Commun.* **54**, 10812–10815 (2018).

56. Lu, K., He, C. & Lin, W. Nanoscale Metal–Organic Framework for Highly Effective Photodynamic Therapy of Resistant Head and Neck Cancer. *J. Am. Chem. Soc.* **136**, 16712–16715 (2014).

57. Gross, S., Kickelbick, G., Puchberger, M. & Schubert, U. Mono-, Di-, and Trimetallic Methacrylate-substituted Metal Oxide Clusters Derived from Hafnium Butoxide. *Monatshefte für Chemie / Chem. Mon.* **134**, 1053–1063 (2003).

58. Kickelbick, G., Wiede, P. & Schubert, U. Variations in capping the Zr6O4(OH)4 cluster core: X-ray structure analyses of [Zr6(OH)4O4(OOC–CH□CH2)10]2(μ-OOC–CH□CH2)4 and Zr6(OH)4O4(OOCR)12(PrOH) (R=Ph, CMe=CH2). *Inorganica Chim. Acta* **284**, 1–7 (1999).

59. Artner, C., Czakler, M. & Schubert, U. New zirconium and zirconium–titanium oxo cluster types by expansion or metal substitution of the octahedral Zr6O8 structural motif. *Inorganica Chim. Acta* **432**, 208–212 (2015).

60. Walther, P., Puchberger, M., Kogler, F. R., Schwarz, K. & Schubert, U. Ligand dynamics on the surface of zirconium oxo clusters. *Phys. Chem. Chem. Phys.* **11**, 3640–3647 (2009).

61. Semrau, A. L. *et al.* Highly Porous Nanocrystalline UiO-66 Thin Films via Coordination Modulation Controlled Step-by-Step Liquid-Phase Growth. *Cryst. Growth Des.* **19**, 1738–1747 (2019).

62. Semrau, A. L. & Fischer, R. A. High-Quality Thin Films of UiO-66-NH2 by Coordination Modulated Layer-by-Layer Liquid Phase Epitaxy. *Chem. – A Eur. J.* **27**, 8509–8516 (2021).

63. Lu, W. *et al.* Tuning the structure and function of metal–organic frameworks via linker design. *Chem. Soc. Rev.* **43**, 5561–5593 (2014).

64. Desai, A. V, Sharma, S., Let, S. & Ghosh, S. K. N-donor linker based metal-organic frameworks (MOFs): Advancement and prospects as functional materials. *Coord. Chem. Rev.* **395**, 146–192 (2019).

65. Yaghi, O. M., Kalmutzki, M. J. & Diercks, C. S. Building Units of MOFs. *Introduction to Reticular Chemistry* 57–81 (2019) doi:https://doi.org/10.1002/9783527821099.ch3.

66. Feng, D. *et al.* A Highly Stable Porphyrinic Zirconium Metal–Organic Framework with shp-a Topology. *J. Am. Chem. Soc.* **136**, 17714–17717 (2014).

67. Feng, D. *et al.* Construction of Ultrastable Porphyrin Zr Metal–Organic Frameworks through Linker Elimination. *J. Am. Chem. Soc.* **135**, 17105–17110 (2013).

68. Jiang, H.-L. *et al.* An Exceptionally Stable, Porphyrinic Zr Metal–Organic Framework Exhibiting pH-Dependent Fluorescence. *J. Am. Chem. Soc.* **135**, 13934–13938 (2013).

69. Cichocka, M. O. *et al.* A Porphyrinic Zirconium Metal–Organic Framework for Oxygen Reduction Reaction: Tailoring the Spacing between Active-Sites through Chain-Based

Inorganic Building Units. *J. Am. Chem. Soc.* **142**, 15386–15395 (2020).

70. Yuan, S. *et al.* Thermodynamically Guided Synthesis of Mixed-Linker Zr-MOFs with Enhanced Tunability. *J. Am. Chem. Soc.* **138**, 6636–6642 (2016).

71. DeStefano, M. R., Islamoglu, T., Garibay, S. J., Hupp, J. T. & Farha, O. K. Room-Temperature Synthesis of UiO-66 and Thermal Modulation of Densities of Defect Sites. *Chem. Mater.* **29**, 1357–1361 (2017).

72. Zhang, J.-L., Liu, Y.-L. & Che, C.-M. Chiral ruthenium porphyrin encapsulated in ordered mesoporous molecular sieves (MCM-41 and MCM-48) as catalysts for asymmetric alkene epoxidation and cyclopropanation. *Chem. Commun.* 2906–2907 (2002) doi:10.1039/B209276J.

73. Chen, L. *et al.* Carbene insertion into N–H bonds with size-selectivity induced by a microporous ruthenium–porphyrin metal–organic framework. *Dalt. Trans.* **47**, 3940–3946 (2018).

74. Jia, Y. *et al.* Improved Performance of Polysulfone Ultrafiltration Membrane Using TCPP by Post-Modification Method. *Membranes* vol. 10 (2020).

75. Roales, J. *et al.* Anchoring effect on (tetra)carboxyphenyl porphyrin/TiO2 composite films for VOC optical detection. *RSC Adv.* **4**, 1974–1981 (2014).

76. Hu, H. *et al.* Metal–organic frameworks embedded in a liposome facilitate overall photocatalytic water splitting. *Nat. Chem.* **13**, 358–366 (2021).

77. Farokhi, A. & Hosseini-Monfared, H. A recyclable Mn–porphyrin catalyst for enantioselective epoxidation of unfunctionalized olefins using molecular dioxygen. *New J. Chem.* **40**, 5032–5043 (2016).

C. Chapter 2: Development of Zirconium and Hafnium Based MOFs Through Layer-by-Layer Molecular Deposition

I. Introduction

The ability to perform tandem reactions through the cooperation of two catalysts in the same reactor would streamline chemistry by reducing the amount of reactors and workups needed to produce a desired product. The synergistic action of two catalysts can often be hindered by catalyst incompatibility. In natural systems such as enzymes, catalytic centers are isolated within a supramolecular assembly so as to enable cooperative action between two or more catalysts. Inspired by these natural phenomena, it was envisioned that molecular-layer deposition would allow for regulation of the position and distance between catalytically relevant porphyrin macrocycles within a MOF film to a degree that is not possible during solvothermal MOF synthesis. The main challenge in this procedure is ligand exchange between the methacrylate cappers of the metal-oxo cluster and the symmetric MOF linkers. Past work on Cu-based MOFs required only repeated exposure of SAM functionalized substrates to solution of copper salt and organic linker,[1,2] a strategy which cannot be applied to the group-IV metal MOFs as formation of the metal-oxo clusters are never afforded. Work on layer-by-layer (LbL) deposition of group-IV metal MOFs was first made successful by Fischer and coworkers with the successful deposition of UiO-66.[3] the LbL deposition of UiO-66 was made possible through the adaptation of two procedural features. Firstly, the discreet synthesis of the zirconium-oxo clusters to be used as a source for the deposition of the metal-oxo nodes, and secondly the use of methacrylic acid as a modulator to enable the exchange of methacrylate cappers with the terephthalate linkers. The use of an acidic modulator for the LbL deposition of MOF thin films was first described by Wannapaiboon et al in 2017,[4] wherein acetic acid was used as a modulator

to produce MOF based films of structure $Zn_4O(L)_3$) (L = 3,5-dialkyl-4-carboxypyrazolate). While this example was the first to use an acidic modulator in thin film synthesis, acidic modulators were previously reported in bulk MOF synthesis.[5] Modulators in MOF synthesis consist of monotopic carboxylate ligands which emulate the coordination of the symmetric organic linkers and serve to compete with desired organic linkers during synthesis.[6] Utilizing modulators during MOF synthesis enables variation and control of MOF crystal shape, allowing for the synthesis of free-standing MOF nanosheets, nanorods, and nanocubes.[7]

Another strategy for the LbL synthesis of MOF films was described by Hinman et al in 2013[8]: in this route; rather than utilize a modulator, tetramethylammonium salts of the symmetric carboxylate linker were used as the organic linker source during MOF growth. Hinman et al were able to perform the LbL deposition of copper-based HKUST-1 on substrates of Au nanorods and attribute the success to the overall negative surface charge of the gold nanorods as brought about by the use of the tetramethylammonium benzoate salt. Inspired by this work, I initiated studies into the use of tetramethylammonium terephthalate as a potential organic linker source to be used in conjunction with $Zr_4(OH)_4O_4(OMc)_{12}$ to deposit thin films on the surface of Au-coated wafers.

To expand the scope of group-IV MOF thin films, it was decided to initiate studies on the LbL deposition of Hf-based MOF films utilizing the aforementioned $Hf_6(OH)_4O_4(OMc)_{12}$ as the metal source for film deposition. Initial studies to develop a reliable protocol for MOF growth focused on the preparation of Hf-UiO-66 thin films; studies were also carried out to determine the effect of substrate chemistry on the structure of Hf-UiO-66 films, with comparisons taking place through x-ray diffraction. After a successful protocol for Hf-UiO-66 was developed efforts then shifted to fabrication of porphyrinic MOF thin films for catalytic applications. Films were characterized with x-ray diffraction, XPS, EDX and scanning electron microscopy.

II. LbL Molecular Deposition of UiO-66 and UiO-66 (Hf)

The UiO-66 topology is one of the most well studied MOF architectures, moreover while at the time of writing methods to grow UiO-66 thin films have been developed by Fischer and co-workers[3,9,10], at the start of these investigations such methods had not been developed. The production of highly crystallin films of UiO-66 through LbL molecular deposition with surface uniformity still remains challenging. Prior to these investigations, work on the LbL molecular deposition of Hf-UiO-66 was non-existent.

1. Preparation of Carboxylate-Functionalized Self-Assembled Monolayers

MOF thin-film deposition most often takes place using Si wafers as a substrate for growth as Si wafers are a widely available, flat substrates: the surface of which can be easily studied. Since the organic linkers of MOFs coordinate to metal nodes via the carboxylate functional group, it was decided to design a carboxylate functionalized surface. To devise this kind of surface it was the known phenomena of self-assembled monolayers (SAMs) was utilized.[11] To enable the use of SAMs the Si wafers were coated with 50 nm layers of gold with a 5 nm adhesion layer of Ti via evaporative deposition. After coating with Au, the substrates were exposed to solutions of 16-mercaptohexadecanoic acid (MHDA), to provide the surface of the wafers with carboxylate functionalization. MHDA is known to adhere to gold via the hard-soft acid/base interaction of the gold surface with the thiol group of MHDA[12], leaving the carboxylic acid group on the other end of the molecule exposed for coordination to the initial layer of metal-oxo clusters (Scheme 2.1). Coating was done by immersing 1 cm x 2 cm Au-coated wafers into 10 mL of 1.0 mM MHDA solutions for 48 hours. Before use in molecular LbL wafers were rinsed with 1.0 mM triethylamine solution then rinsed with ethanol and dried under a gentle stream of N_2 before use.

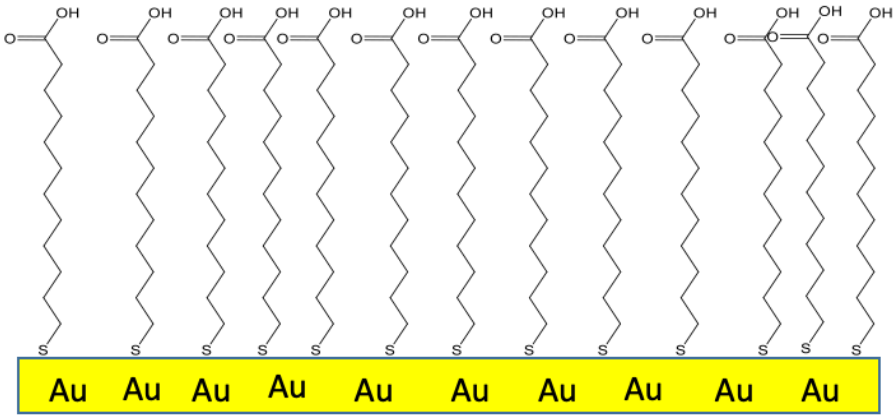

Scheme 2.1: Self-assembled monolayer of MHDA on a gold surface.

2. LbL Deposition of ZrMOF Film-10

Efforts to enact the LbL deposition of a UiO-66 thin film through the use of the $Zr_6O_4(OH)_4(OMc)_{12}$ in conjunction with the tetramethylammonium terephthalate salt began by simple affixing MHDA-functionalized Au covered Si wafers onto a pair of reverse grip tweezers and punctured through a septum which was fitted to the top of multiple 20 mL vials, which were filled with the mother solutions of the film synthesis as well as rinsing solutions. The wafer was moved between the vials while attached to the septum and the vials sealed while the wafer was not immersed. To mitigate the effect any potential degradation of the $Zr_6O_4(OH)_4(OMc)_{12}$ cluster would have on the fabrication, fresh $Zr_6O_4(OH)_4(OMc)_{12}$ solution was placed in the vial after every 10 cycles. A depiction of the vial setup is depicted in Scheme 2.2. Tetramethylammonium terephthalate was prepared by mixing tetramethylammonium hydroxide and terephthalic acid in water at a 2:1 molar ratio followed by removal of water by lyophilizer. $Zr_6O_4(OH)_4(OMc)_{12}$ (**1.4**) was prepared as described in Chapter 1.

Initial studies required several optimizations in regards to solution temperatures and amount and species of acid modulator. Conditions were tested by exposing MHDA-functionalized wafers to 30 cycles of metal-rinsing-linker-rinsing steps. After every 10 cycles the wafers would by analyzed with X-ray diffraction, to determine if diffraction peaks correlating the UiO-66 structure could be determine as well as scanning electron microscopy to determine if any film deposition could be observed at all.

Depiction of the LbL Molecular Deposition by Hand using Tetramethylammonium Terephthalate and the $Zr_6O_4(OH)_4(OMc)_{12}$ Cluster

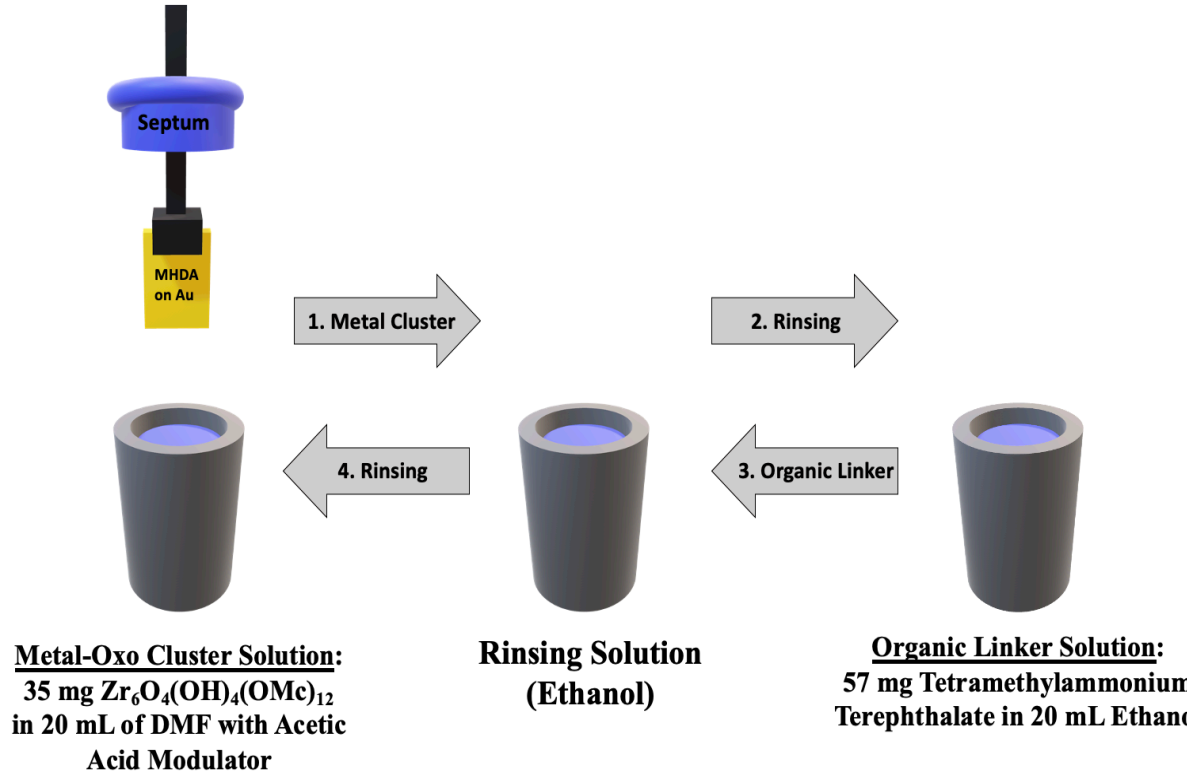

Scheme 2.2: Schematic depicting the procedure for the LbL deposition of UiO-66 onto MHDA-functionalized Au-coated wafers. Wafer attached to the reverse grip tweezers and affixed to a septum allowing for the wafer to be suspended into each solution for the desired dipping time. Arrows numbered from 1-4 denote one full metal-rinsing-linker-rinsing cycle. All solutions were stirred with magnetic stirring.

The acidic modulator selected for testing was acetic acid as it has been shown that for UiO-66 modulation of crystallization process produces the highest level of crystallinity.[13] Ethanol was chosen as the solvent of choice for the tetramethylammonium terephthalate linker solutions and DMF was selected for the metal-oxo cluster solutions. Initial experiments consisted of testing rations of acetic acid to metal-oxo cluster ranging from 0-50 in increments of ten to determine which amount led to reliable deposition, temperatures were varied between room temperature and 60 C for the metal-oxo and tetramethylammonium terephthalate. Tested conditions for the modulator quantity and temperature for the $Zr_6O_4(OH)_4(OMc)_{12}$ solutions are listed in Table 2.1, the complete condition which resulted in successful deposition of films which diffracted (condition 10) is listed in Table 2.2. Equivalent conditions were tested for the $Zr_6O_4(OH)_4(OBA)_{12}$ but did not yield films which diffracted.

Variations in the Modulator Quantity and Temperature for the $Zr_6O_4(OH)_4(OMc)_{12}$ Solutions During UiO-66 LbL Deposition Optimization

Condition No.	µL AcOH	Molar ratio (AcOH/ Zr-oxo cluster)	Temp (C)	Film Diffraction
1	0	0	r.t	No
2	0	0	60	No
3	20	10	r.t.	No
4	20	10	60	No
5	40	20	r.t	No
6	40	20	60	No
7	60	30	r.t.	No
8	60	30	60	No
9	80	50	r.t.	No
10	80	50	60	Yes

Table 2.1: All solutions were 20 mL in volume. Film diffraction was tested every 10 cycles and all conditions were tested up to 100 cycles. All conditions used 35 mg of the $Zr_6O_4(OH)_4(OMc)_{12}$ cluster and the substrate was placed into the solutions 5 min per cycle.

Condition for The LbL Molecular Deposition of ZrMOF Film-10

Cluster amount*	Cluster Solution Solvent (mL/Solvent)	Acetic Acid Amount	Dipping Time for Cluster Solution	Temperature of Cluster Solution	Rinsing solvent**	Linker amount***	Linker Solution Solvent (solvent/ml)	Dipping Time for Linker Solution	Temperature of Linker Solution
35 mg	20 mL DMF	80 uL	5 mins	60 C	20 mL ethanol	57 mg	20 mL Ethanol	5 mins	60 C

Table 2.2: Conditions leading to films which gave diffraction patters with peaks correlating to the diffraction pattern of UiO-66. * Cluster used was $Zr_6O_4(OH)_4(OMc)_{12}$ and solutions were replenished with fresh solution every 10 cycles. ** Rinsing solvent was kept at room temperature ***Linker refers to tetramethylammonium terephthalate.

Films acquired from the use of 80 uL of acetic acid modulator (50:1 molar excess over the cluster) gave diffraction peaks matching the expected (111) peak from UiO-66. Films synthesized via this setup (condition 10) were analyzed with XRD, SEM and XPS (Figure 2.1). The films showed a diffraction peak 7.2° 2Θ which correlates to the most intense peak of UiO-66 arising from the diffraction of the (111) index. Attempts to match the entire diffraction pattern of UiO-66 were not successful but as evidenced by diffraction patterns of the films from condition 10 between 70-100 cycles of deposition it is clear that structural similarity exists between an idealized UiO-66 film and the observed films. Analyzing such films by X-ray diffraction is the difficult as thin films may show broadened diffraction peaks,[14] later efforts at thin film characterization will attempt to overcome this obstacle with diffraction techniques specialized for thin films. The crystalline film was so name ZrMOF Film-10.

Cross-sectional EDX analysis confirms the presence of Zr and C isolated to the surface of the wafer. The appearance of only the (111) peak of UiO-66 can be the result of either oriented growth, or a large number of defects. While a total match to the UiO-66 calculated diffraction pattern is not made, there is clear evidence for a deposition of a crystallin Zr based film with structural similarities to UiO-66. The growth of ZrMOF Film-10 was monitored by X-ray diffraction from start of deposition to 100 cycles with a diffraction pattern being taken every 10

cycles. A 2Θ peak at 7.2° is detectable after only 10 cycles (Figure 2.2) and at this time other peaks correlating to the diffraction pattern of UiO-66 can also be noted. After 20 cycles evidence of a film becomes apparent by SEM, and after 30 cycles even an optical microscope can detect the presence of a clear white film.

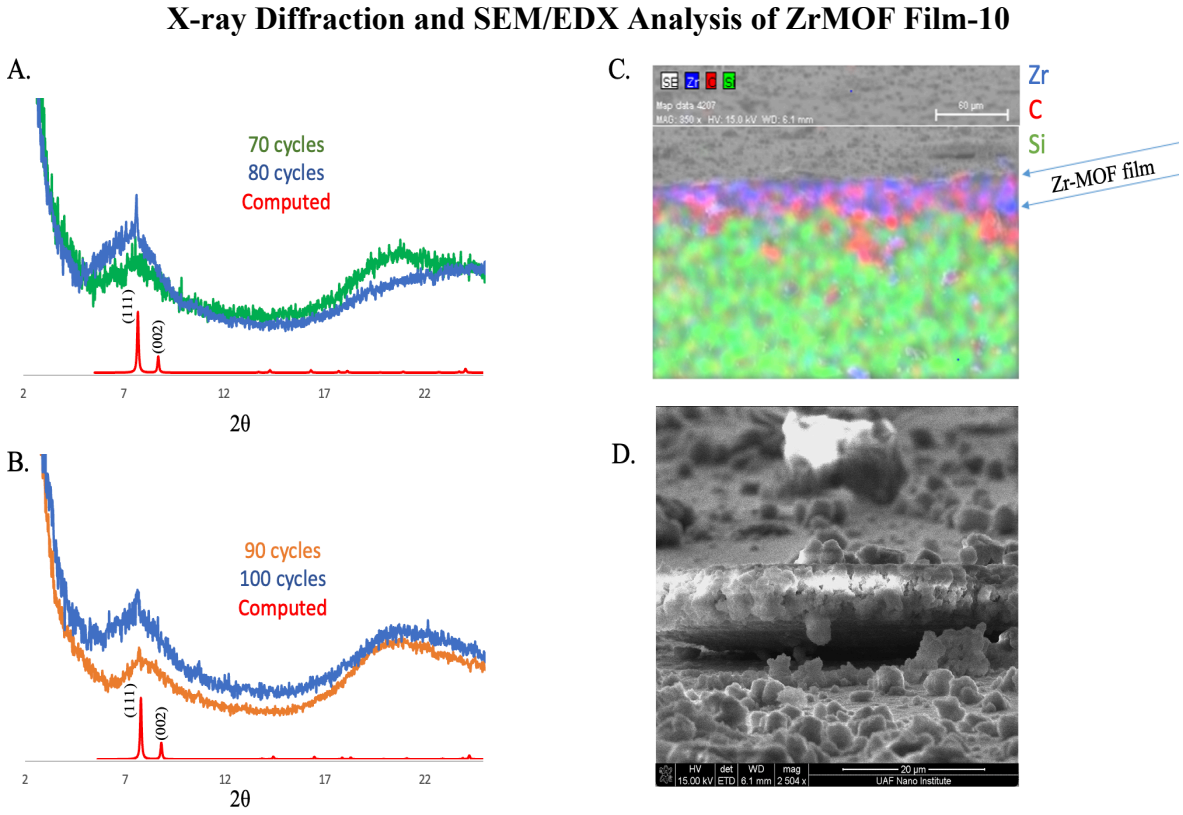

Figure 2.1: Characterization of the ZrMOF Film-10 by X-ray diffraction and SEM/EDX. **A**: X-ray diffraction pattern of Zr-MOF Film-10 after 70 cycles (green) and 80 cycles (blue). **B**: X-ray diffraction pattern of ZrMOF Film-10 after 90 cycles (orange). In both A and B the computed diffraction pattern of UiO-66 is shown in red for comparison. Strong correlation exists between the first peak of UiO-66 (arising from the (1,1,1) Miller index) and the diffraction peak of ZrMOF Film-10. **C**: Cross-sectional scanning-EDX analysis of ZrMOF Film-10 after 100 cycles of deposition. ZrMOF Film-10 composition is evident by the presence of Zr and C isolated to the surface of the Si wafer. **D**: A SEM cross-sectional analysis of the ZrMOF Film-10 after 100 cycles of deposition.

X-ray Diffraction and Microscopy Data of Wafers Subjected to Condition 10

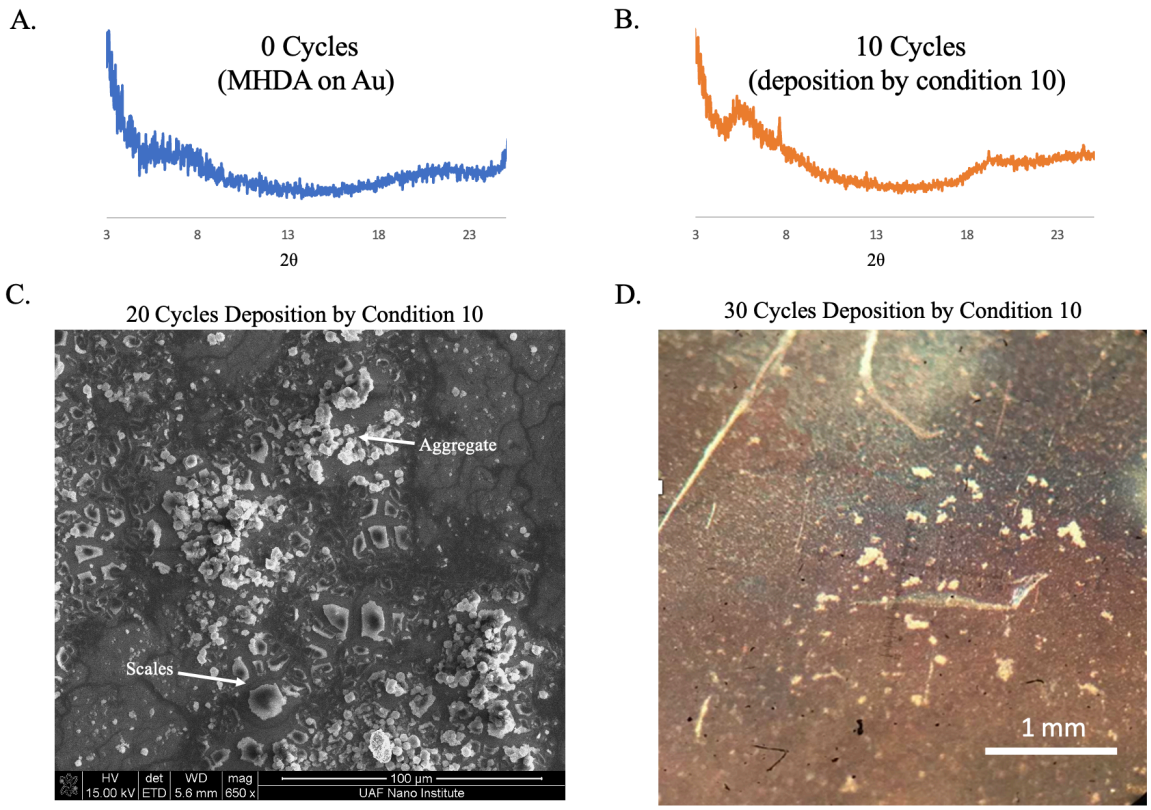

Figure 2.2: Characterization of early stages of ZrMOF-Film 10 deposition. **A**: X-ray diffraction of a blank substrate, consisting of just a gold-coated Si wafer which has been functionalized with a monolayer of 16-MHDA and **B**: X-ray diffraction pattern of the substrate after 10 cycles of deposition by condition 10, a peak between 7-8° 2Θ is present indicating detectable growth of the ZrMOF-Film 10 material. **C**: SEM images of ZrMOF-Film 10 after 20 cycles of deposition, at this point the film is visible and two morphologies, scales and aggregated particles are visible. **D**: Optical microscope images ZrMOF-Film after 30 cycles of deposition by condition 10, a film on the gold surface is present.

Cross-sectional SEM analysis of the ZrMOF-Film 10 wafers after 100 cycles of deposition do reveal uniform coverage of the wafer surface however structural uniformity is lacking. Microscopic images at 100 cycles also reveals the existence of two morphologies for the film, flat scales which grow in plane to the surface and as well as some round particles growing outwards from the plane of the substrate the which seem to aggregate (Figure 2.3**)**. One factor which limited investigations regarding new techniques for the molecular LbL deposition of UiO-

66 was the need to perform deposition by hand, making it difficult to test a wide range of conditions. However, it is clear that the utilization of tetramethylammonium salts present a promising alternative to the traditional carboxylic acids as precursors for MOF synthesis, especially for molecular LbL deposition. It should be noted that control experiments which matched exactly condition 10 but replaced the tetramethylammonium terephthalate with terephthalic acid did not display any diffraction.

SEM Analysis of ZrMOF-Film 10 After 100 Deposition Cycles

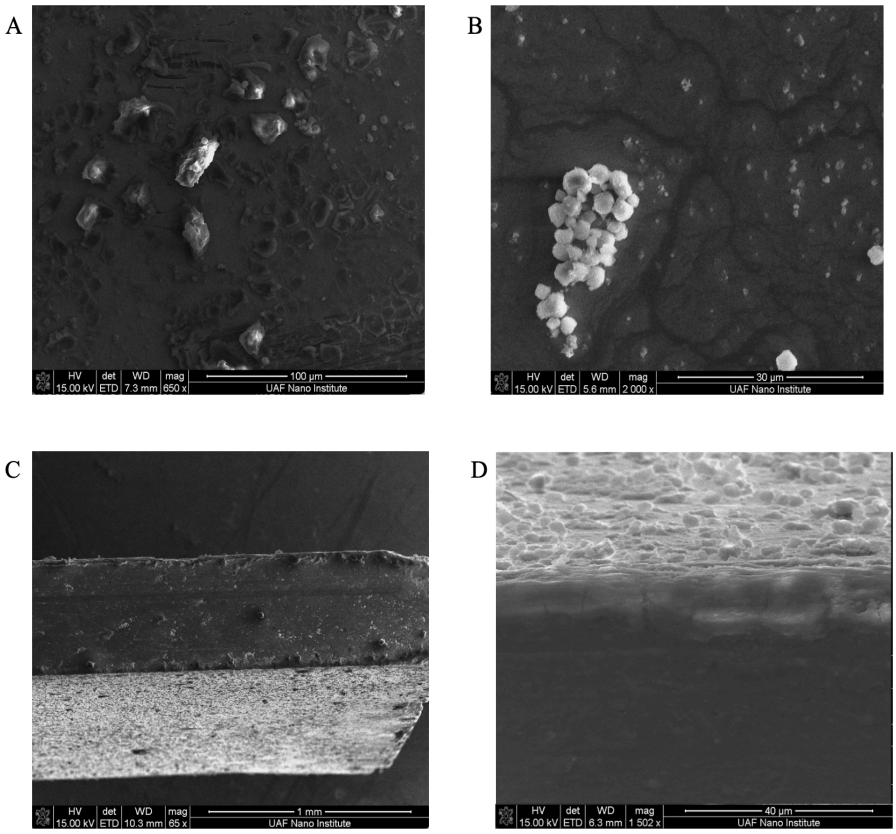

Figure 2.3: SEM images of ZrMOF-Film 10 which showing two distinct morphologies of the film and the overall coverage of the gold surface. All images are of the ZrMOF-Film 10 after 100 cycles of deposition. **A**: Image taken by SEM showing scales-like structure of ZrMOF-Film 10. **B**: SEM image showing the circular particles, another distinct morphology. **C**: An SEM cross section image showing the uniform coverage of ZrMOF-Film 10 on the surface of the Au covered wafer. **D:** SEM cross-section at a higher magnification showing the distinct morphologies on the same surface.

3. LbL Molecular Deposition of UiO-66 (Hf)

After work on the molecular LbL deposition of ZrMOF-Film 10 using the tetramethyl ammonium salt had been initiated, recent communications in the literature had been made regarding the molecular LbL deposition of UiO-66 by Semrau et al.[3] To initiate a novel study onto the LbL deposition of group-IV metal base MOFs and with a synthetic route to the $Hf_6O_4(OH)_4(OMc)_{12}$ cluster in hand, it was decided to initiate studies onto molecular LbL deposition of the isostructural UiO-66(Hf) MOF. The Hf analogs of UiO-66 are especially important in the field of gas capture, particularly of interest for showing higher adsorption of CO_2 when compared to the Zr analogs.[15] In order to overcome the procedural challenges faced during the molecular LbL deposition of ZrMOF-Film 10, a robot for the automated movement of substrates between reaction vessels was designed and manufactured (Scheme 2.3).

A.

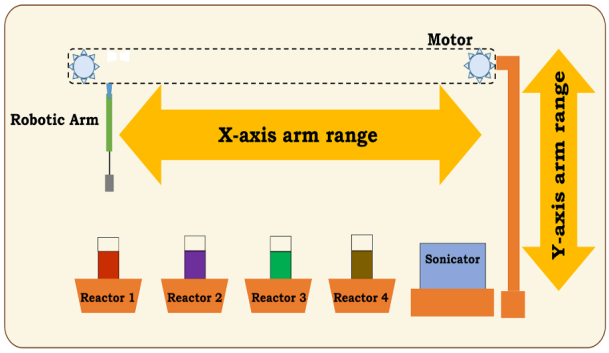

B.

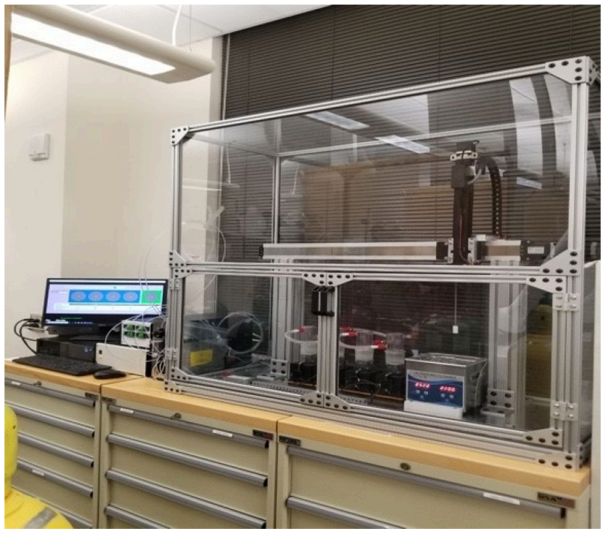

Scheme 2.3: Automated molecular LbL workstation featuring a robotic arm capable of moving substrates to any position in a (X, Y) plane, including 4 built in reactor stations and a sonicator rinsing station. **A**) Cartoon schematic showing a summary of the automated workstation and **B**) Photograph of the completed automated workstation including the plexiglass showed allowing for ventilation and the computer controller. All reactors are connected to a solvent pumping unit and heating elements. Rather than magnetic stirring the robotic arm itself can rotate the substrate. The robot was assembled by JKEM scientific in St. Louis, MO and is a custom robot designed specifically for the molecular LbL deposition of reticular materials.

Semrau and coworkers discovered that the addition of methacrylic acid can work in conjunction with water to enable the molecular LbL of UiO-66 on films of SiO_2.[3] This same methodology was found to be appliable to the LbL deposition of UiO-66 (Hf) on the surface of MHDA functionalized gold. LbL deposition of the UiO-66 (Hf) produced films which matched the calculated diffraction patterns of UiO-66 (Hf) only when the correct ratios of water and methacrylic acid were used and when dipping times per solution were held to 5 minutes using the epitaxial workstation, rotation speed of the wafers was held at 100 rpm. Reflux was available for the reactors in the epitaxial workstation and temperatures of the ethanol solutions could be held at 70 C during the dipping procedure without loss of solvent to evaporation. A full list of the conditions which yielded crystallin films of UiO-66 (Hf) can be found in Table 2.3 and Scheme 2.4.

Schematic for the Molecular LbL Deposition of UiO-66 (Hf) Using the Automated Epitaxial Work Station

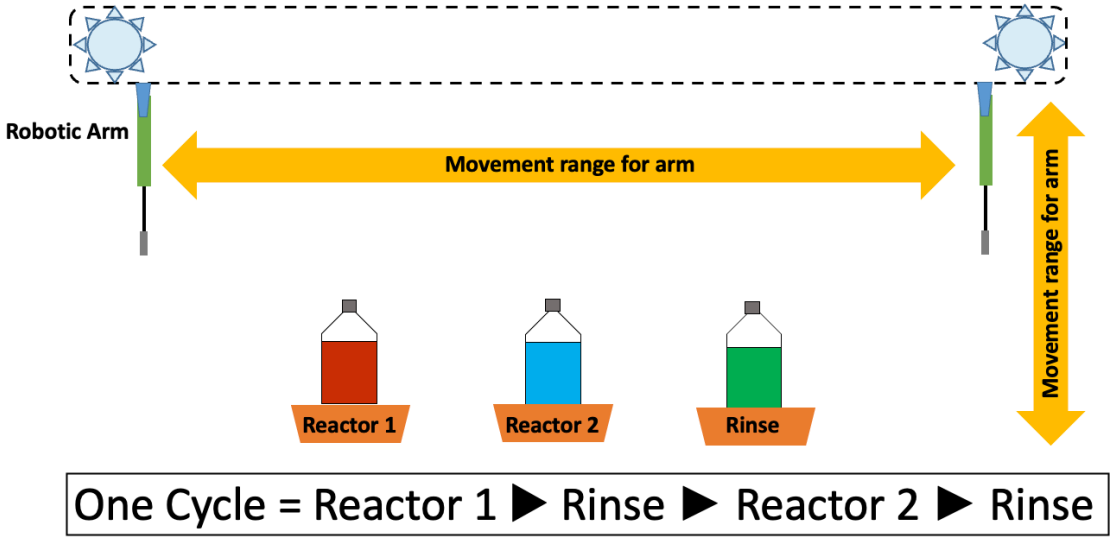

Scheme 2.4: The substrate was attached to the robotic arm via a Teflon screw then robotically moved between reactors, being rotated at 100 rpm while submersed in the solution of each reactor. For the molecular LbL molecular deposition of each UiO-66 (Hf) 3 distinct reactors were used and each reactor solution was replaced after 10 cycles via an automated pump connected to fresh solutions and waste containers.

	Reactor 1	Reactor 2	Rinse
Reactants	38.5 mg $Hf_6O_4(OH)_4(OMc)_{12}$ (0.5 mM)	17.44 mg Terephthalic Acid (3.0 mM)	N/A
Modulators	0.903 g Methacrylic acid	0.903 g methacrylic acid 1.26 g H_2O	N/A
Solvents	35 mL Ethanol	35 mL Ethanol	70 mL Ethanol
Temp/Time	70 C / 5 min	70 C / 5 min	70 C / 5 min

Table 2.3: Contents of the Reactors for the Molecular LbL Deposition of UiO-66 (Hf)

UiO-66 (Hf) films fabricated through the automated LbL molecular deposition were monitored with X-ray diffraction every 10 cycles. Growth of UiO-66 (Hf) was monitored on both MHDA-functionalized Au as well as bare Au. All substrates were Au deposited on Si wafers and diced to 2cm x 1cm rectangles. The surface chemistry of the substrates did affect the overall structure of the UiO-66 (Hf) film as the MHDA functionalized substrates gave films with diffraction peaks associated with both the (111) and the (002) Miller indices of UiO-66 (Hf) however the films grown on bare Au only showed a diffraction peak associated with the (111) Miller index. This surprising result is promising in that control over the orientation of growth can be a useful option during MOF film synthesis, as preferred orientations can have effects on gas separation applications.[16] The substrate-dependent orientation was evidenced by a difference in diffraction patterns (Figure 2.4); UiO-66 (Hf) films grown on bare Au gave only a diffraction peak at 7.2° while the films grown on MHDA functionalized wafers gave two diffraction peaks (7.2° and 9.2°). For both UiO-66 (Hf) films, the differences in diffraction patterns were noted after 120 layers of automated growth. One notable observation in the films grown on the MHDA functionalized wafers was that the peak which most closely correlated to the (002) Miller index has shifted 0.6° higher (to 9.2° as opposed to the calculated 8.6°). This shift in diffraction peak to a higher 2Θ angle is caused by compression of the unit cell. Reasons for this strain in the unit cell likely have to do with the substitution of the Zr atom with Hf in the MOF formula. It should

be mentioned that the calculated diffraction patterns used for comparison are calculated using Zr-containing UiO-66; which is standard practice as the diffraction patterns for UiO-66 and UiO-66 (Hf) are known to the same for the (111) and (002) Miller index as was exhaustively proven by Jakobsen et al.[17]

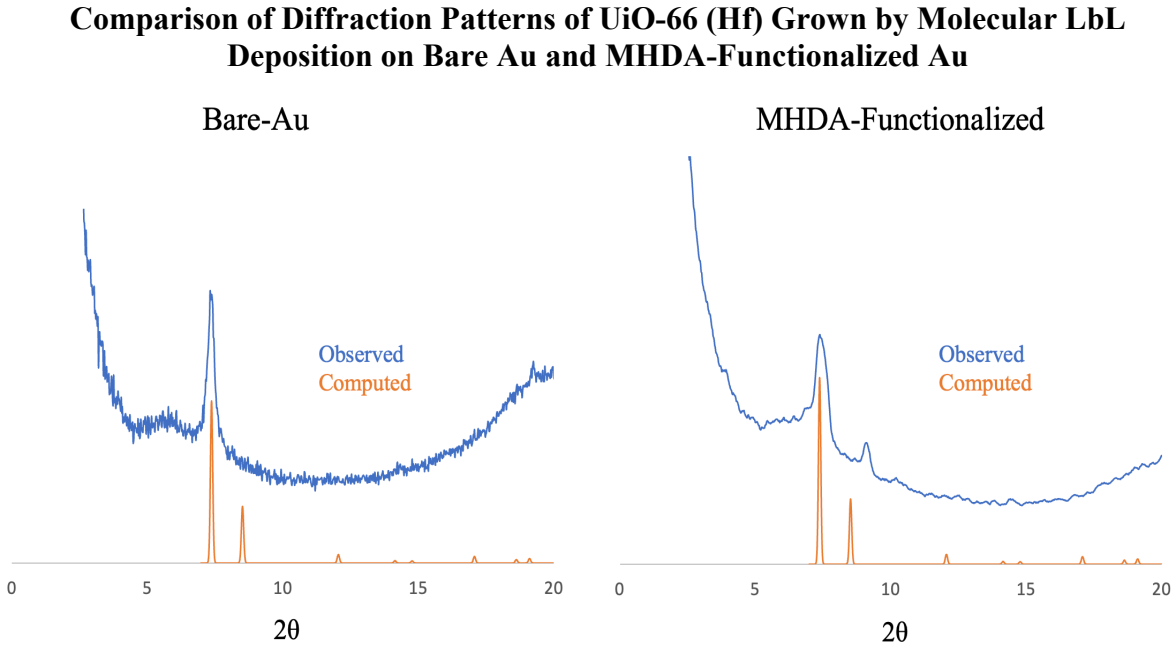

Figure 2.4: Diffraction patters of UiO-66 (Hf) films after 120 cycles of deposition. On the left is the diffraction pattern of UiO-66 (Hf) grown on bare Au and on the right is the diffraction pattern of the UiO-66 (Hf) grown on MHDA-functionalized Au. The diffraction pattern of the samples grown on bare Au shows only a peak for the (111) Miller index while the MHDA-functionalized substrate also shows a peak for the (002) Miller index.

To further explore the degree to which orientation and structure of the of the substrate can be altered by substrate selection SAMs consisting of 3-mercaptopropionic acid (MPA) were also prepared according to the literature method[18] and tested as substrates for the molecular LbL deposition of UiO-66 (Hf). After 120 cycles of deposition films grown on MPA functionalized-Au also showed a preferred orientation for growth along the (111) Miller index however when this was increased to 180 cycles evidence for growth along the (002) index was present in the form of a broad shoulder centered around 8.5° 2Θ (Figure 2.5). This result further enhances the

potential for structural control over the UiO-66 (Hf) films which and shows that selection of the substrate can be used to exert structural control over MOF films.

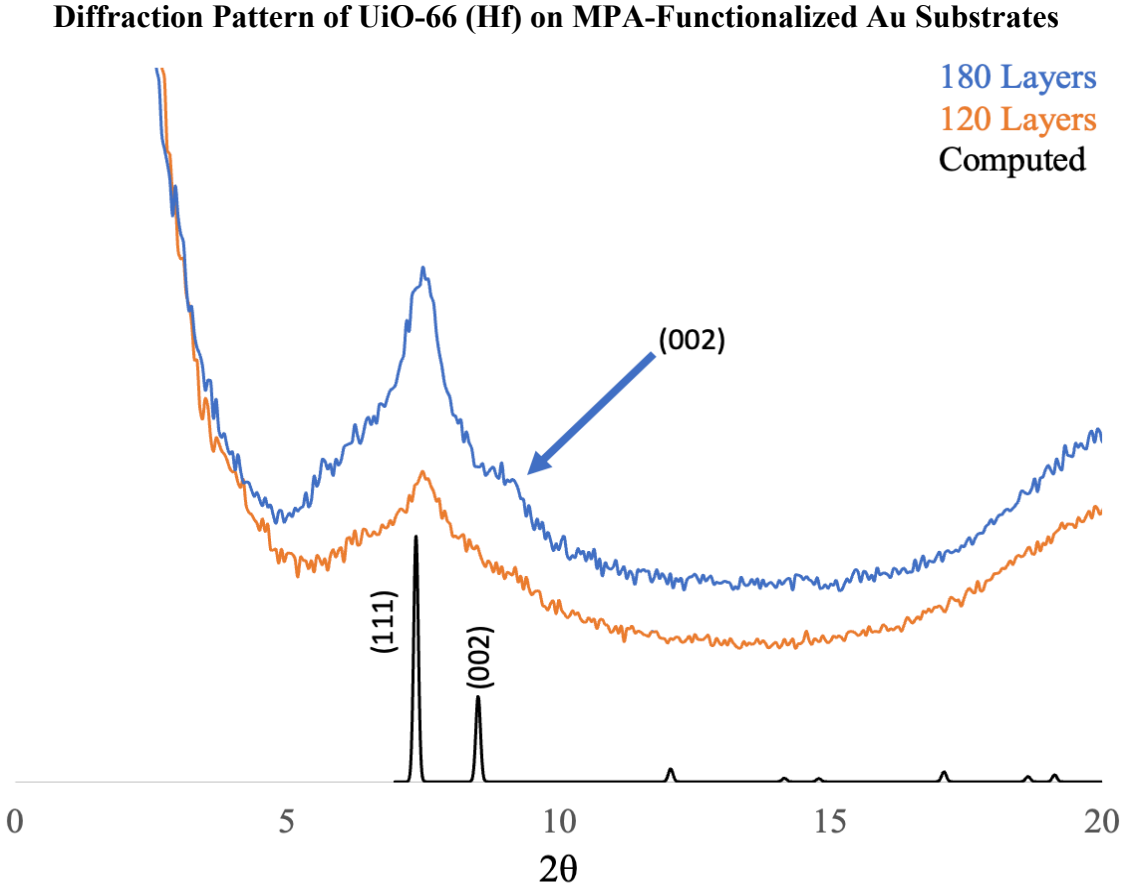

Figure 2.5: Diffraction patterns of UiO-66 (Hf) grown on MPA-functionalized Au after 120 cycles of deposition (orange) and 180 cycles (blue). The diffraction pattern after 120 cycles shows only a peak correlated only to the (111) Miller index, after 180 cycles crystallinity has increased and a new peak showing which correlates to the (002) Miller index is beginning to be detectable.

Morphological assessment of films by UiO-66 (Hf) thin films took place by SEM analysis of the films at 180 cycles of deposition for films grown both on MHDA and MPA functionalized substrates. Despite differences in the x-ray diffraction peaks neither films grown on MHDA or MPA were indistinguishable with SEM microscopy. In both films the cross sectional analysis reveals that the UiO-66 (Hf) is isolated to the surface of the substrates in a

uniform coating (Figure 2.6). Similar to ZrMOF-Film 10, scale-like film growth was observed consisting of a coating parallel to the surface of the substrate (**Figure 2.6 C & D**).

Scanning Electron Microscope Images of UiO-66 (Hf) After 180 Cycles of Molecular LbL Deposition on a MHDA and MPA Functionalized Au Surfaces

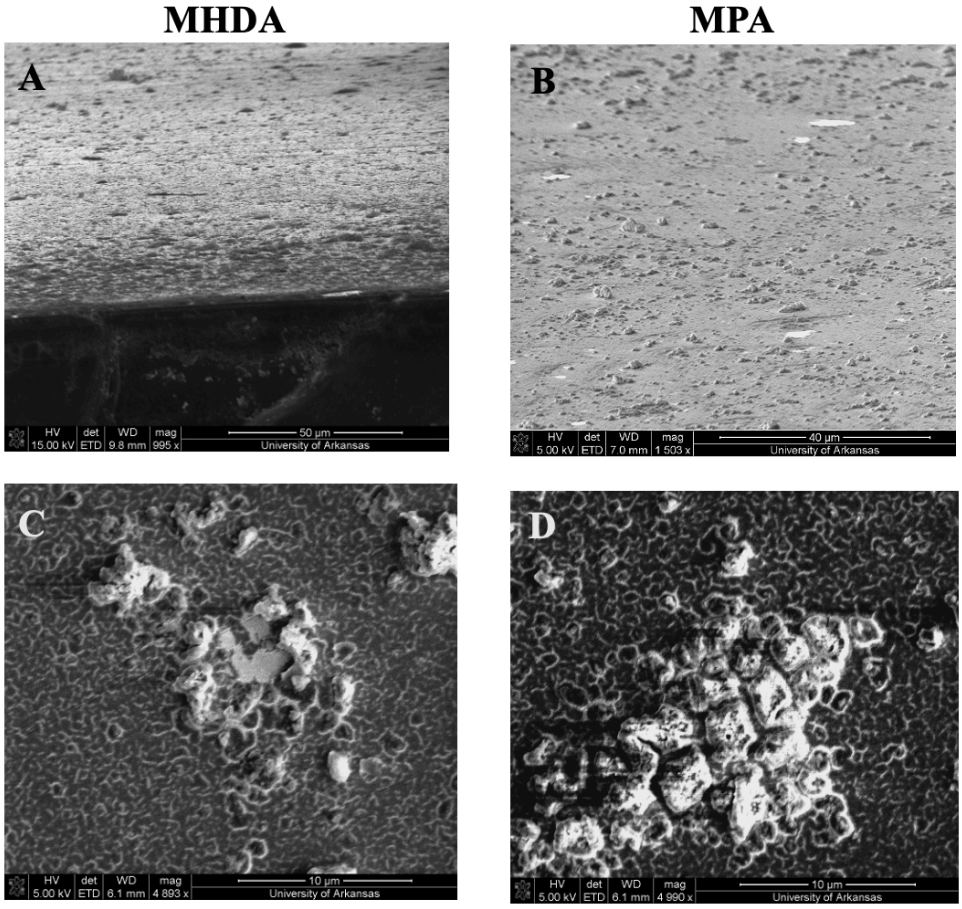

Figure 2.6: SEM analysis of UiO-66 (Hf) revealing the surface uniformity and complete coverage of the surface. **A**: Cross sectional analysis at 1200 times magnification showing the MOF film isolated on the surface of the MHDA-functionalized substrate **B**: Cross sectional analysis at 2000 times magnification showing UiO-66 (Hf) grown on the top of a MPA-functionalized substrate. **C**: Top-down view of the UiO-66 at ~5000 times magnification showing scale-like growth of MOF sheets parallel to the surface of the film on MHDA-functionalized substrates **D**: Zoomed in image (~5000 times magnification) the same scale-like growth of the MOF films this time on MPA-functionalized substrates.

III. Molecular LbL Deposition of PCN (Hf) MOFs

1. Molecular LbL of PCN Type Films

The development of UiO-66 (Hf) films represented the first instance of molecular deposition of Hf MOFs and served as a relevant proof of concept for the use of the $Hf_6O_4(OH)_4(OMc)_{12}$ clusters as a precursor for MOF films. To continue with investigations into the molecular LbL deposition of MOF films it was decided to attempt the deposition of porphyrin-containing Hf-based MOFs. Specifically, it was decided to utilize the 5,10,15,20-tetrakis(carboxyphenyl) porphyrin (TCPP) as the organic linker to connect the Hf-oxo clusters which would result in the deposition of PCN-type MOFs. This linker was selected because the tetratopic porphyrin can be synthesized in high purity with just two simple steps. Since multiple PCN species, exist each with metal-oxo clusters with different levels of connectivity, screening the diffraction patterns of synthesized films against several calculated patterns was necessary. All experiments utilized MHDA-functionalized Au coated wafers as a substrate and took place

Table 2.4: Contents of the Reactors for the Molecular LbL Deposition of Porphyrinic-Hf MOF Films

	Reactor 1	Reactor 2	Rinse
Reactants	38.5 mg $Hf_6O_4(OH)_4(OMc)_{12}$ (0.5 mM)	82 mg TCPP (3.0 mM)	N/A
Modulators	0.903 g Methacrylic acid	0.903 g methacrylic acid 1.26 g H_2O	N/A
Solvents	35 mL Ethanol	35 mL Ethanol	70 mL Ethanol
Temp/Time	70 C / 10 min	70 C / 10 min	70 C / 5 min

using the epitaxial workstation. The precise condition for the molecular deposition for the porphyirnic Hf MOF films were deposited is listed in Table 2.4.

To deposit the PCN-type Hf MOFs films; conditions analogous to the deposition of UiO-66 (Hf) were utilized, with TCPP replacing terephthalic acid in molar quantities. For deposition

of PCN-type Hf MOF films dipping time in the reactor vessels was increased to 10 minutes. Films were analyzed with x-ray diffraction and only after 120 cycles could the diffraction peaks associated with PCN-type MOFs be detected. Ultimately, after screening the acquired diffraction patterns against calculated patterns of PCN-(222, 225, 225 and 226) it was determined that PCN-222 was the closest match especially the strong correlation to the peak at 2.44° which arises from the diffraction of PCN-222. When the number for cycles was increased to 240 the intensity of the peak increases however this is a slight shift of the observed diffraction peak to a lower 2Θ (2.06°) which correlates to an expansion of the unit cell size, which can be a result of missing linker defects (Figure 2.7).[19] The observed diffraction patterns also reveal a broad signal between 2Θ = 5° and 2Θ = 10°, these broad humps in x-ray diffraction patterns arise from the presence of amorphous phases within the film and often arise in thin film analysis form interference by the substrate.[20] Since comparison to the computed diffraction patterns of PCN-type MOFs did not provide an exact match for the observed patterns, further X-ray methods were needed to

characterize the molecular structure of the films. Towards this end, X-ray diffraction experiments designed specifically for thin-film analysis were utilized.

Further investigation into the structure of the deposited porphyrinic films required surface sensitive x-ray diffraction techniques to both increase the diffraction pattern arising from crystalline samples and to decrease the effect of amorphous contaminates. To achieve surface sensitivity grazing-incidence diffraction X-ray diffraction (GIXRD) was used. GIXRD, often referred to as "in-plane" diffraction is different from traditional "out of plane" diffraction in that the X-ray source is held at a steady position with a low relative angle to the sample. This type of scattering geometry was utilized to ensure that the interaction of X-rays with the samples would be isolated to the synthesized thin films. For the analysis of MOF films GIXRD is used to increased peak intensity of low 2Θ diffraction peaks and to higher surface selectivity towards the MOF film.[21] For analysis of the porphyrinic MOF film by GIXRD, an MHDA-functionalized Au substrate underwent 210 cycles of molecular LbL deposition under the conditions listed in Table

Comparison of Diffraction Patterns of Films of Porphyrinic MOF Grown by Molecular LbL Deposition

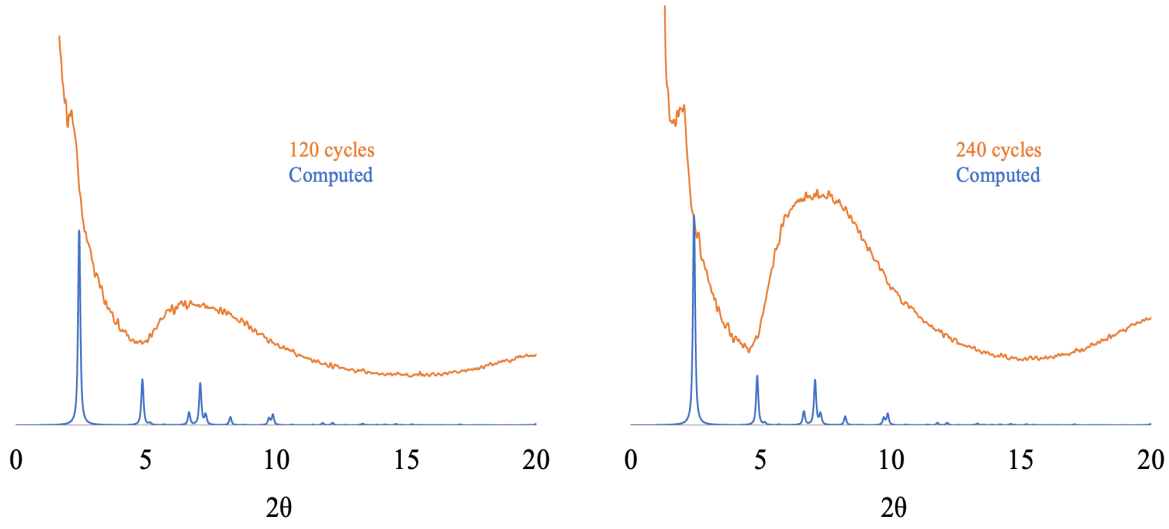

Figure 2.7: X-ray diffraction patterns of porphyrinic MOF films grown through the molecular LbL deposition. Observed diffraction patterns are shown in orange and the computed diffraction pattern for PCN-222 is shown in blue.

GIXRD Analysis of (Hf)PCN-Film Compared to the Computed PCN-222 Diffraction Pattern

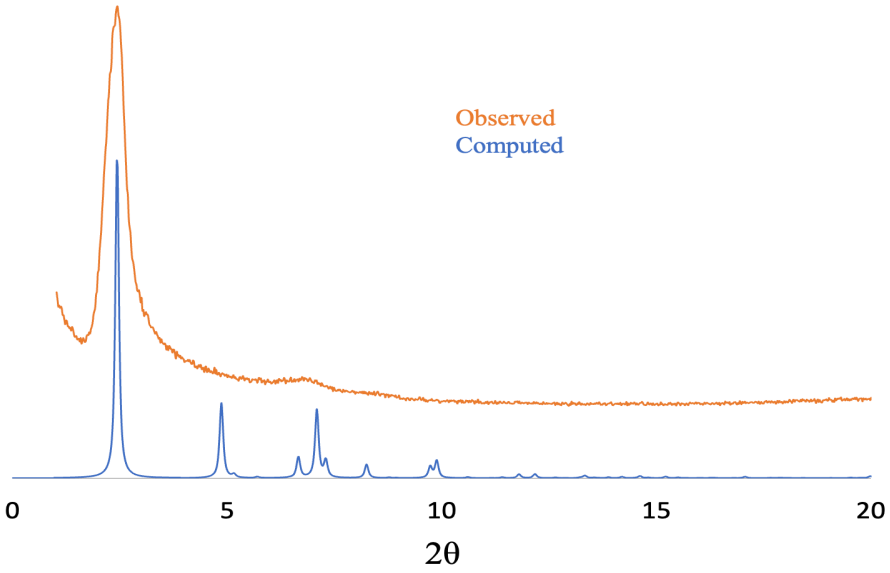

Figure 2.8: GIXRD analysis at an incident angle of 1.0° of (Hf)PCN-Film after 210 cycles of deposition reveals a strong diffraction peak at 2.4° which correlates to the (100) Miller index of PCN-222.

2.4 then the film was diffracted using a incidence angle of 1°. To the great pleasure of the experimenter, GIXRD provided a strong diffraction peak at 2.4°, which strongly matches the main diffraction peak of the computed PCN-222 diffraction pattern (Figure 2.8). This result provides evidence for high correlation between the overall structure of the film and PCN-222. Absence of the large hump from 5-10 2Θ seen in the out-of-plane diffraction experiments indicates that this signal likely arises from the substrate and not the film itself. Despite the single peak which strongly correlates to the PCN-22 diffraction pattern a total structural match is not possible. The MOF film is so named (Hf)-PCN-Film.

2. (Hf)PCN-Films Incorporating Zn and Mn Metalloporphyrins

After the successful deposition of (Hf)PCN-Film it was decided to investigate the deposition of metalloporphyrin analogs which hold great potential for catalytic applications.[22–24] The porphyrinic films once again relied on interlinkage via coordination to Hf-oxo clusters. Of

particular interest was the ability to perform tandem catalysis by the action of two porphyrins in unison. The overall goal was to develop a film which could catalyze the synthesis of cyclic carbonates from alkenes via the action of an oxidation catalyst to form the epoxide followed by

Scheme 2.5: Depiction of Catalysis on a MOF Film Via the Tandem Action of Two Porphyrin Linkers

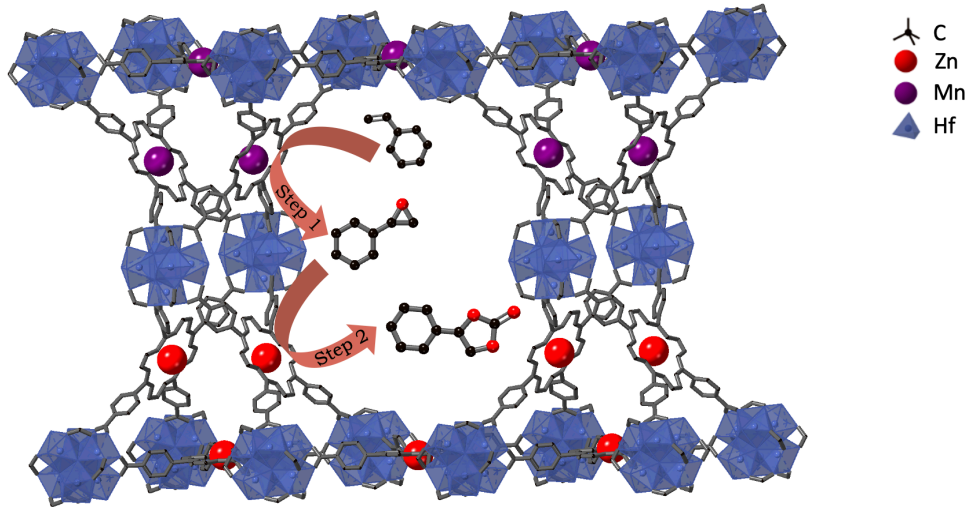

the action of a Lewis acid to promote ring expansion of the epoxide with CO_2 to form the carbonate (Scheme 2.5). This two-in-one reaction would be an important development as cyclic carbonates hold potential as industrially relevant solvents and could represent a method for the valorization of CO_2 captured from the atmosphere.[25] Especially appealing would be the development of a reaction which utilizes two gases; O_2 and CO_2, for the transformations. The ability to utilize two gases which are found in the atmosphere would be a meaningful development towards showcasing the abilities of MOF films for tandem catalysis.

For the initial oxidation step, there any many metalloporphyrins which can produce epoxides from an alkene: including Ru, Fe and Mn porphyrins.[26–28] Regarding the ring-opening expansion of the epoxide, literature sources were referenced and it was determined that either the Zn or Co metalloporphyrin would be able to serve as a suitable Lewis acid catalyst for the CO_2 fixation.[29] It should also be noted that the Hf-oxo clusters also display Lewis acidity enough to

promote ring expansion of epoxides to cyclic carbonates in the presence of CO_2.[30] One final consideration is not just how each catalytic system behaves alone, but how all the two catalytic systems will behave in tandem. Both the epoxidation and ring expansion step require the use of co-catalysts to perform the respective steps: oxidants in the case of epoxidation and tetrabutylammonium bromide (TBAB) in the case of ring expansion, and the compatibility of these co-catalysts must also be assured.

The fabrication of metalloporphyrin films and the subsequent characterization, with initial emphasis set on developing methods for the deposition of Zn-porphyrin and Mn-porphyrin MOF films respectively. After confirmation that each unique metalloporphyrin could be incorporated into a film, the two metalloporphyrins would be deposited onto a film in a

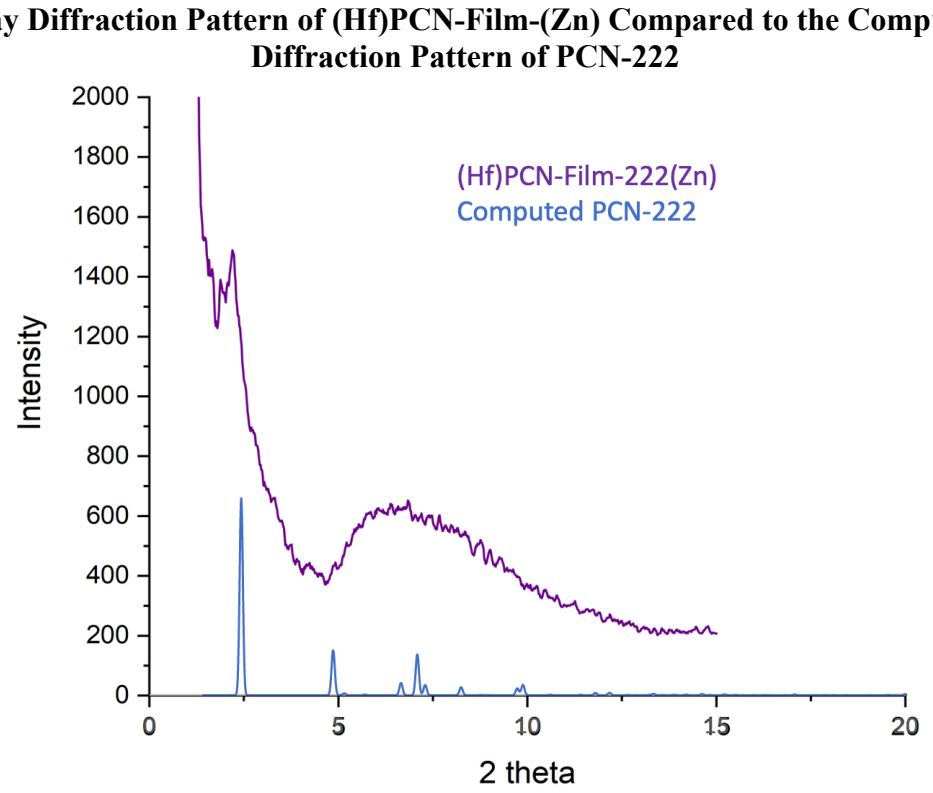

Figure 2.9: Comparison of the out-of-plane diffraction pattern of (Hf)PCN-Film-(Zn) (purple) to the computed diffraction pattern of PCN-222 (blue).

sequential fashion. Initial work began on the deposition of (Hf)PCN-Film-(Zn), a materials of

which the Zr analog has been previously synthesized in bulk and used for CO_2 fixation.[31] Conditions for the molecular LbL deposition of (Hf)PCN-Film-(Zn) mirrored the deposition of

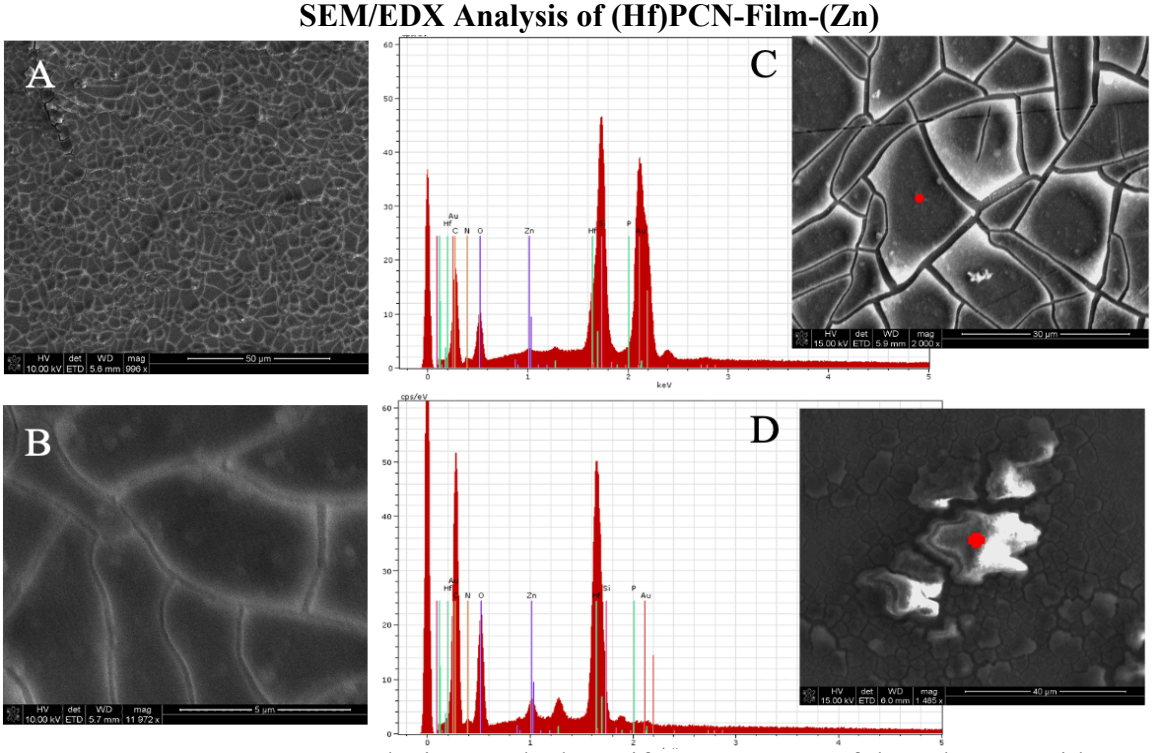

Figure 2.10: A & B SEM analysis reveals the uniform coverage of the substrate with (Hf)PCN-Film-(Zn) **C & D**: EDX analysis shows the presence of Zn and Hf on the film.

(Hf)PCN-Film except TCPP was replaced with a molar equivalent of Zn-TCPP. The resultant films have an out-of-plane diffraction pattern which correlated to calculated PCN-222 structure (Figure 2.9). SEM and EDX analysis revealed a uniform film which gave the spectral signals for Zn through EDX (Figure 2.10**)**, which in conjunction with the matching diffraction patterns gave strong evidence for the fabrication of the Zn-TCPP analogue.

(Hf)PCN-Film-(Zn) was then tested for catalytic activity for ring expansion of an epoxide with CO_2 to form a cyclic carbonate. The films were tested using at 15 bar of CO_2 with 4.3 mol% TBAB co-catalyst. The films tested consisted of 120 cycles of deposition on MHDA-functionalized Au-coated wafers. To determine the mass of the film deposited; the substrates were weighed before and after deposition. It was revealed that the mass of the deposited

(Hf)PCN-Film-(Zn) after 120 cycles of deposition was 0.98 mg. Catalysis was conducted at 15 bar of CO_2 pressure (Scheme 2.6), a stainless-steel Parr pressure vessel was used as a reactor.

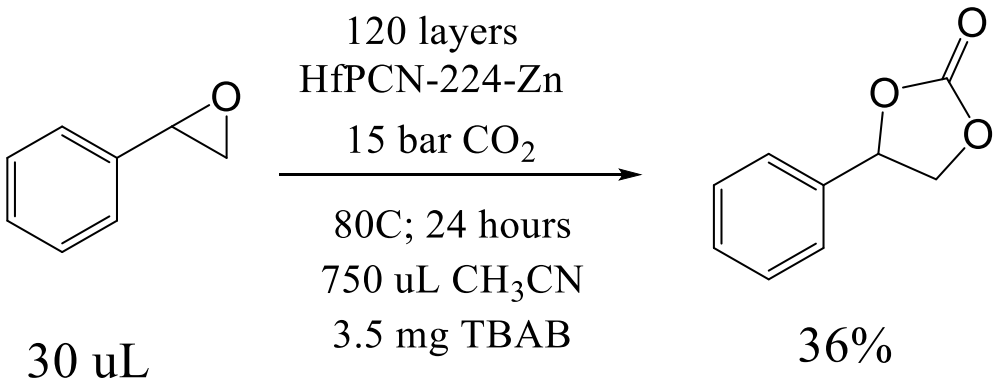

Scheme 2.6: (Hf)PCN-Film-(Zn) catalyzed ring expansion of styrene oxide to 1-phenyl-1,2-ethylene carbonate.

(Hf)PCN-Film-(Zn) was able to obtain a 36% conversion in 24 hours, which represents a 15% increase in performance when compared to just the TBAB. With just TBAB after 48 hours the reaction under the same conditions gave only 31% conversion. All yields were determined by ^{1}H NMR (Section III, Figures 1.19, 1.20 and 1.21).

Following the successful fabrication of the (Hf)PCN-Film-(Zn) material, the next step towards the development for a film that could affect tandem catalysis was the development of the Mn analog. Molecular LbL deposition of the (Hf)PCN-Film-(MnCl) films onto MHDA-functionalized Au-coated wafers took place through the same procedure as the deposition of (Hf)PCN-Film-(Zn) but with the Mn-Cl TCPP replacing the Zn-TCPP in molar quantities. Surprisingly, X-ray diffraction of the film after 60 cycles of deposition showed several differences than the previous TCPP-based films. The lowest 2Θ peak was shifted even further down to 1.88° 2Θ and a new diffraction peak at 9.02° was also detected (Figure 2.11). To further investigate the structure surface sensitive grazing-incidence wide angle X-ray scattering (GIWAXS) was utilized. One interesting correlation that was made is that the new diffraction

peak at 9.02° seemed to match the highest intensity peak of just powder Mn-Cl TCPP, however no amount of rinsing with DMF would remove this peak. Despite complications with the X-ray analysis, it was noted that even after only 60 layers of deposition optimal microscope images showed the development of a visible film on the surface of the substrate. The (Hf)PCN-Film-(Mn-Cl) films were tested as epoxidation catalysts for the reaction of styrene to styrene-oxide using conditions previously described by Chan et al.[32] The films showed catalytic activity, promoting a 32% conversion after only 14 hours.

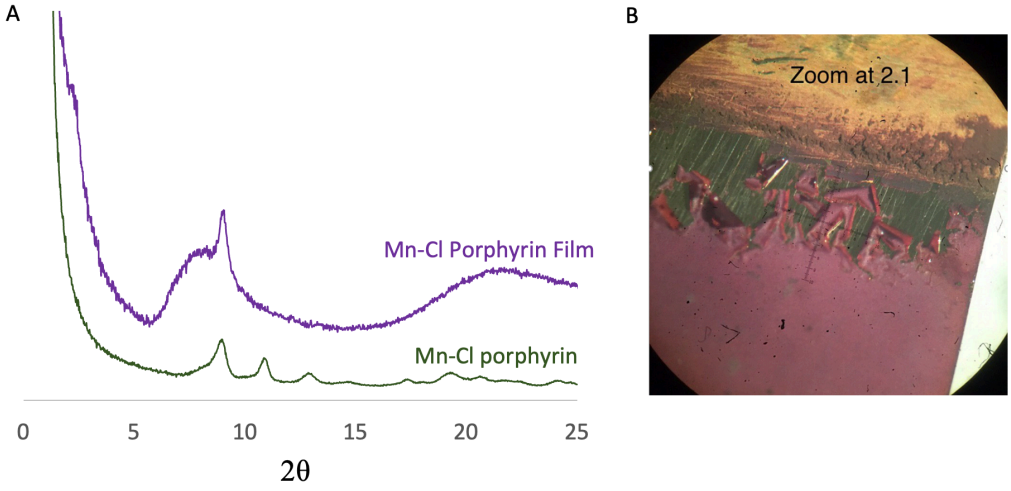

Figure 2.11: XRD and optical microscope analysis of the (Hf)PCN-Film-(Mn-Cl). A) Out-of-plane X-ray diffraction spectra of (Hf)PCN-Film-222(Mn-Cl) after 60 cycles of molecular LbL deposition in purple compared to the powder-diffraction pattern of the Mn-Cl Porphyrin small molecule in green. B) An optical microscope image of the (Hf)PCN-Film-(Mn-Cl) grown after 60 cycles of deposition.

After successful deposition of (Hf)PCN-Film-Mn-Cl) and (Hf)PCN-Film-(Zn) work began in the deposition of Zn/Mn interchanged porphyrinic MOF films. In this procedure the number of reactors was increased to four, so that the substrate could be dipped into two unique porphyrin solutions. The goal was to develop a MOF film where the two distinct porphyrins could be held in place one molecular layer apart where cooperative action was optimized. Before catalytic testing the developed films were first characterized by X-ray diffraction and SEM/EDX

analysis. All films were grown on MHDA-functionalized Au-coated wafers. The X-ray diffraction studies consisted of out-of-plane diffraction experiments and showed that a diffraction peak in the 2.0° range which has become distinctive to the PCN-222 type films and still displays the diffraction peak at 9.02° which was observed in the (Hf)PCN-Film-(Mn-Cl) film. SEM analysis of the film shows uniform coverage and SEM cross-section after shearing the film on one end shows a film of uniform thickness (Figure 2.12). EDX point scan was used to show that Hf, Zn and Mn are all present in the film.

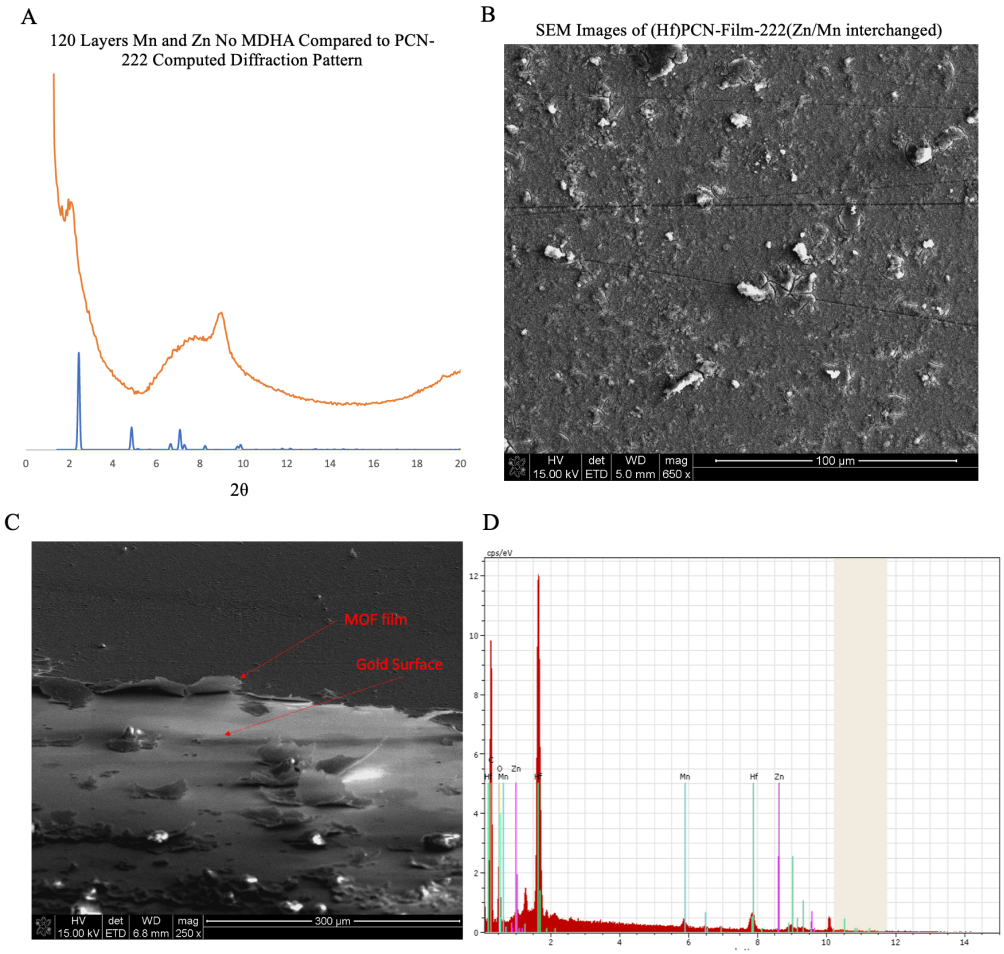

Figure 2.12: Characterization of (Hf)PCN-Film-222(Zn/Mn interchanged). A) Out-of-plane XRD analysis of (Hf)PCN-Film-222(Zn/Mn interchanged). B) SEM micrograph of (Hf)PCN-Film-222(Zn/Mn interchanged) after 120 cycles of molecular LbL deposition magnified at 650 times and C) SEM cross-sectional analysis of the (Hf)PCN-Film-222(Zn/Mn interchanged) film. D) EDX analysis of the (Hf)PCN-Film-222(Zn/Mn interchanged), point scan reveals the spectral lines of Hf, Zn and Mn.

3. Fabrication of Interchanged Metalloporphyrin PCN-type MOF Films and Catalytic Applications

Following characterization, the (Hf)PCN-Film-(Zn/Mn interchanged) films were explored as catalysts for the transformation of styrene to 1-phenyl-1,2-ethylene carbonate. This reaction would transform a cheap starting materials to a useful solvent through the capture of CO_2 in a facile manner. All reactions took place using H_2O_2 as a oxidant for the epoxidation and TBAB as a co-catalyst for the CO_2 fixation. $CNCD_3$ was used as a solvent which made monitoring the reactions with 1H NMR simple. Based on the initial experiments with the single-porphyrin films conditions for the tandem catalysis reaction was optimized to increase reaction yields, the overall amount of styrene starting material was reduced to 20 uL and the reaction time was increased to 48 hours. Overall; the reaction was able to convert the majority of the styrene to styrene carbonate with styrene oxide also detected. Reactions were carried out in acetonitrile-d_6 so that the reaction mixtures could be transferred directly to an NMR tube and analyzed with a 400 MHz NMR. While the (Hf)PCN-Film-(Zn/Mn interchanged) did succeed at carrying out the tandem catalysis, future work should be aimed at finding a two-porphyrin system which would carry out tandem catalysis using two gasses, O_2 and CO_2.

4. Molecular LbL Deposition of (Hf)PCN MOFs Atop a Basement Layer of UiO-66 (Hf)

While investigating the molecular LbL deposition of PCN-type Hf MOFs one recurring problem was the lack of crystallinity in the films. A potential solution for this problem was to use the developed UiO-66 (Hf) films to serve as an anchor layer for more complicated MOF films to be grown. After development of successful techniques for the molecular LbL deposition of UiO-66 (Hf) efforts were made to find an application for these MOF films to serve as a basement

layer for the further deposition of PCN-type MOF films. The use of a basement layer for MOF growth during molecular LbL deposition was first explored by Wang et al where a basement layer of HKUST was first deposited on the substrate so that a intentionally defective mixed-linker HKUST derivatives could then be deposited.[33] In a similar fashion, it was determined to effect the molecular LbL deposition of PCN-type MOFs on the top of a basement layer of UiO-66 (Hf) (Scheme 2.6).

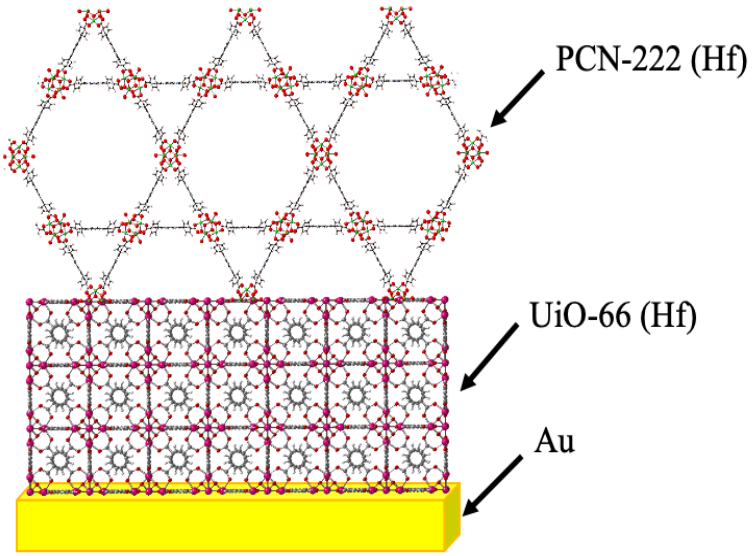

Scheme 2.6: Depiction of a film consisting of PCN-222(Hf) grown on top of UiO-66(Hf).

The UiO-66 topology serves as an excellent basement layer as it has greater density than MOFs of the PCN topology owing to the smaller linker distance and higher connectivity of the metal-oxo nodes.[34] The resultant material will be a hybrid film with two distinct MOF topologies, both based on the Hf-oxo cluster, combined onto the same film. Production of hybrid UiO-PCN films combines two of the most highly-utilized MOF topologies into one film, opening up a litany of potential applications with the ability to merge several functionalities into one film. The hybrid UiO-PCN (Hf) films were characterized by XRD and SEM analysis.

The growth of UiO-PCN (Hf) films was carried out using the conditions optimized of UiO-66 (Hf) and the automated epitaxial workstation. Hybrid films were fabricated using MHDA functionalized films which first were subject to 120 cycles of UiO-66 (Hf) deposition, then subject to deposition of PNC MOFs. Molecular deposition of the PCN MOFs was carried out by substituting (5,10,15,20)-tetra(4-carboxyphenyl)porphyrin for terephthalic acid during the epitaxy step. Conditions for the molecular LbL Epitaxy are laid out in detail in the Experimental Section Figure 2.23. Deposition of the films was monitored by X-ray diffraction with the first analysis taking place after 120 layers of UiO-66 (Hf) deposition, followed by the deposition of (Hf)PCN-Film. The film was analyzed with X-ray diffraction after every 30 cycles of (Hf)PCN-Film deposition (Figure 2.13). The XRD analysis shows the progress of the (Hf)PCN-Film on the top of the (Hf)UiO-66, the so-named (Hf)UiO-PCN Hybrid Film was analyzed by SEM microscopy after 240 cycles of deposition (120 cycles of UiO-66 (Hf) then 120 cycles of (Hf)PCN-Film. While the growth of the (Hf)PCN film was apparent by XRD analysis, the overall crystallinity was not apparently improved in that still only one diffraction peak associated with the computed PCN-222 pattern was detected. SEM analysis did reveal a uniform film which covered the surface of the MHDA-functionalized Au substrate.

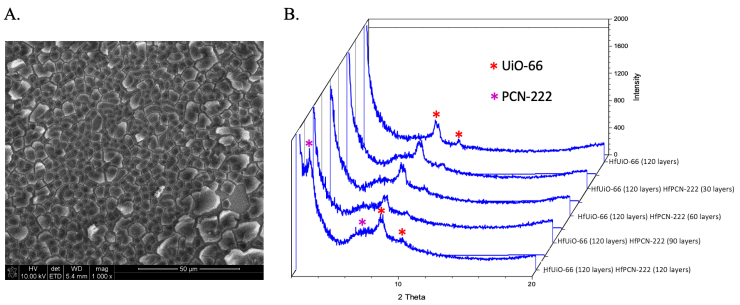

Figure 2.13: Analysis of the (Hf)UiO-PCN Hybrid Film. **A**) SEM analysis shows a morphology similar to previously fabricated films and uniform coverage of the surface. **B**) Step-wise X-ray diffraction experiments show the growth of the PCN type film atop the basement layer of the UiO-66 (Hf) film after 120 cycles of deposition of both topologies.

IV. Experimental Section and Spectral Data

1. GIWAXS Data

GIWAXS experiments took place on beamline 8-ID-E at the Advanced Photon Source (Argonne National Lab). The incident angle of diffraction was 0.14° and the X-ray energy was 10.92 keV which correlates to a wavelength of 11.353 nm. Analysis was carried out in MATLAB using the GIXSGUI software developed by Zhang Jiang.[35] The goal of carrying out these GIWAXS experiments was to gather diffraction data which could be used to confirm a precise structure of the MOF thin films. While exact structural assignment was not possible with the gathered data, the presence of specific d-spacings were recorded. Overall, these GIWAXS experiments provide a template and procedure by which future GIWAXS of MOF thin films can be guided. GIWAXS data is presented as follows. First an overall image of the 2D diffraction pattern is presented, for each sample many sample heights were tested and the image shown represents a selected height which gave the most usable spectra. After this a series of linecuts across various phi values are shown. All samples were analyzed by taking linecuts at 180°-160°, 180°-90°, 180°-135°, and 135°-90°. Linecuts were then analyzed to find the maxima of the diffraction peaks and the d-spacing associated with these peaks were indexed using the publicly available instaNANO calculator.[36] This analysis examines the thin-film samples for any potential diffraction signals which might arise of the presence of crystalline MOF films on the wafer. One complication arising from this analysis is that correlating specific peaks to specific lattice plans become difficult, for the purpose of analysis the d-spacing provided are assumed to arise form first order diffraction. Before the GIWAXS analysis of the MOF films it was required to carry out analysis on the relevant blank substrates, these included an Au-coated Si wafer then an MHDA-functionalized Au-coated Si wafer (Figures 2.14 and 2.15 respectively). This testing of

blanks was necessary to determine any effects the substrate would have on the analysis. Samples tested include the (Hf)PCN-Film wafers (Figure 2.16), (Hf)PCN-Film-(Mn-Cl) (Figure 2.17), (Hf)UiO-PCN Hybrid Film (Figure 2.18).

GIWAXS Analysis of Au-Coated Si Wafer.

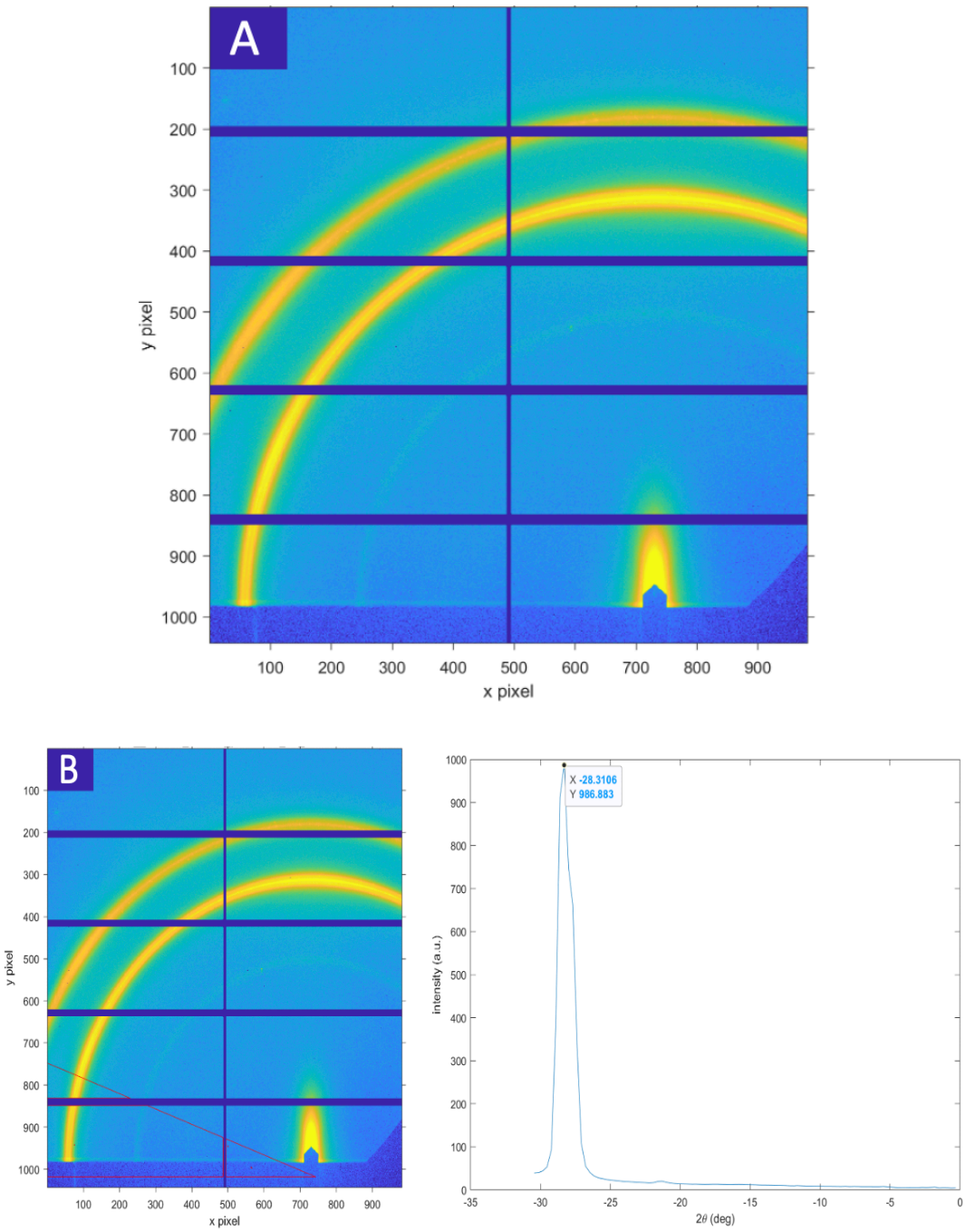

Figure 2.14: GIWAXS analysis of an Au-coated Si wafer. A) Overall 2D diffraction pattern. B) Linecut analysis of 180°-160°

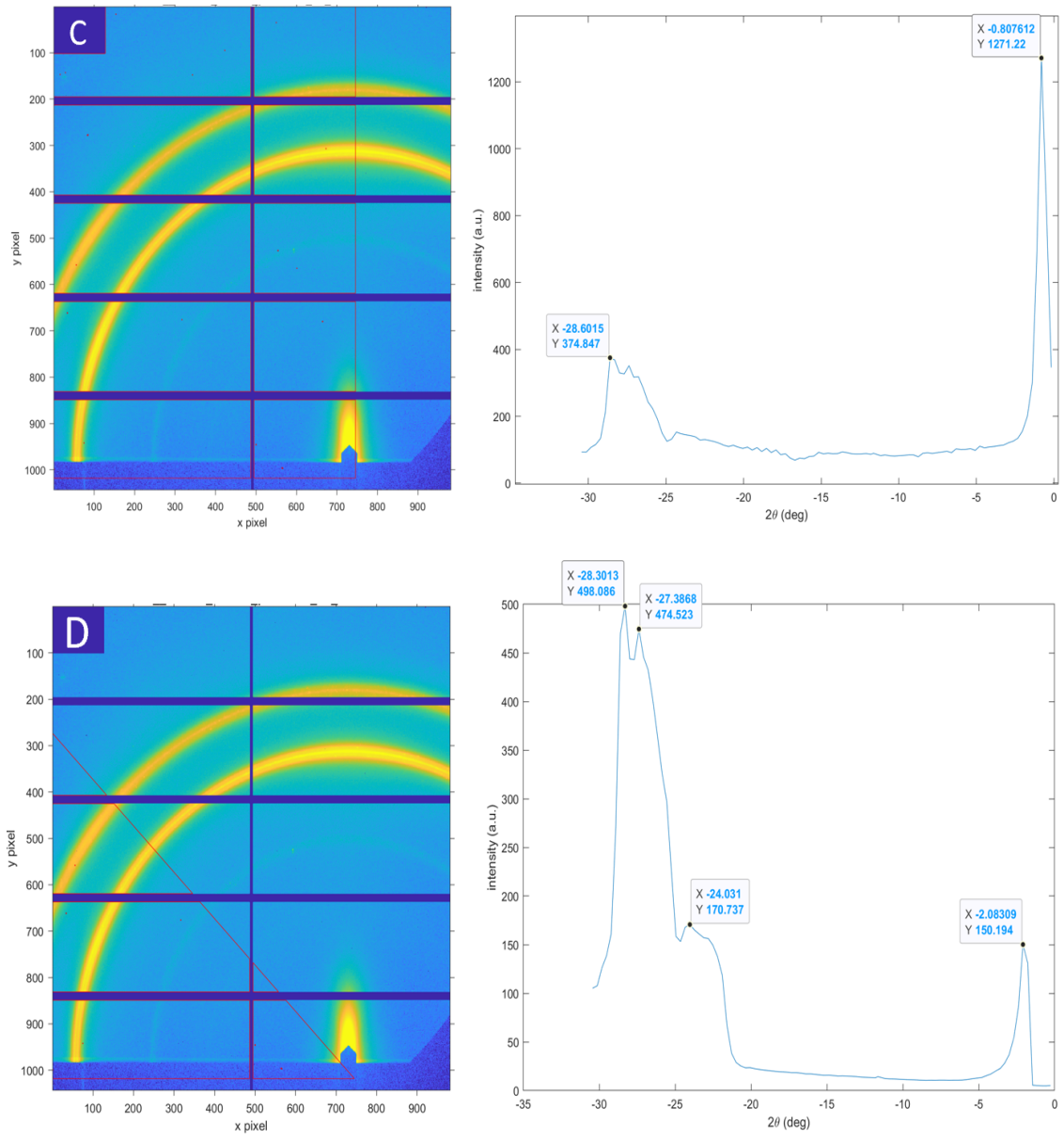

Figure 2.14 Cont.: C) Linecut analysis of 180°-90° phi. D) Linecut analysis of 180°-135° phi.

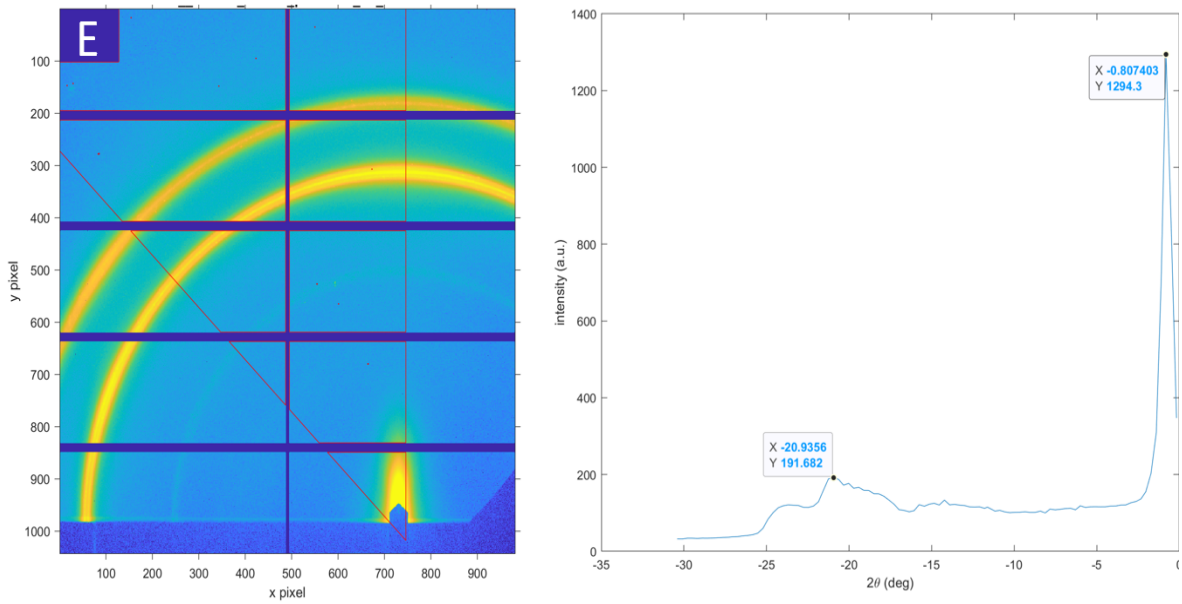

Figure 2.14 Cont.:. E) Linecut analysis of 135°-90° phi.

Table 2.5 Indexed Peaks and Associated d-Spacings

Entry	Phi Values	Peak Max	d-Spacing (if 1st Order)
	180°-160°		
1		28.3106°	0.23 nm
	180°-90°		
2		0.807612°	8.5 nm
3		28.6051°	0.23 nm
	180°-135°		
4		2.08309°	3.12 nm
5		24.031°	0.27 nm
6		27.3868°	0.24 nm
7		28.3013°	0.23 nm
	135°-90°		
8		0.807403°	8.06 nm
9		20.9356°	0.31 nm

Table 2.5 reveals only the peaks associated with Au crystal structure, entries 1,3,6 and 7 all arise from the (111) lattice plane of gold.[37] Peaks 2, 4 and 8 are assumed arise from reflections and should not be considered the result of diffraction

GIWAXS Analysis of MHDA-Functionalized Au-Coated Si Wafer.

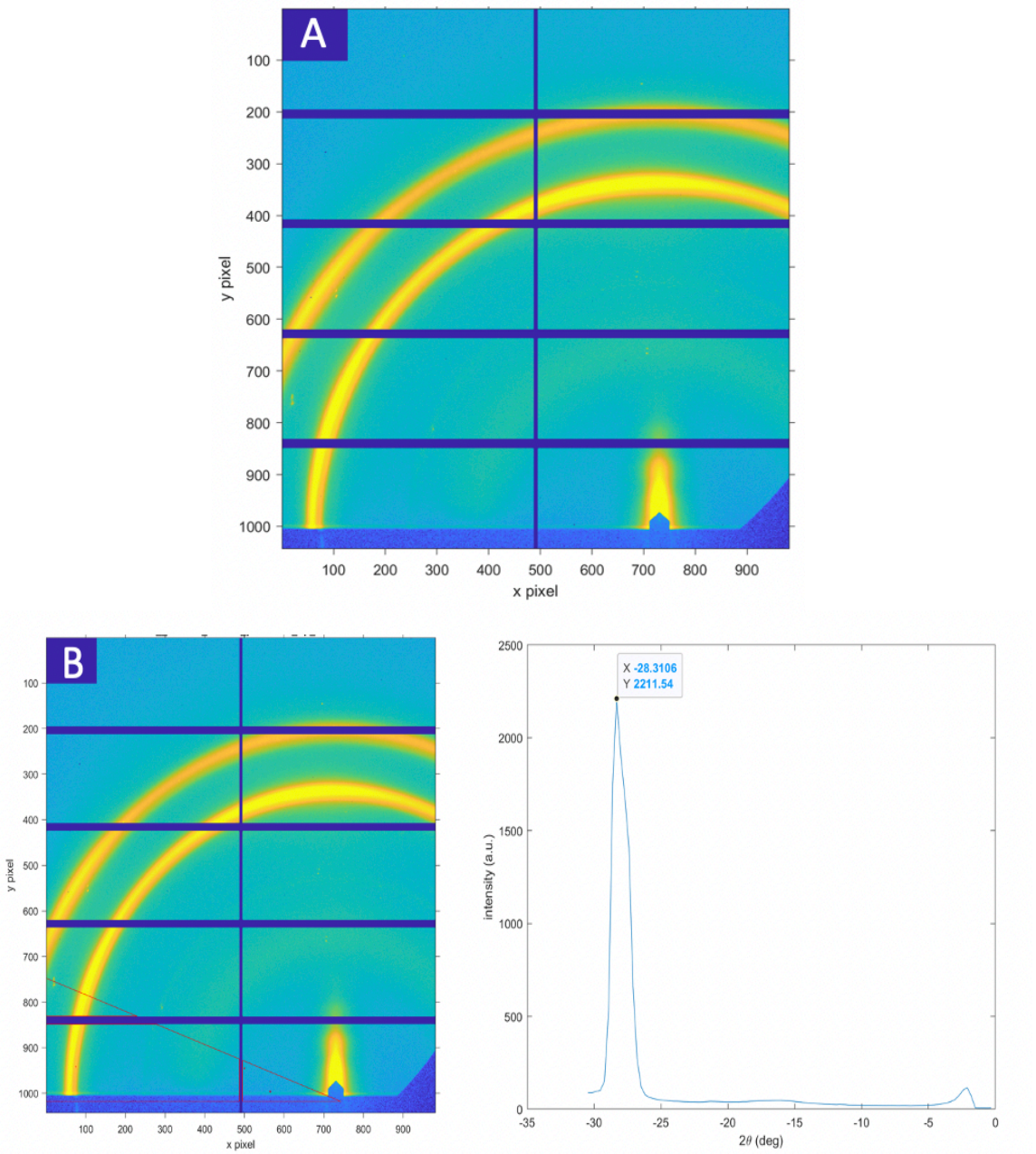

Figure 2.15: GIWAXS analysis of an MHDA-functionalized Au-coated Si wafer. A) Overall 2D diffraction pattern. B) Linecut analysis of 180°-160° phi.

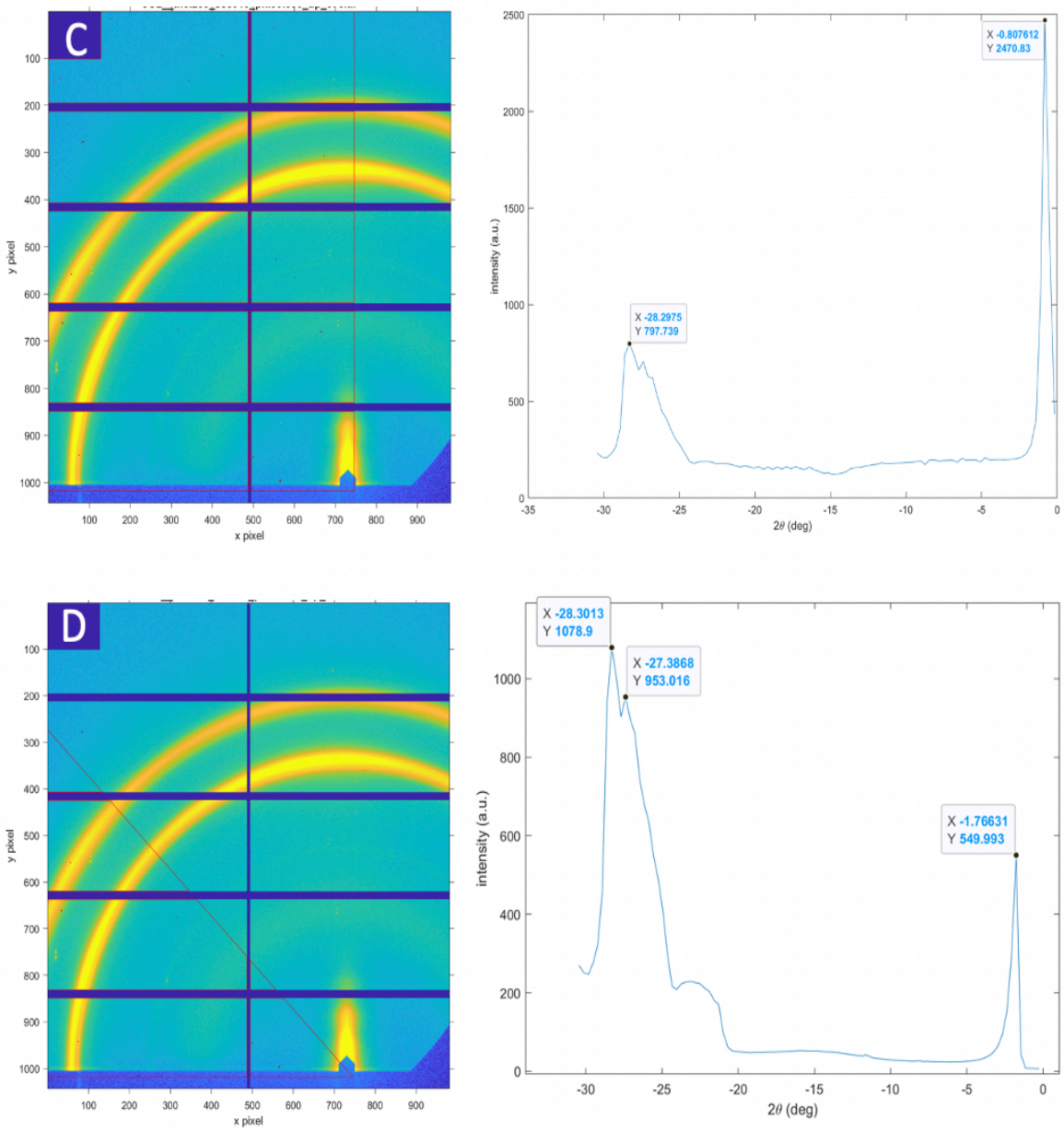

Figure 2.15 Cont.: C) Linecut analysis of 180°-90° phi. D) Linecut analysis of 180°-135° phi.

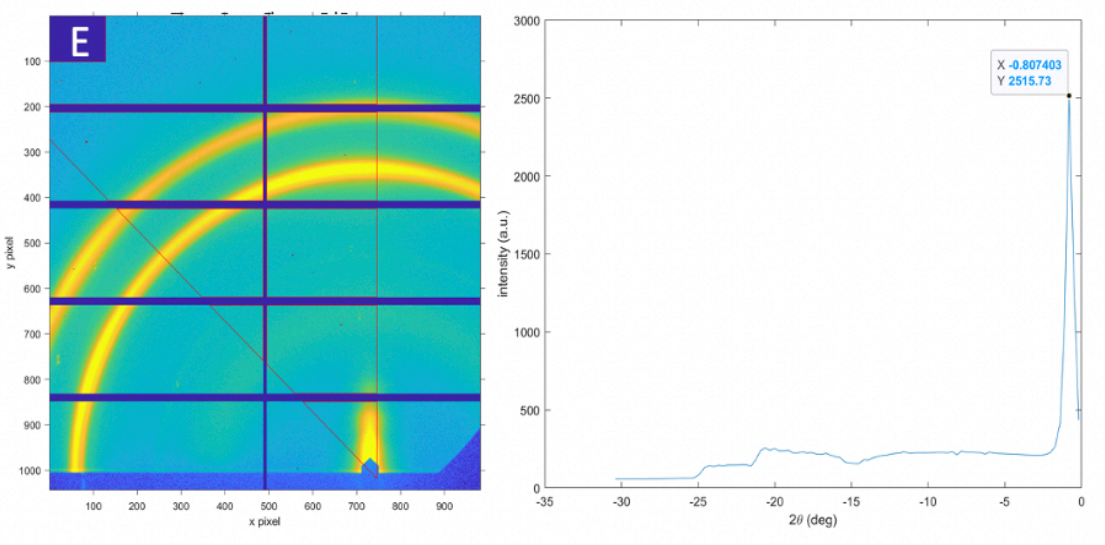

Figure 2.15 Cont.: E) Linecut analysis of 135°-90° phi.

Table 2.6 Indexed Peaks and Associated d-Spacings

Entry	Phi Values	Peak Max	d-Spacing (if 1st Order)
	180°-160°		
1		28.3106°	0.23 nm
	180°-90°		
2		0.807612°	8.5 nm
	180°-135°		
3		1.76631°	3.68 nm
4		27.3868°	0.24 nm
5		28.3013°	0.23 nm
	135°-90°		
6		0.807403°	8.06 nm

Table 2.6 reveals only the peaks associated with Au crystal structure. It is apparent that the addition of an MHDA SAM does not affect the diffraction of the gold film and so should not pose any problems to GIWAXS analysis. Entries 1,4 and 5 arise from the (111) lattice plane of Au. Entries 2,3 and 6 are the result of reflectance and should not be considered diffraction peaks.

GIWAXS Analysis of (Hf)PCN-Film

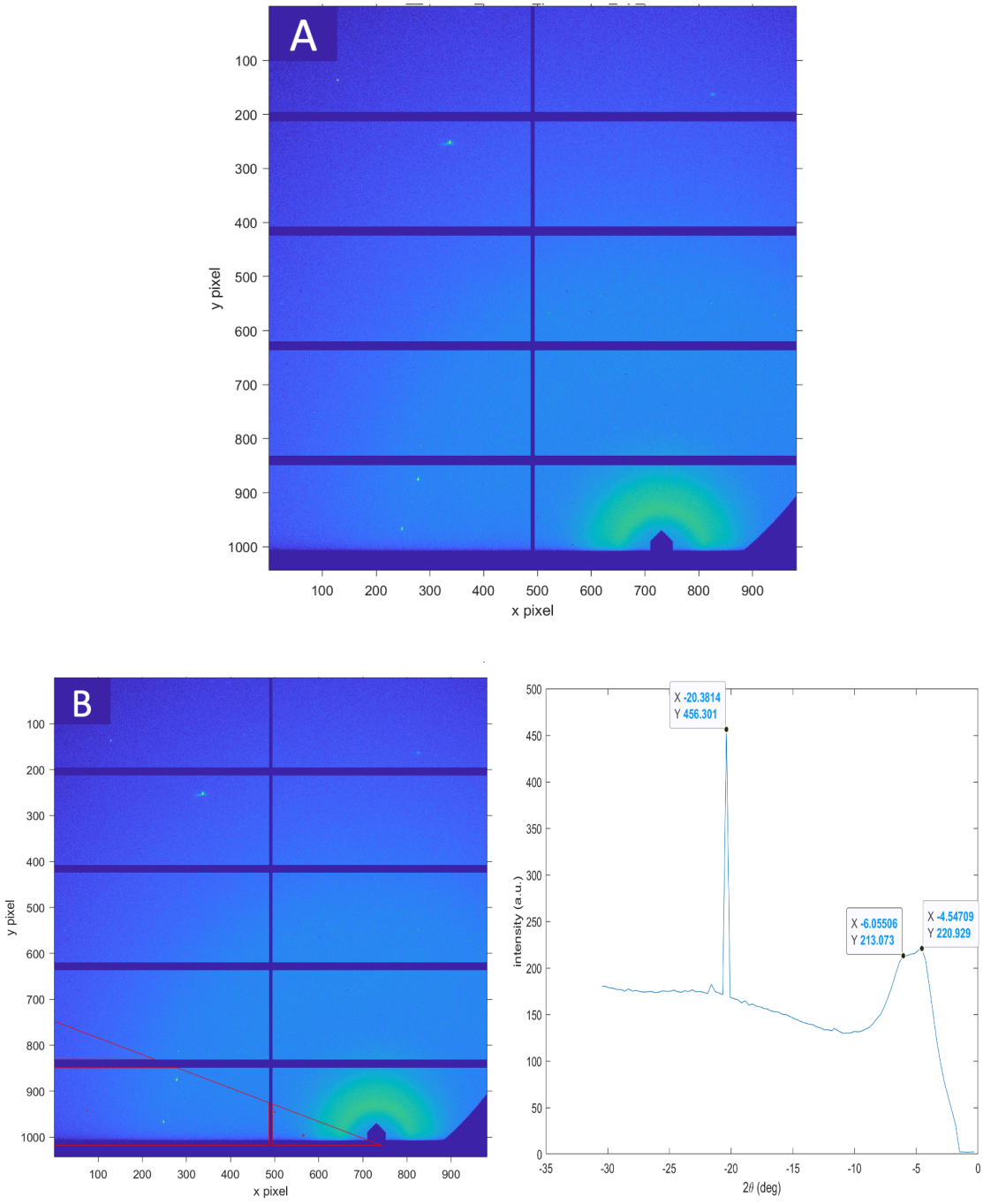

Figure 2.16: GIWAXS analysis of an (Hf)PCN-film wafer. A) Overall 2D diffraction pattern. B) Linecut analysis of 180°-160° phi.

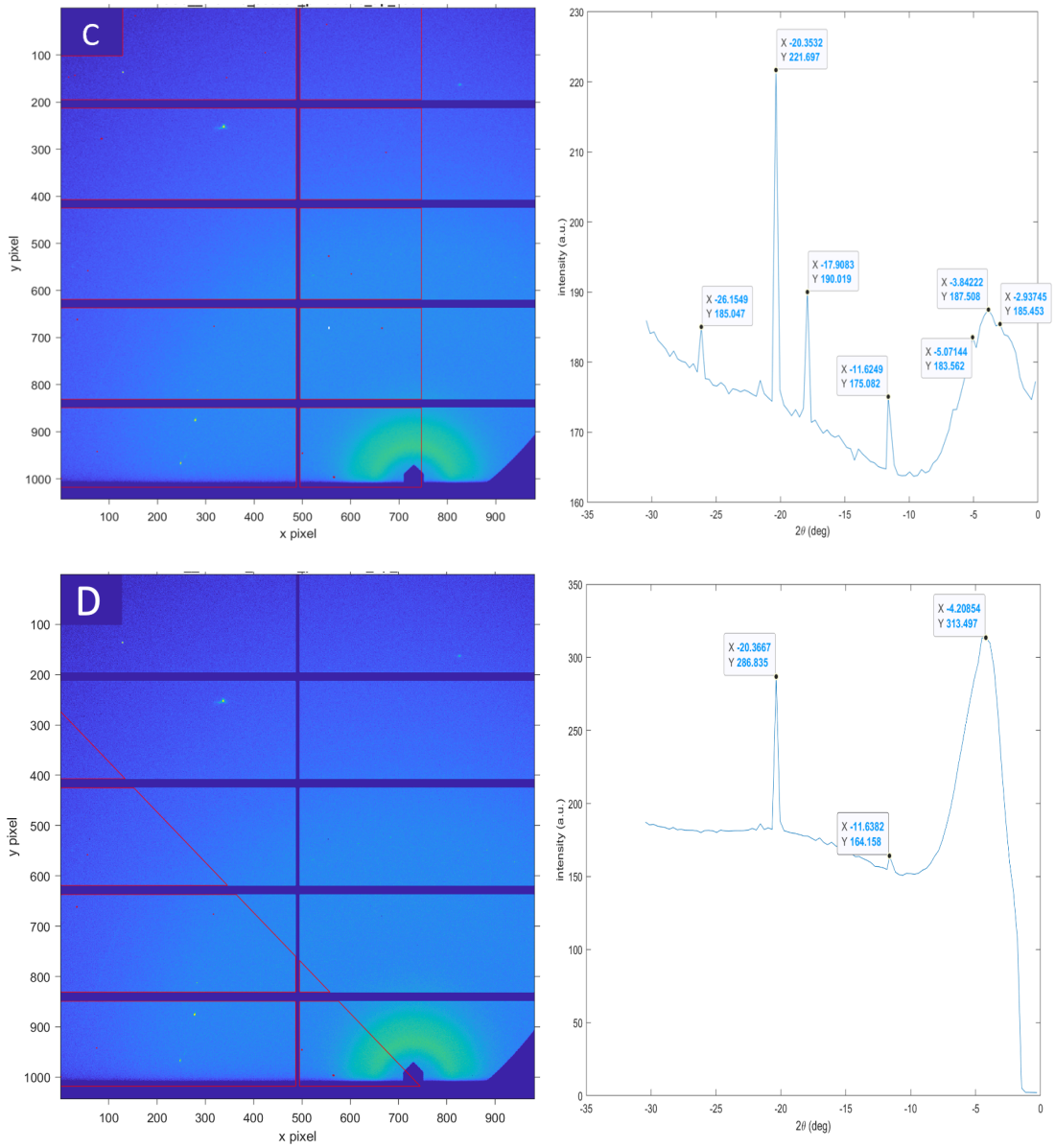

Figure 2.16 Cont.:) Linecut analysis of 180°-90° phi. D) Linecut analysis of 180°-135° phi.

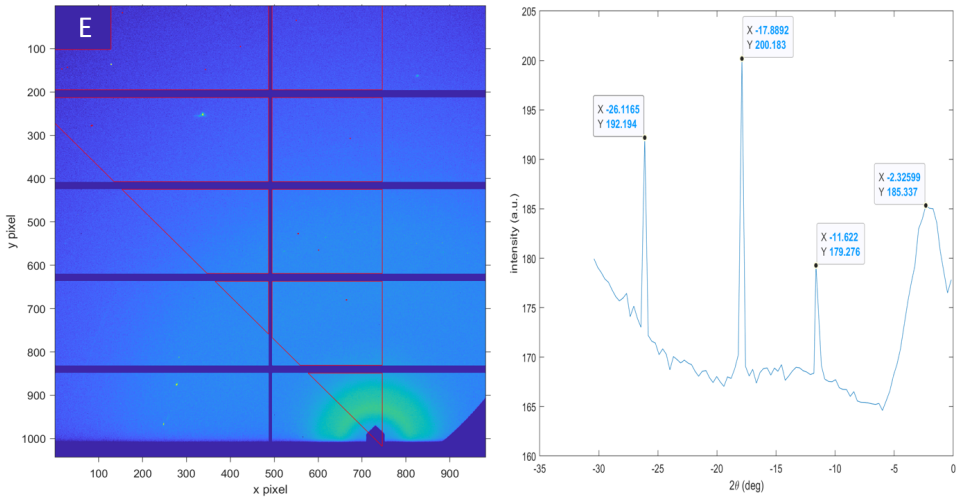

Figure 2.16 Cont.: E) Linecut analysis of 135°-90° phi.

Table 2.7 Indexed Peaks and Associated d-Spacings

Entry	Phi Values	Peak Max	d-Spacing (if 1st Order)
	180°-160°		
1		4.54709°	1.43 nm
2		6.05506°	1.07 nm
3		20.3814°	0.32 nm
	180°-90°		
4		2.93745°	2.21 nm
5		3.84222°	1.69 nm
6		5.07144°	1.28 nm
7		11.6249°	0.56 nm
8		17.9083°	0.36 nm
9		20.3532°	0.32 nm
10		26.1549°	0.25 nm
	180°-135°		
11		4.20854°	1.55 nm
12		11.6382°	0.56 nm
13		20.3667°	0.32 nm
	135°-90°		
14		2.32599°	2.80 nm
15		11.622°	0.56 nm
16		17.8892°	0.37 nm
17		26.1165°	0.25nm

Table 2.7 reveals only the peaks associated with (Hf)PCN-Film. It can be said that several of the diffraction peaks are associated with d-spacing close to those which would be found in a MOF films with TCPP linker (i.e 1.4-3nm).[38,39]

GIWAXS Analysis of (Hf)PCN-Film-(Mn-Cl)

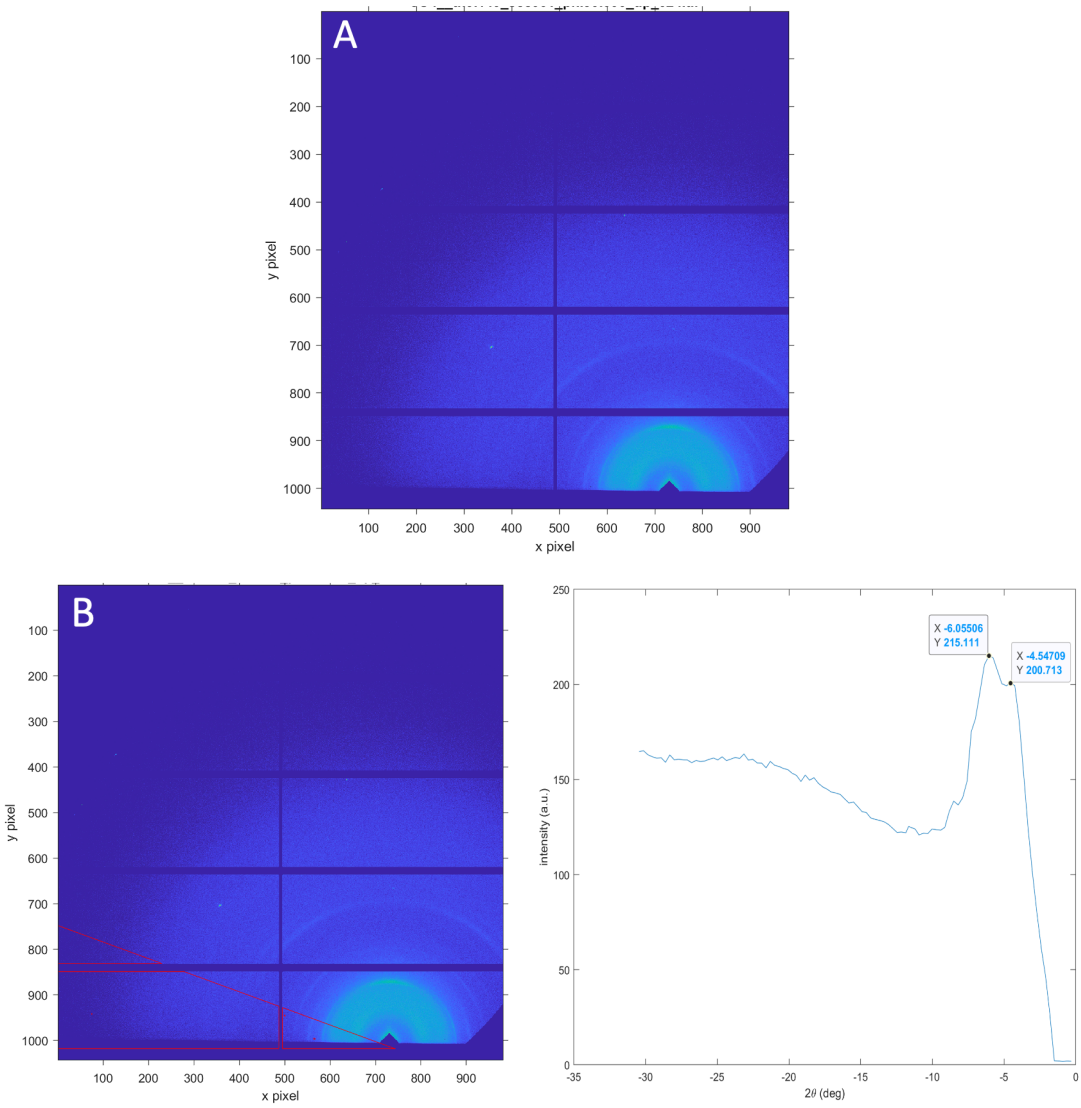

Figure 2.17: GIWAXS analysis of an (Hf)PCN-Film-(Mn-Cl). A) Overall 2D diffraction pattern. B) Linecut analysis of 180°-160° phi.

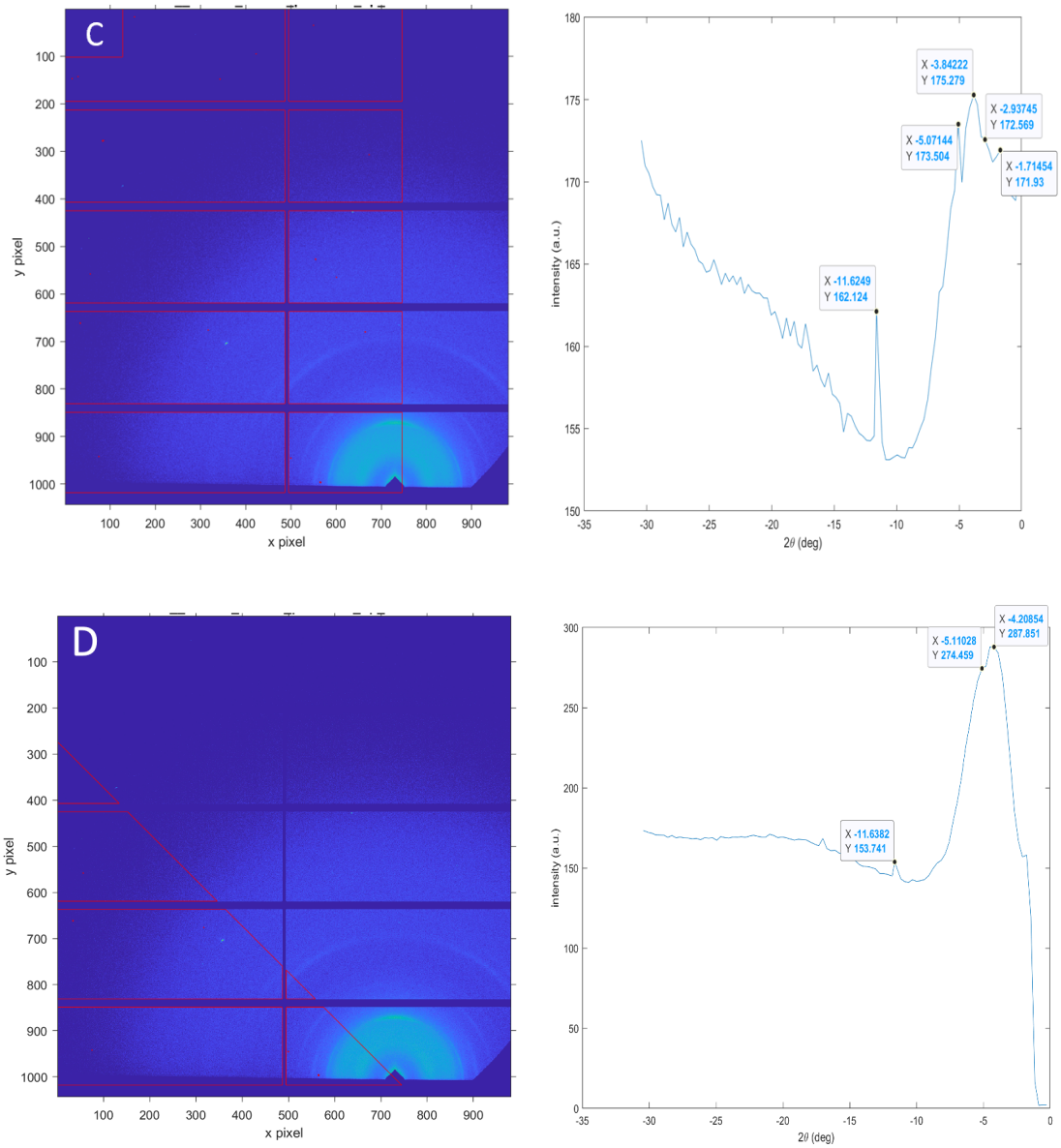

Figure 2.17 Cont.: C) Linecut analysis of 180°-90° phi. D) Linecut analysis of 180°-135° phi.

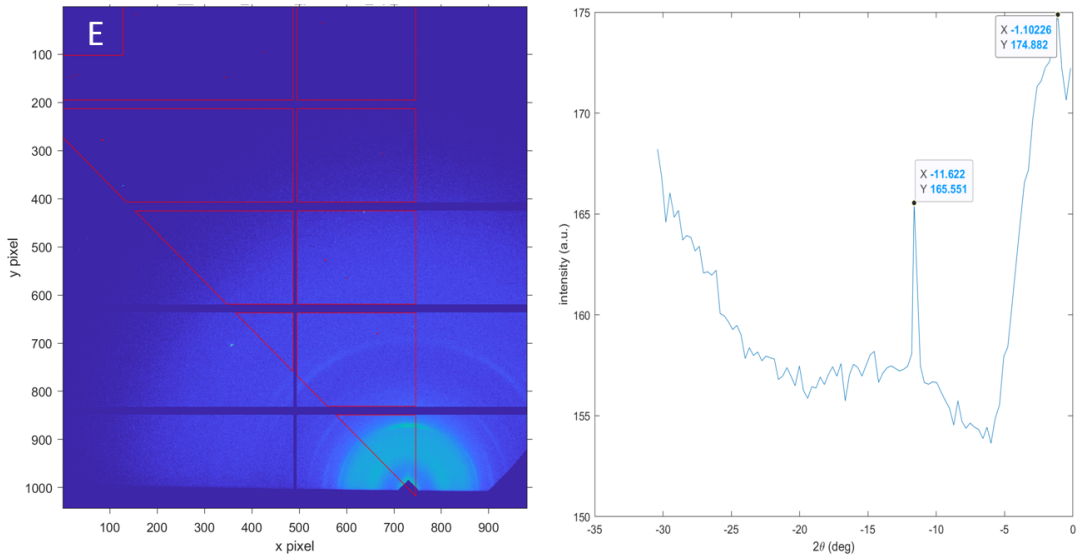

Figure 2.17 Cont.: E) Linecut analysis of 135°-90° phi.

Table 2.8 Indexed Peaks and Associated d-Spacings

Entry	Phi Values	Peak Max	d-Spacing (if 1st Order)
	180°-160°		
1		4.45709°	1.46 nm
2		6.05506°	1.07 nm
	180°-90°		
3		1.71454°	3.79 nm
5		2.93745°	2.21 nm
6		3.84222°	1.69 nm
7		5.07144°	1.28 nm
8		11.6249°	0.56 nm
	180°-135°		
9		4.20854°	1.55 nm
10		5.11028°	1.27 nm
11		11.6382°	0.56 nm
	135°-90°		
12		1.10226°	5.90 nm
13		11.622°	0.56 nm

Table 2.8 reveals the peaks associated with the (Hf)PCN-Film-(Mn-Cl). PCN-type MOFs are often characterized by peaks in the 2θ range for 2°-10°;[40] peaks 1, 2, 5, 6, 7, 9 and 10 are all within this range.

GIWAXS Analysis of (Hf)UiO-PCN Hybrid Film

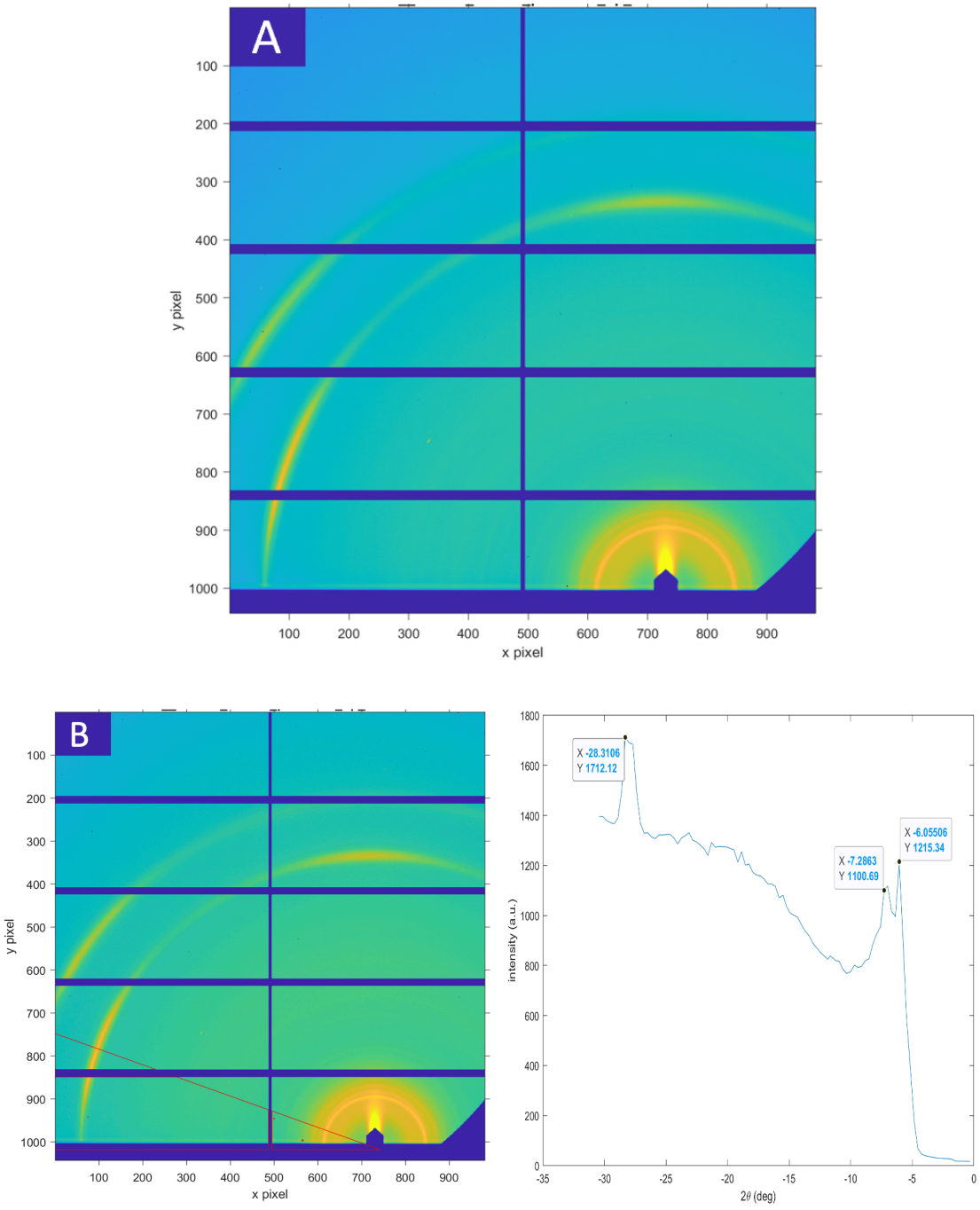

Figure 2.18: GIWAXS analysis of an (Hf)UiO-PCN Hybrid Film. A) Overall 2D diffraction pattern. B) Linecut analysis of 180°-160° phi.

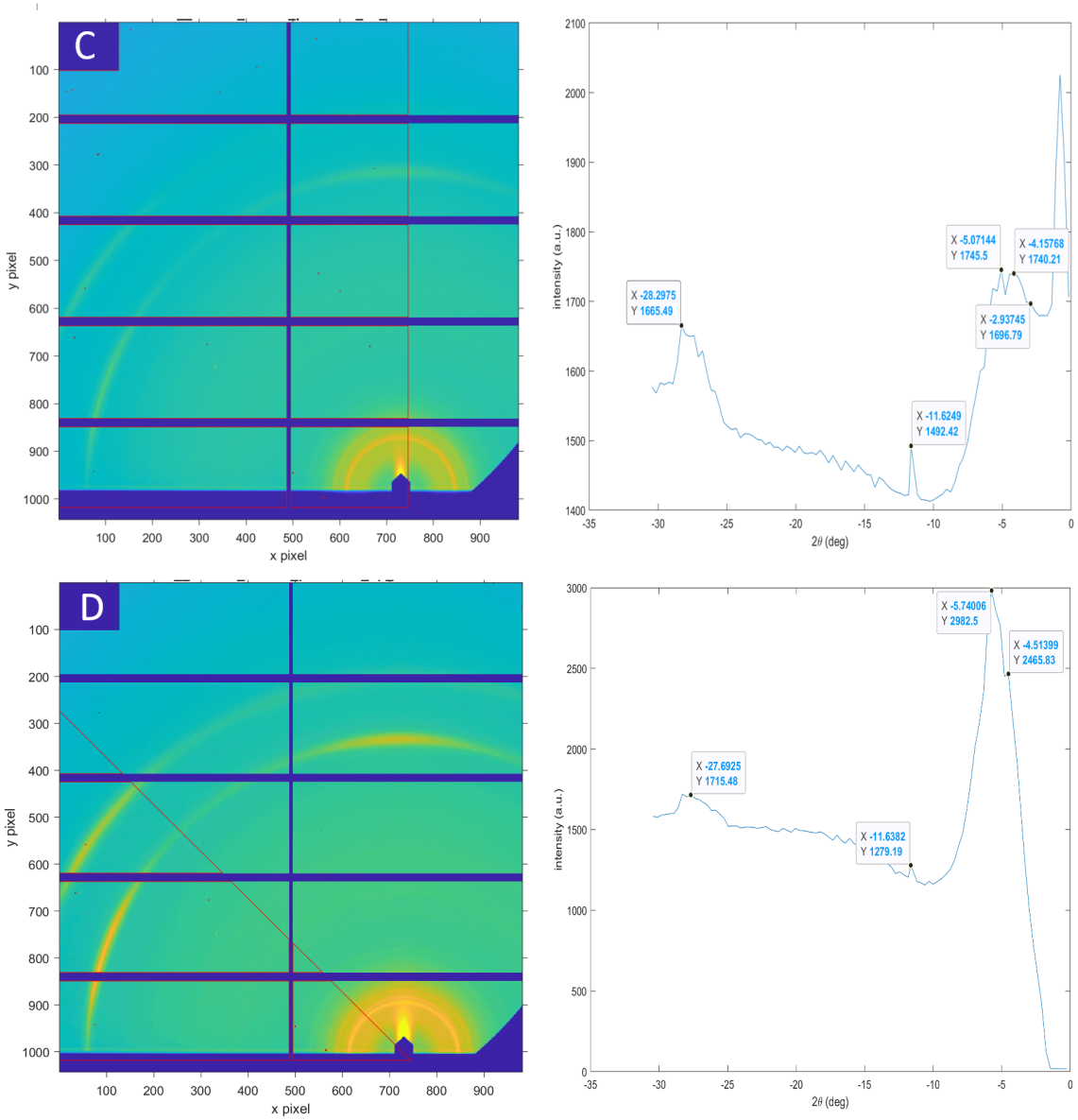

Figure 2.18 Cont.: C) Linecut analysis of 180°-90° phi. D) Linecut analysis of 180°-135° phi.

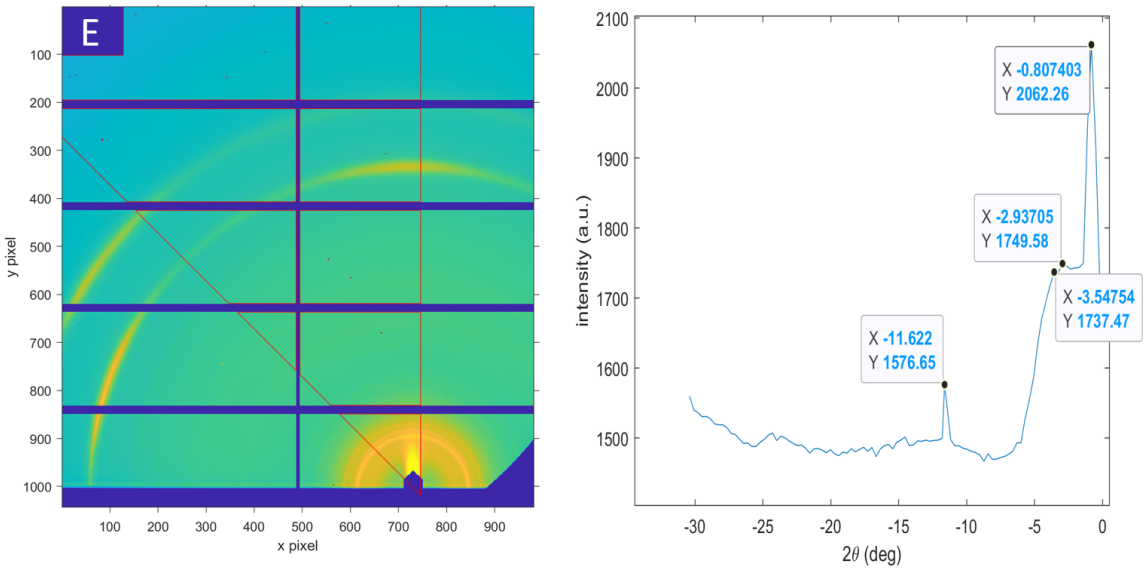

Figure 2.18 Cont.: E) Linecut analysis of 135°-90° phi.

Table 2.9 Indexed Peaks and Associated d-Spacings

Entry	Phi Values	Peak Max	d-Spacing (if 1st Order)
	180°-160°		
1		6.05506°	1.07 nm
2		7.2863°	0.89 nm
3		28.3106°	0.23 nm
	180°-90°		
4		2.93745°	2.21 nm
5		4.15768°	1.56 nm
6		5.07144°	1.28 nm
7		11.6249°	0.56 nm
8		28.2975°	0.23 nm
	180°-135°		
9		4.51399°	1.44 nm
10		5.74006°	1.13 nm
11		11.6382°	0.56 nm
12		27.6925°	0.24 nm
	135°-90°		
12		0.807403°	8.06 nm
13		2.93705°	2.21 nm
14		3.54754°	1.83 nm
15		11.622°	0.56 nm

Table 2.9 reveals the diffraction peaks of the (Hf)UiO-PCN Hybrid Film. Diffraction peaks associated with both the UiO-66(Hf) MOF layer as well as the PCN-type MOF layer. Entries 1 and 2 strongly correlate with the expected signals arising from the (111) and (002) lattice planes of a UiO-66(Hf) MOF, meanwhile the entries 4, 5, 6, 9, 10, 13 and 14 all seem to correlate with signals which would arise from a PCN-type MOF film. Entry 12 is likely a signal arising from reflectance rather than diffraction.

2. CO_2 Fixation by (Hf)PCN-Film-(Zn)

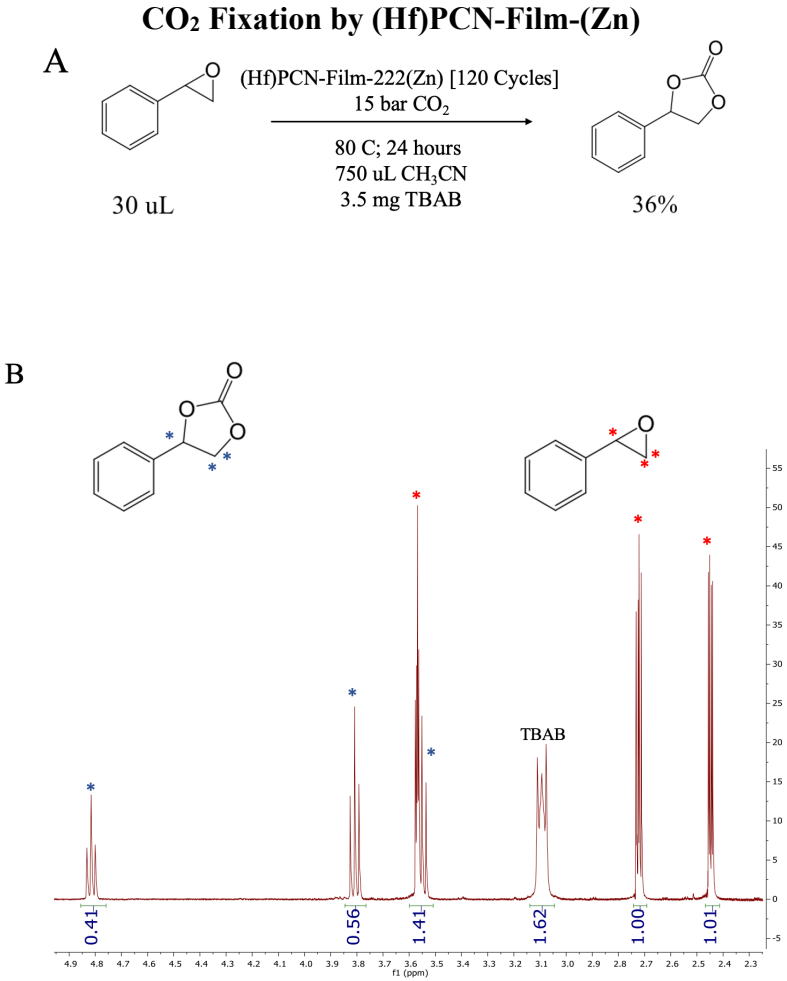

Figure 1.19: CO_2 fixation as catalyzed by the (Hf)PCN-Film-(Zn). A) Overall reaction scheme. B) ^1H NMR analysis of the reaction mixture in acetonitrile-d_3 showing the integrated peaks of styrene oxide (denoted by red asterisks) and styrene carbonate (blue asterisks).

24 Hour CO_2 Fixation Control; Just TBAB

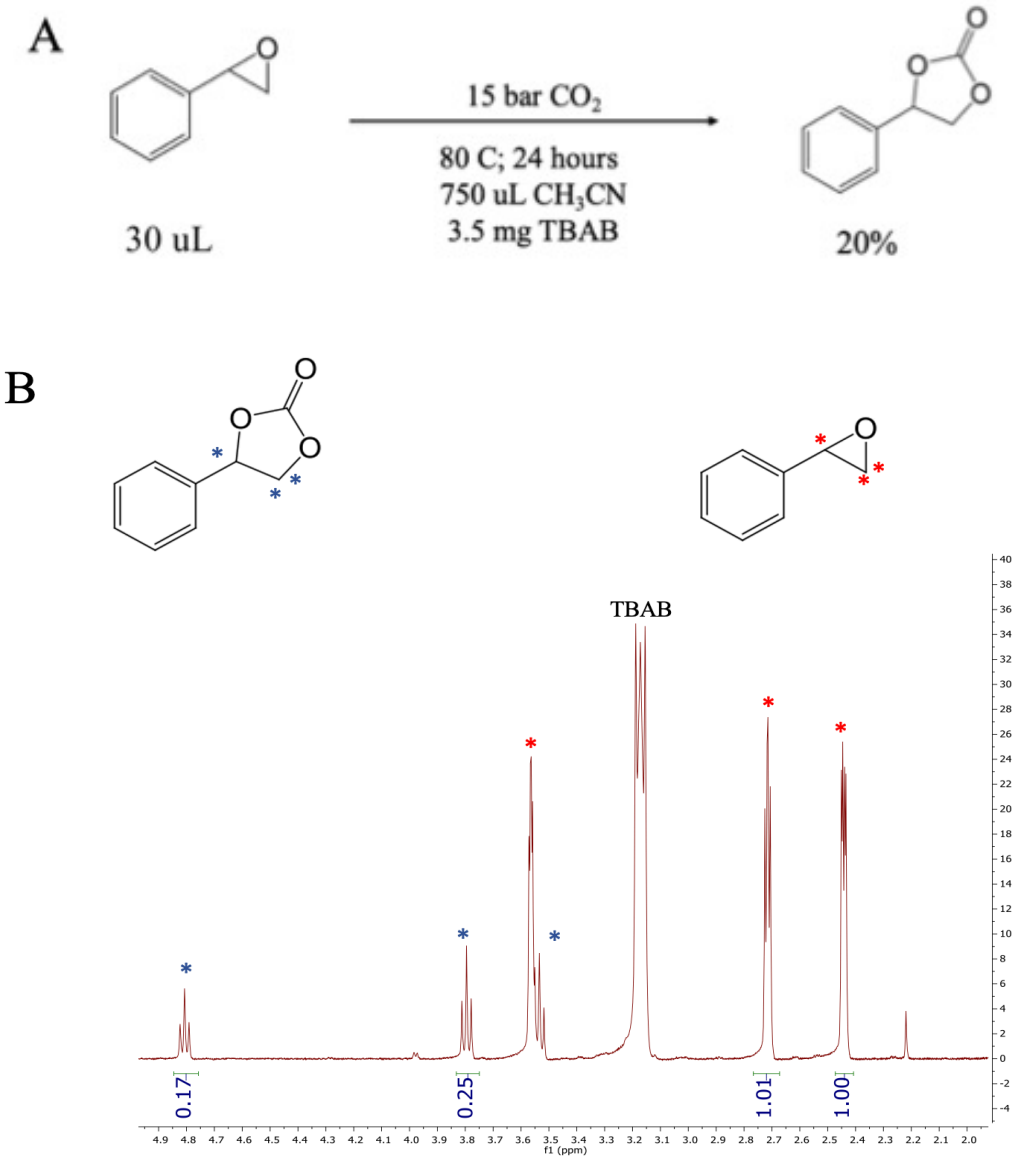

Figure 1.20: CO_2 fixation control reaction at 24 hours. A) Overall reaction scheme. B) ^1H NMR analysis of the reaction mixture in acetonitrile-d_3 showing the integrated peaks of styrene oxide (denoted by red asterisks) and styrene carbonate (blue asterisks).

48 Hour CO_2 Fixation Control; Just TBAB

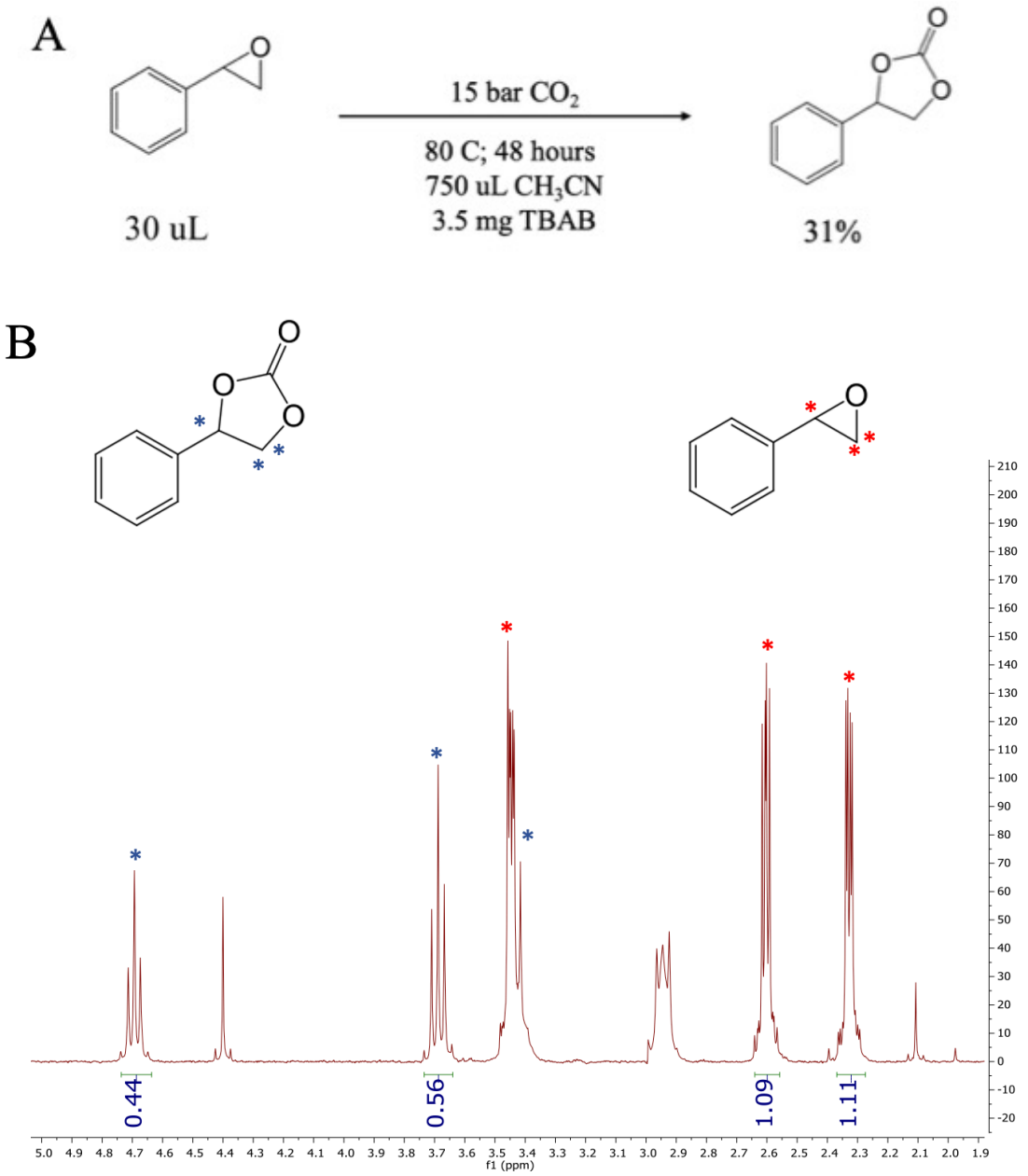

Figure 1.21: CO_2 fixation control reaction at 48 hours. A) Overall reaction scheme. B) ^{1}H NMR analysis of the reaction mixture in acetonitrile-d_3 showing the integrated peaks of styrene oxide (denoted by red asterisks) and styrene carbonate (blue asterisks).

3. Tandem Catalysis by Interchanged Films

Transformation of Styrene to Styrene Carbonate by the Tandem Catalysis of (Hf)PCN-Film-(Zn/Mn interchanged)

A)

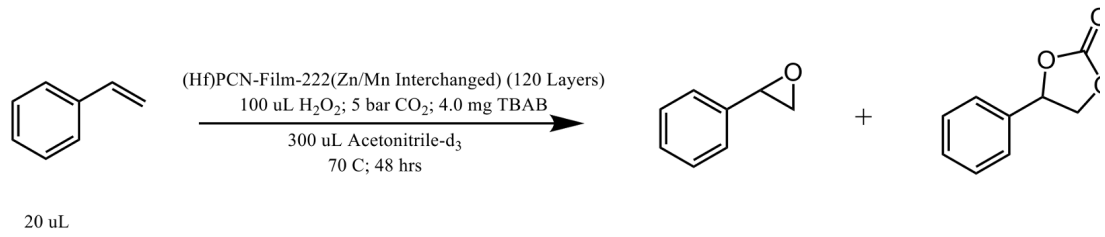

B)

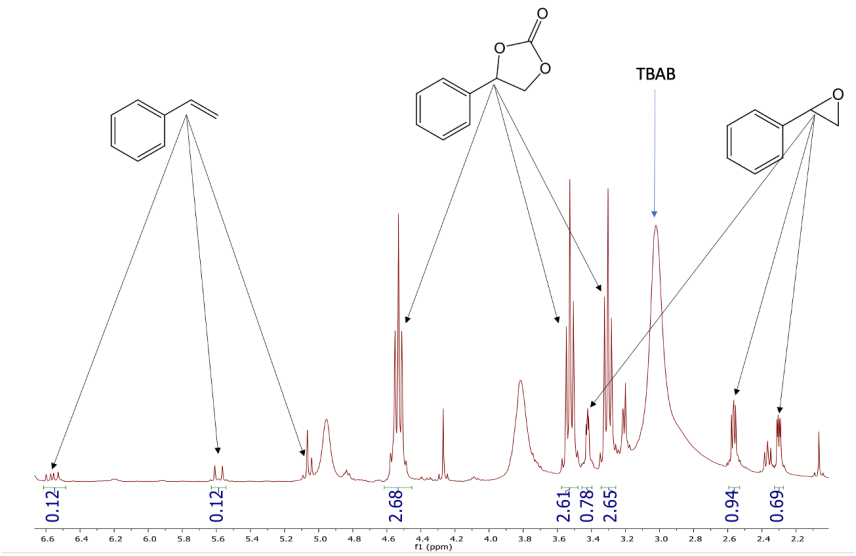

Figure 1.22: Tandem catalysis of the (Hf)PCN-Film-(Zn/Mn interchanged) film for the transformation of styrene to styrene carbonate. A) Overall reaction scheme with the Hf)PCN-Film-(Zn/Mn interchanged) film. B) ^{1}H NMR analysis of the reaction taken in acetonitrile-d_6 on a 400 MHz NMR spectrometer. Peaks associated with styrene, styrene oxide, styrene carbonate and TBAB area all noted. The majority of the styrene has been consumed.

4. Molecular LbL Conditions for the (Hf)UiO-PCN Hybrid Film

Deposition Conditions for the (Hf)UiO-PCN Hybrid Film

A) PCN-222(Hf)	g (SBU) (Hf Cluster)	Minutes in SBU sln/ Temp of sln	SBU modulator solution	Organic linker amount	Minutes in organic linker sln/ Temp of linker sln	Organic Linker Solution	Rinsing (solvent and protocol)	Cycles
Amounts	38.5 mg (0.5 mM)	10 min 70C	0.903 g McOH in 35 mL Ethanol (300 mM)	17.44 mg (3 mM) terephthalic acid	10 min 70 C	0.903 g McOH (300 mM) 1.26 g H_2O (2000 mM) In 35 mL EtOH	Ethanol rinsing, sonication in ethanol every third cycle	120

B) UiO-66 (Hf)	g (SBU) (Hf Cluster)	Minutes in SBU sln/ Temp of sln	SBU modulator solution	Organic linker amount	Minutes in organic linker sln/ Temp of linker sln	Organic Linker Solution	Rinsing (solvent and protocol)	Cycles
Amounts	38.5 mg (0.5 mM)	10 min 70C	0.903 g McOH in 35 mL Ethanol (300 mM)	17.44 mg (3 mM) terephthalic acid	10 min 70 C	0.903 g McOH (300 mM) 1.26 g H_2O (2000 mM) In 35 mL EtOH	Ethanol rinsing, sonication in ethanol every third cycle	120

Figure 2.23: The deposition conditions for the (Hf)UiO-PCN Hybrid Film. A) The conditions used for the deposition of the PCN-(Hf) portion of the film which was deposited atop B) the UiO66 (Hf) portion of the film.

V. References

1. Shekhah, O., Wang, H., Zacher, D., Fischer, R. A. & Wöll, C. Growth Mechanism of Metal–Organic Frameworks: Insights into the Nucleation by Employing a Step-by-Step Route. *Angew. Chemie Int. Ed.* **48**, 5038–5041 (2009).

2. Shekhah, O. *et al.* Step-by-Step Route for the Synthesis of Metal−Organic Frameworks. *J. Am. Chem. Soc.* **129**, 15118–15119 (2007).

3. Semrau, A. L. *et al.* Highly Porous Nanocrystalline UiO-66 Thin Films via Coordination Modulation Controlled Step-by-Step Liquid-Phase Growth. *Cryst. Growth Des.* **19**, 1738–1747 (2019).

4. Wannapaiboon, S. *et al.* Enhanced properties of metal–organic framework thin films fabricated via a coordination modulation-controlled layer-by-layer process. *J. Mater. Chem. A* **5**, 13665–13673 (2017).

5. Tsuruoka, T. *et al.* Nanoporous Nanorods Fabricated by Coordination Modulation and Oriented Attachment Growth. *Angew. Chemie Int. Ed.* **48**, 4739–4743 (2009).

6. Forgan, R. S. Modulated self-assembly of metal–organic frameworks. *Chem. Sci.* **11**, 4546–4562 (2020).

7. Pham, M.-H., Vuong, G.-T., Fontaine, F.-G. & Do, T.-O. Rational Synthesis of Metal–Organic Framework Nanocubes and Nanosheets Using Selective Modulators and Their Morphology-Dependent Gas-Sorption Properties. *Cryst. Growth Des.* **12**, 3091–3095 (2012).

8. Hinman, J. G., Turner, J. G., Hofmann, D. M. & Murphy, C. J. Layer-by-Layer Synthesis of Conformal Metal–Organic Framework Shells on Gold Nanorods. *Chem. Mater.* **30**, 7255–7261 (2018).

9. Semrau, A. L. & Fischer, R. A. High-Quality Thin Films of UiO-66-NH2 by Coordination Modulated Layer-by-Layer Liquid Phase Epitaxy. *Chem. – A Eur. J.* **27**, 8509–8516 (2021).

10. Semrau, A. L. *et al.* Substantial Turnover Frequency Enhancement of MOF Catalysts by Crystallite Downsizing Combined with Surface Anchoring. *ACS Catal.* **10**, 3203–3211 (2020).

11. Guo, Q. & Li, F. Self-assembled alkanethiol monolayers on gold surfaces: resolving the complex structure at the interface by STM. *Phys. Chem. Chem. Phys.* **16**, 19074–19090 (2014).

12. Weisbecker, C. S., Merritt, M. V & Whitesides, G. M. Molecular Self-Assembly of Aliphatic Thiols on Gold Colloids. *Langmuir* **12**, 3763–3772 (1996).

13. Wei, R. *et al.* Tuning the Properties of Zr6O8 Nodes in the Metal Organic Framework UiO-66 by Selection of Node-Bound Ligands and Linkers. *Chem. Mater.* **31**, 1655–1663 (2019).

14. Dengfa, L. & Yuming, W. The "Hook Effect" of X-Ray Diffraction Peak Broadening of Multilayer Thin Films. *Powder Diffr.* **2**, 180–182 (1987).

15. Hu, Z., Nalaparaju, A., Peng, Y., Jiang, J. & Zhao, D. Modulated Hydrothermal Synthesis of UiO-66(Hf)-Type Metal–Organic Frameworks for Optimal Carbon Dioxide Separation. *Inorg. Chem.* **55**, 1134–1141 (2016).

16. Sun, Y., Song, C., Guo, X. & Liu, Y. Concurrent Manipulation of Out-of-Plane and Regional In-Plane Orientations of NH2-UiO-66 Membranes with Significantly Reduced Anisotropic Grain Boundary and Superior H2/CO2 Separation Performance. *ACS Appl. Mater. Interfaces* **12**, 4494–4500 (2020).

17. Jakobsen, S. *et al.* Structural determination of a highly stable metal-organic framework with possible application to interim radioactive waste scavenging: Hf-UiO-66. *Phys. Rev. B* **86**, 125429 (2012).

18. Sawaguchi, T., Sato, Y. & Mizutani, F. Ordered structures of self-assembled monolayers of 3-mercaptopropionic acid on Au(111): in situ scanning tunneling microscopy study. *Phys. Chem. Chem. Phys.* **3**, 3399–3404 (2001).

19. Wu, H. *et al.* Unusual and Highly Tunable Missing-Linker Defects in Zirconium Metal–Organic Framework UiO-66 and Their Important Effects on Gas Adsorption. *J. Am. Chem. Soc.* **135**, 10525–10532 (2013).

20. Gilles, B. *Grazing incidence diffraction : A review*. http://inis.iaea.org/search/search.aspx?orig_q=RN:28044557 (1996).

21. Lausund, K. B., Olsen, M. S., Hansen, P.-A., Valen, H. & Nilsen, O. MOF thin films with bi-aromatic linkers grown by molecular layer deposition. *J. Mater. Chem. A* **8**, 2539–2548 (2020).

22. Pereira, M. M., Dias, L. D. & Calvete, M. J. F. Metalloporphyrins: Bioinspired Oxidation Catalysts. *ACS Catal.* **8**, 10784–10808 (2018).

23. Singh, R. & Mukherjee, A. Metalloporphyrin Catalyzed C–H Amination. *ACS Catal.* **9**, 3604–3617 (2019).

24. Nakagaki, S., Ferreira, G. K., Ucoski, G. M. & Dias de Freitas Castro, K. A. Chemical Reactions Catalyzed by Metalloporphyrin-Based Metal-Organic Frameworks. *Molecules* vol. 18 (2013).

25. Sakamaki, Y. *et al.* Metal–Organic Frameworks and Covalent Organic Frameworks as Platforms for Photodynamic Therapy. *Comments Inorg. Chem.* **38**, 238–293 (2018).

26. Zhang, J.-L., Liu, Y.-L. & Che, C.-M. Chiral ruthenium porphyrin encapsulated in ordered mesoporous molecular sieves (MCM-41 and MCM-48) as catalysts for asymmetric alkene epoxidation and cyclopropanation. *Chem. Commun.* 2906–2907 (2002) doi:10.1039/B209276J.

27. Yang, D. & Gates, B. C. Catalysis by Metal Organic Frameworks: Perspective and Suggestions for Future Research. *ACS Catal.* **9**, 1779–1798 (2019).

28. Rayati, S. & Nafarieh, P. A practical innovative method for highly selective oxidation of alkenes and alkanes using Fe (III) and Mn (III) porphyrins supported onto multi-wall carbon nanotubes as reusable heterogeneous catalysts. *Appl. Organomet. Chem.* **33**, e4789 (2019).

29. Chen, A., Zhang, Y., Chen, J., Chen, L. & Yu, Y. Metalloporphyrin-based organic polymers for carbon dioxide fixation to cyclic carbonate. *J. Mater. Chem. A* **3**, 9807–9816 (2015).

30. Beyzavi, M. H. *et al.* Metal–Organic Framework-Based Catalysts: Chemical Fixation of CO2 with Epoxides Leading to Cyclic Organic Carbonates . *Frontiers in Energy Research* vol. 2 63 (2015).

31. Carrasco, S., Sanz-Marco, A. & Martín-Matute, B. Fast and Robust Synthesis of Metalated PCN-222 and Their Catalytic Performance in Cycloaddition Reactions with CO2. *Organometallics* **38**, 3429–3435 (2019).

32. Chan, W.-K., Liu, P., Yu, W.-Y., Wong, M.-K. & Che, C.-M. Highly Diastereoselective Epoxidation of Allyl-Substituted Cycloalkenes Catalyzed by Metalloporphyrins. *Org. Lett.* **6**, 1597–1599 (2004).

33. Wang, Z. *et al.* Defect Creation in Surface-Mounted Metal–Organic Framework Thin Films. *ACS Appl. Mater. Interfaces* **12**, 2655–2661 (2020).

34. Connolly, B. M. *et al.* Tuning porosity in macroscopic monolithic metal-organic frameworks for exceptional natural gas storage. *Nat. Commun.* **10**, 2345 (2019).

35. Jiang, Z. {\it GIXSGUI}: a MATLAB toolbox for grazing-incidence X-ray scattering data visualization and reduction, and indexing of buried three-dimensional periodic nanostructured films. *J. Appl. Crystallogr.* **48**, 917–926 (2015).

36. InstaNANO. https://instanano.com/characterization/calculator/xrd/d-value/.

37. Torres-Mendieta, R. *et al.* In situ decoration of graphene sheets with gold nanoparticles synthetized by pulsed laser ablation in liquids. *Sci. Rep.* **6**, 30478 (2016).

38. Yu, C.-J., Krzyaniak, M. D., Fataftah, M. S., Wasielewski, M. R. & Freedman, D. E. A concentrated array of copper porphyrin candidate qubits. *Chem. Sci.* **10**, 1702–1708 (2019).

39. Chen, B. *et al.* Ultrasensitive, rapid and selective sensing of hazardous fluoride ion in aqueous solution using a zirconium porphyrinic luminescent metal-organic framework. *Anal. Chim. Acta* **1145**, 95–102 (2021).

40. Yu, K., Won, D.-I., Lee, W. I. & Ahn, W.-S. Porphyrinic zirconium metal-organic frameworks: Synthesis and applications for adsorption/catalysis. *Korean J. Chem. Eng.* **38**, 653–673 (2021).

D. Chapter 3: Bulk Deposition of UiO-66(Hf) Films for the Fixation of CO_2 to Epoxides for the Synthesis of Cyclic Carbonates

I. Introduction:

The release of CO_2 into the atmosphere as a result of human action has increased the level of CO_2 in the atmosphere such that current levels of CO_2 are the highest in 20 million years.[1] Current scientific consensus states that elevated levels of CO_2 pose a severe threat to the ecosystems across the globe, causing a rise in global temperatures and acidification of the planet's oceans. A potential strategy to reducing the amounts of CO_2 gas in the atmosphere is to make possible the valorization of CO_2 as a chemical feedstock, and towards this end reactions which utilize CO_2 are highly desirable.[2] One potential reaction which has been identified as a promising method to valorize CO_2 is the ring expansion of epoxides to cyclic carbonates.[3,4] MOFs which serve as heterogenous catalysts to enhance the rate of this ring expansion are well known.[5,6] Action of the MOF catalysts proceeds through the Lewis acidity of metal centers which activate the epoxide through coordination to the oxygen atom thus encouraging ring-opening of the epoxide by the Br^- of TBAB (**Figure 3.1**).

The UiO-66 MOF has been of particular interest as a reliable platform for the CO_2 fixation noted for its reliable synthesis and high stability.[7–9] It has also been shown that Hf-MOFs have a greater Lewis acidity at the metal-oxo center and so perform greater for CO_2 fixation.[10] Of further interest to the author was the study my Semrau et al which describes the increased turnover frequency number of Lewis-acid catalysis in UiO-66 thin films.[11] Considering these two developments, it was decided to pursue the development of UiO-66 (Hf) thin films as catalysts for the fixation of CO_2 to epoxides. While the molecular LbL deposition of UiO-66 (Hf) was shown to be possible, it is a technically difficult procedure which requires specialized

instrumentation and can only produce one wafer at a time. Seeking to develop a simpler method for the deposition of UiO-66 (Hf) films the author decided to investigate the strategies for the bulk deposition of UiO-66 (Hf) films onto substrates. It was envisioned that the development of such films would prove to be a valuable material for the sequestration of CO_2.

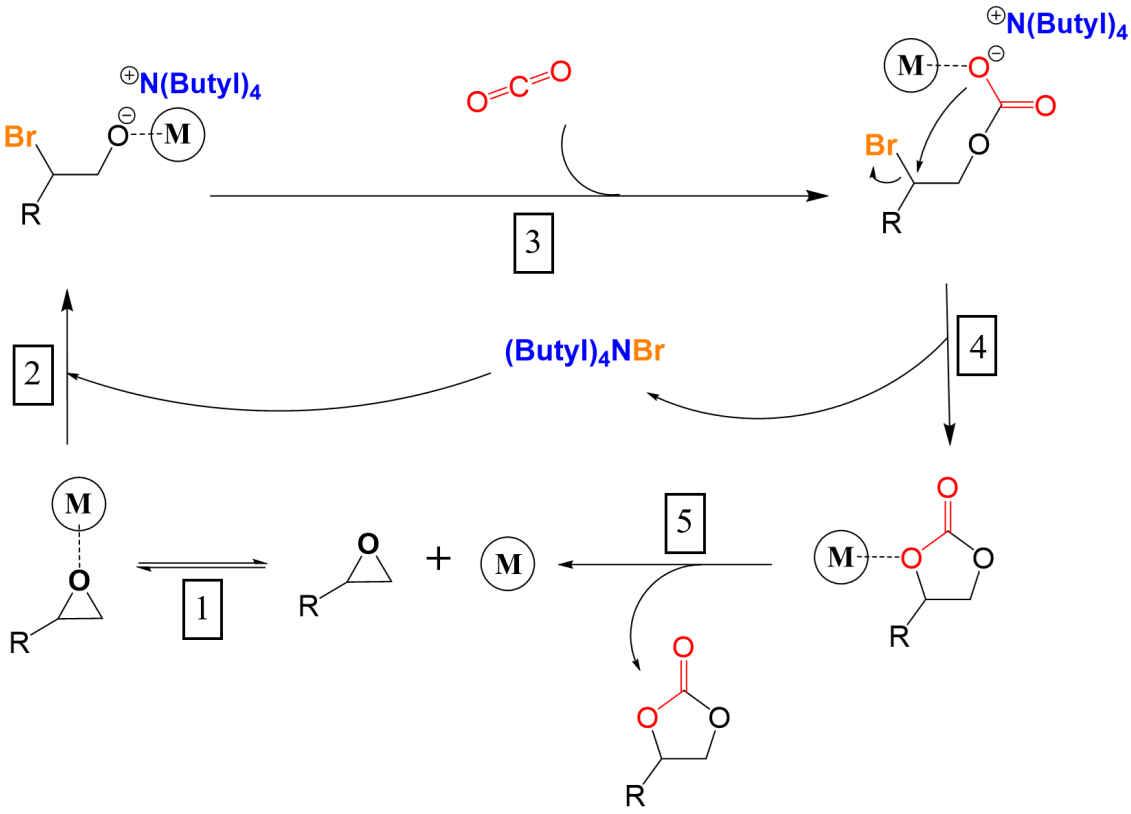

Figure 3.1: Mechanism for the fixation of CO_2 to an epoxide for the synthesis of a cyclic carbonate. Step 1: Activation of the epoxide through coordination of the metal (M) Step 2: Ring opening of the epoxide by the TBAB co-catalyst. Step 3: Insertion of CO_2 followed by Step 4: Ring closure for formation of the cyclic carbonate. Step 5: Regeneration of the Lewis acid center.

II. Bulk Deposition of UiO-66 and UiO-66 (Hf)

Some previous methods for the deposition of UiO-66 films included molecular LbL deposition,[12] gas-phase atomic layer deposition[13] and solution shearing;[14] however all these methods are labor intensive and require specialized instrumentation. Having met success with the

deposition of UiO-66 (Hf) onto the MHDA-functionalized wafers via molecular LbL deposition, it was decided that the same substrates would be used for the bulk deposition. It was hoped that the COOH functionalized surface would serve as an appropriate method to initiate crystal growth onto the surface of the film. While traditional methods for the bulk synthesis of UiO-66 require only solvothermal synthesis, which is suitably simple, long crystallization times are required and efforts to immerse substrates into the solvothermal synthesis of UiO-66 (Hf)[15] did not provide films which readily diffracted after rinsing. Seeing as the traditional solvothermal syntheses are not suitable, alternative routes were explored with the goal of finding a method for the bulk deposition of films suitable for catalysis. Ultimately it was discovered that a procedure developed for the room-temperature synthesis of UiO-66 developed by DeStefano et al[16] was capable of depositing films of both UiO-66 and UiO-66(Hf) onto MHDA-functionalized films. High quality films of both UiO-66 and UiO-66 (Hf) were developed and the films of UiO-66(Hf) were shown to be excellent catalysts for the fixation of CO_2 to epoxides for cyclic carbonate synthesis.

1. Bulk Deposition of UiO-66, UiO-66 (OH) and UiO-66 (NH_2)

The MOF synthesis itself takes place in several steps in one reactor (Scheme 3.1), first the metal alkoxide is mixed into a DMF/acetic acid solution and heated for two hours, then the organic linker is added and heating terminated while stirring is maintained for 12 hours. Coating of the wafers took place by suspending the wafers into the reaction mixture directly after the dissolution of the organic linker. Similar to the procedure used to coat the wafers by hand, the wafers were suspending in the mixture by piercing a pair of reverse grip tweezers through a septum. The complete procedure can be found in the experimental section. To begin explorations into the development of bulk deposited thin films the initial explorations aimed to successfully

deposit films of UiO-66, only after successful deposition of UiO-66 would the more expensive Hf analogues be used for the synthesis of UiO-66 (Hf). One interesting feature of this procedure was the adaptability of the bulk deposition technique to be used for the deposition of various functionalized UiO-66 analogues including UiO-66-OH[17] and UiO-66-NH_2.[18]

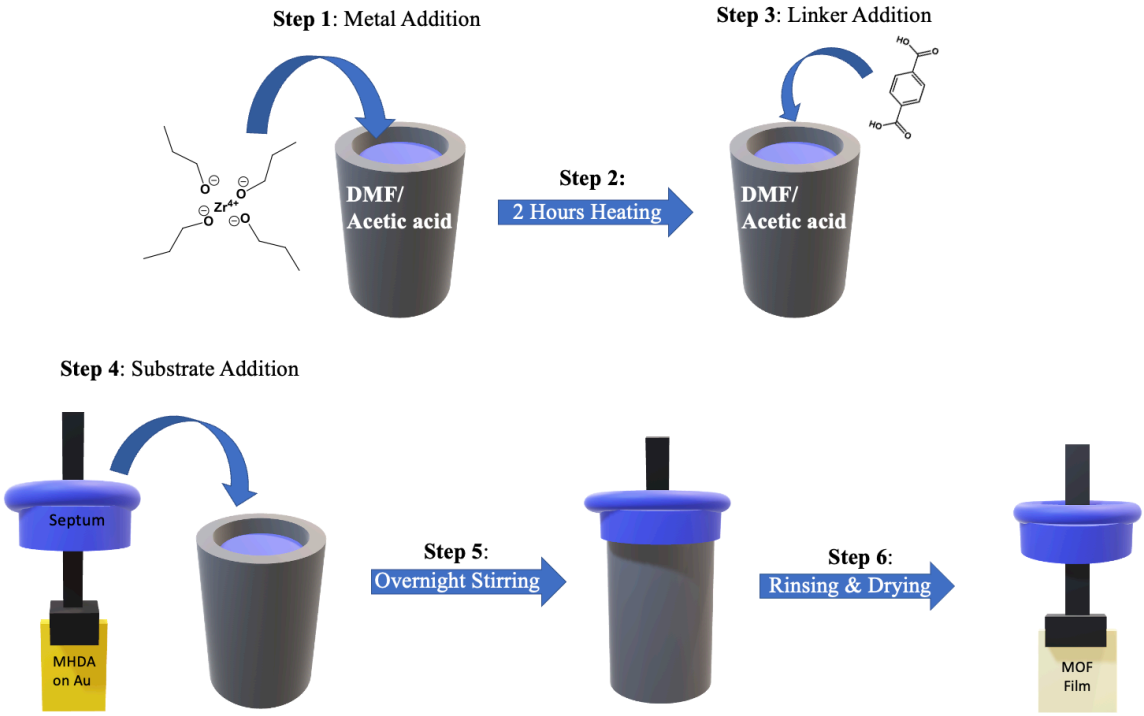

Scheme 3.1: Depiction of the bulk deposition procedure. The procedure begins by adding the metal alkoxide into a 4/7 mixture of acetic acid/DMF while stirring is initiated (Step 1) the solution is then heated for 2 hours at 130 C (Step 2). After heating the metal alkoxide the solution the organic linker is added (Step 3) then the suspended wafer which is fixed to a septum is fixed to the top of the vial and the wafer is suspended in the solution (Step 4) while it is left to stir overnight (Step 5). After stirring overnight the wafer is rinsed in DMF and Acetone then dried for 12 hours in a vacuum oven at 80C (Step 6).

The procedure for the UiO-66 was adapted from the procedure by DeStefano et al,[16] with the only difference being that films of UiO-66 were synthesized onto MHDA-Functionalized Au-coated silicon wafers of dimension 1cm x 2cm. First a solution of 22 mL solution of acetic acid/DMF (4:7) was charged into a glass vial, 71 uL of zirconium isopropoxide (70% in propanol) was added to the solution and the solution heated to 130 C under stirring, open to atm.

After 2 hours of heating, 75 mgs of terephthalic acid is added to the solution and upon dissolution of the acid the heating is turned off but stirring continues. A rubber septum with the MHDA functionalized wafer is affixed to the top of the septum such that the wafer is suspended in the solution, stirring is maintained and the height of the wafer in the solution is such that the stir bar will not come into contact with the wafer. The solution is left to stir overnight with the wafer suspended in the solution. After roughly 12 hours of stirring the wafer can be removed and is rinsed with DMF three times by suspending in clean DMF for 10 minutes per rinse, then rinsed for 10 minutes in acetone 3 times. The wafers were then dried overnight in a vacuum oven set to 80 C and 100 mbar. The wafers were then diffracted by standard out-of-plane X-ray diffraction to reveal the pattern of UiO-66. This procedure was able to also produce films of UiO-66-OH and UiO-66-NH_2. These isostructural analogs of UiO-66 differ only in the structure of their organic linkers: UiO-66-OH utilizes 2-hydroxyterephthalic acid and UiO-66-NH_2 utilizes 2-amino terephthalic acid. In the case of UiO-66-OH, 21 mg of 2-hydroxyterephthalic acid is used, in the case of the UiO-66-NH_2 82 mg of 2-amino terephthalic acid is used. The diffraction patterns of the wafers can be seen in Figure 3.2.

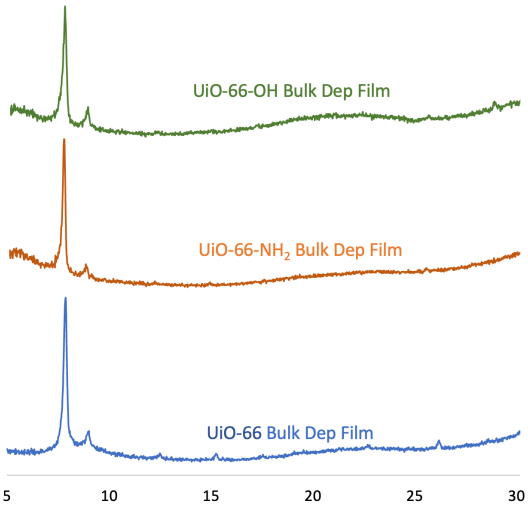

Figure 3.2: Diffraction patterns of the UiO-66, UiO-66-OH and UiO-66-NH_2 Bulk Dep Films

2. Bulk Deposition UiO-66 (Hf), UiO-66-OH (Hf) and UiO-66-NH_2 (Hf)

For the deposition of the UiO-66 (Hf) a Hf alkoxide was used as the metal source. The deposition was initiated by heating 75 uL of hafnium butoxide in 20 mL of a 4/7 acetic acid/DMF solution at 130 C for two hours. Just like the procedure for the UiO-66 bulk deposited film, 75 mg of terephthalic acid was then added to the mixture and the solution allowed to cool to room temperature. After addition of the organic linker the wafer is added to the mixture and solution stirred while the wafer is suspended in the mixture. After overnight suspension in the mixture wafers were removed from solution coated in a UiO-66 (Hf) film. Replacing the terephthalic acid with 2-hydroxy terephthalic acid (21 mg) or 2-amino terephthalic (82 mg) acid gives UiO-66-OH (Hf) and UiO-66-NH_2 (Hf) respectively. Wafers were analyzed with X-ray diffraction to confirm the structure of the film (Figure 3.3). Bulk deposited films of UiO-66 (Hf) were also analyzed with GIWAXS analysis to show that highly anisotropic crystallinity.

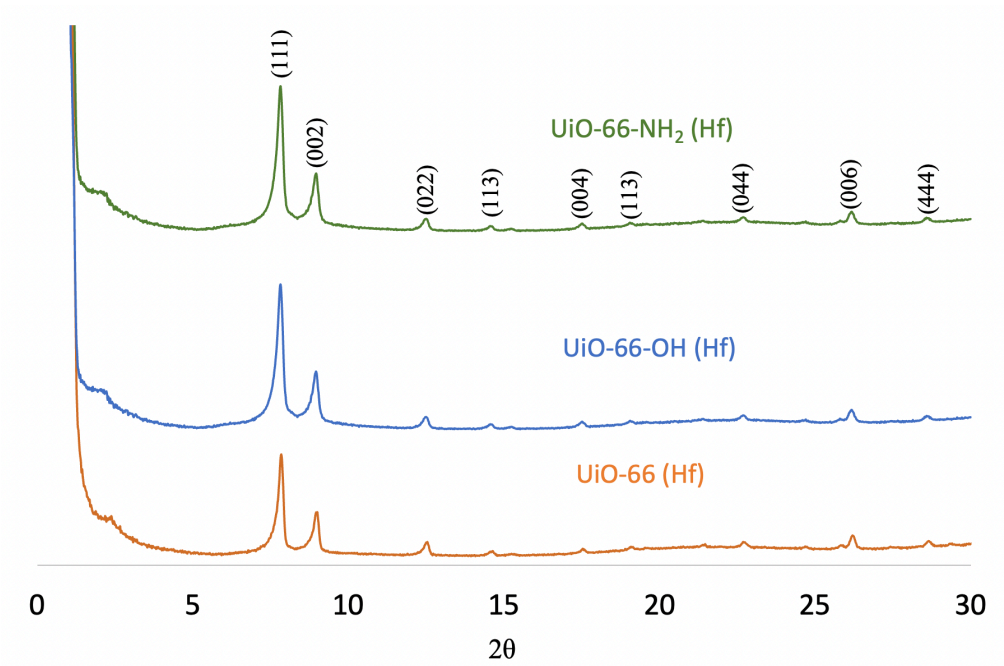

Figure 3.3: X-ray diffraction pattern of UiO-66 (Hf) Bulk Dep films and the functionalized structural analogs, UiO-66-OH (Hf) and UiO-66-NH_2 (Hf).

It is the belief of the author that the bulk deposition for UiO-66 and UiO-66 (Hf) is especially effective in this method due to the two-step MOF solvothermal synthesis process. Namely the initial heating step wherein the metal alkoxide is first reacted with acetic acid in DMF. It is probable that during this step the formation of discreet metal-oxo clusters, similar to the methacrylate or benzoate capped clusters are forming, but with acetic acid as a capping ligand. Upon addition of the organic linker ligand exchange between the organic linkers and acetic acid cappers might be the initiator for MOF crystallization. This unique route to MOF synthesis might be the reason that bulk deposition of a film on the surface of the MHDA-functionalized wafers is possible. It should be noted that through this method deposition of a stable MOF film only takes place on the Au-coated wafer surface. The side of the wafer which remains bare Si is devoid of a MOF film after rinsing with stirred DMF and acetone.

Compared to the thin films fabricated by molecular LbL deposition, the bulk deposited wafers UiO-66 (Hf) thin films showed a higher level of crystallinity, as indicated by greater intensity of diffraction peaks as well as the appearance of a greater number of peaks associated with lattice planes of the UiO-66 topology. For the molecular LbL grown films only the (111) and (002) peaks were observed however for the bulk deposited UiO-66 (Hf) films nine Miller indices could be identified. SEM analysis also shows that that bulk deposited films of UiO-66 (Hf) were robust and covered the surface uniformly, the film was also visible as a white film coating the gold surface (Figure 3.4). One interesting note that should be made concerning the XRD pattern is the presence of a small hump at roughly 2.5°, this signal in the XRD diffraction pattern can be the result of defects in the MOF structure, specifically missing cluster defects.[19,20] GIWAXS analysis was also carried out on samples of UiO-66 (Hf) bulk deposition samples with the intent of further confirming the crystallinity of the film and to reveal any potential orientation

of the growth. Ultimately the GIWAXS analysis did reveal a highly crystallin film with the streaking of diffraction peaks indicating isotropic growth of crystal domains (Section IV: Experimental Data).

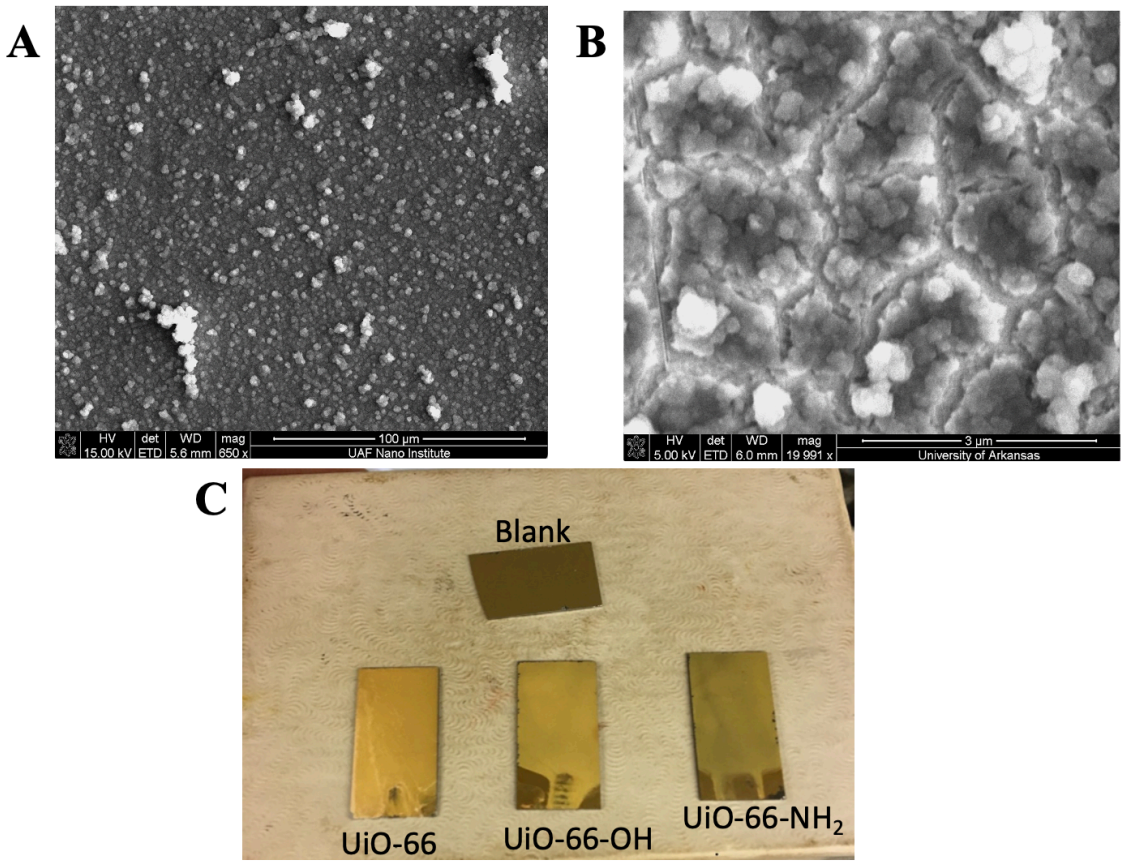

Figure 3.4: Visual analysis of the bulk deposited film A) SEM analysis at 650x magnification of UiO-66 (Hf) shows the uniform coverage of the surface with a MOF film B) SEM analysis of UiO-66 (Hf) at ~20000x magnification showing the rough texture of the film in detail. C) Visual inspection of the UiO-66 (Hf), UiO-66-OH (Hf) and UiO-66-NH_2 (Hf) films showing the obvious visual coverage.

In comparison to the UiO-66 (Hf) films grown by molecular LbL deposition, the bulk deposited UiO-66 (Hf) films were had a much rougher as observed by AFM (Figure 3.5). Increased roughness as the surface will increase the overall external surface area of the film and might aid in catalysis. The amount of MOF was also greater, the amount was determined by massing wafers before and after deposition, rinsing and thorough drying. Out of three massed

UiO-66 (Hf) wafers the average difference in mass was found to be 0.11 mg, the same experiment for the wafers subject to molecular LbL epitaxy did not yield a detectable change in mass. This increased in MOF loading also can increase the catalytic activity.

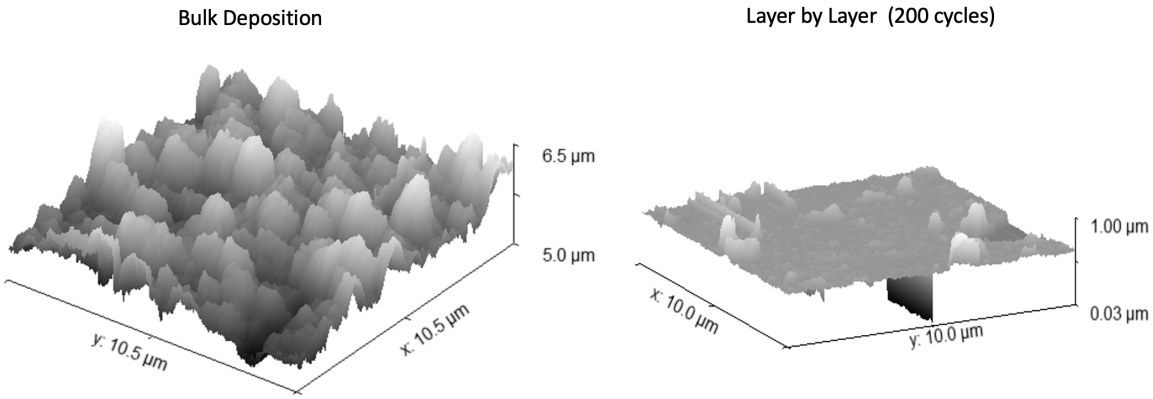

Figure 3.5: Atomic force microscopy analysis of the bulk deposited UiO-66 (Hf) film and a UiO-66 (Hf) film synthesized by 200 cycles of molecular LbL deposition.

III. Bulk Deposited UiO-66 (Hf) Films as a Catalyst for CO_2 Fixation

With the development of a reliable procedure for the synthesis of UiO-66(Hf) films it was decided to then pursue investigations into the ability of such films to catalyze the fixation of CO_2 to epoxides for the synthesis of cyclic carbonates. It was hypothesized that bulk deposited UiO-66(Hf) films would be a exceptional heterogenous catalyst that would promote ring expansion of epoxides to cyclic carbonates through the action of the TBAB salt. The two model epoxides selected for the catalytic tests were propylene oxide and styrene oxide. Styrene oxide is a known carcinogen and teratogen and proper ventilation should be used in handling both styrene oxide and propylene oxide. For experimental purposes, these two molecules were different in size and electronics such that some differences in the catalytic action would be expected.

1. Control Reactions for CO_2 Fixation to Propylene Oxide and Styrene Oxide for the Synthesis of Cyclic Carbonates

The first tests were conducted were control reaction which took place to monitor the effectiveness of just TBAB to promote the ring expansion of epoxides with CO_2. The reactions were tested with 505 mg of propylene oxide (8.7 mmol) with 280 mg of TBAB (0.87 mmol) added, 250 uL of CH_3CN was added to the reaction for the purpose of solvating the TBAB. The reactions took place at 60 C and were monitored by 1H NMR analysis every 12 hours for 48 hours total. Reactions were tested at 1 bar and 5 bar CO_2, reactions at 1 bar refer to gauge pressure. Reactions of styrene oxide took place on the same molar scale (10:1 styrene oxide to TBAB) and took place a 60 C as well, no acetonitrile was needed for the styrene oxide reactions as the reactant itself suitable solvent enough. At the 5 bar control condition for the conversion of propylene oxide to propylene carbonate was complete after 48 hours, at 1 bar the percent conversion after 48 hours was 86%. For the conversion of styrene oxide to styrene carbonate at 5 bar 87.9% conversion was achieved after 48 hours, at 1 bar only 52.7% conversion was achieved after 48 hours (Figure 3.6).

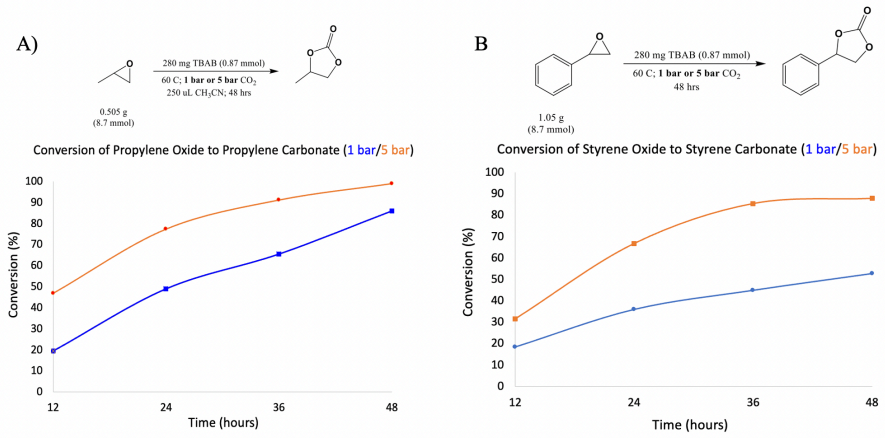

Figure 3.6: Control reactions to investigate ring expansion of epoxides with CO_2 to form cyclic carbonates. Lines in orange represents conversions at 5 bar and lines in blue represent conversion at 1 bar. A) The ring expansion of propylene oxide to propylene carbonate. B) The ring expansion of styrene oxide to styrene carbonate.

2. Catalytic CO_2 Fixation by the UiO-66 (Hf) Bulk Deposited Film

The control reactions provided an essential baseline to compare the effect of the UiO-66 (Hf) bulk deposited films. While the use of 5 bar of CO_2 was able to achieve high yields for both molecules; at 1 bar total conversion was much more challenging with only TBAB, so it was decided to test the bulk deposited films in the 1 bar of CO_2 condition. Films were tested by simply placing the coated wafer into the pressure reactor vessel face up so that the MOF film is exposed to the solution. For both the propylene oxide and the styrene oxide reactions the MOF film resulted in a major increase in the reaction rate as observed by proton nmr. In the case of propylene oxide the MOF film was able to bring the reaction to total completion in 15 hours. The conversion of styrene oxide did prove to be more challenging, with the percent conversion after 24 hours being 83.1%, however this was a serious improvement over the 52.7% yield of the reaction without the wafer after 48 hours (Figure 3.7). The decreased activity for the larger

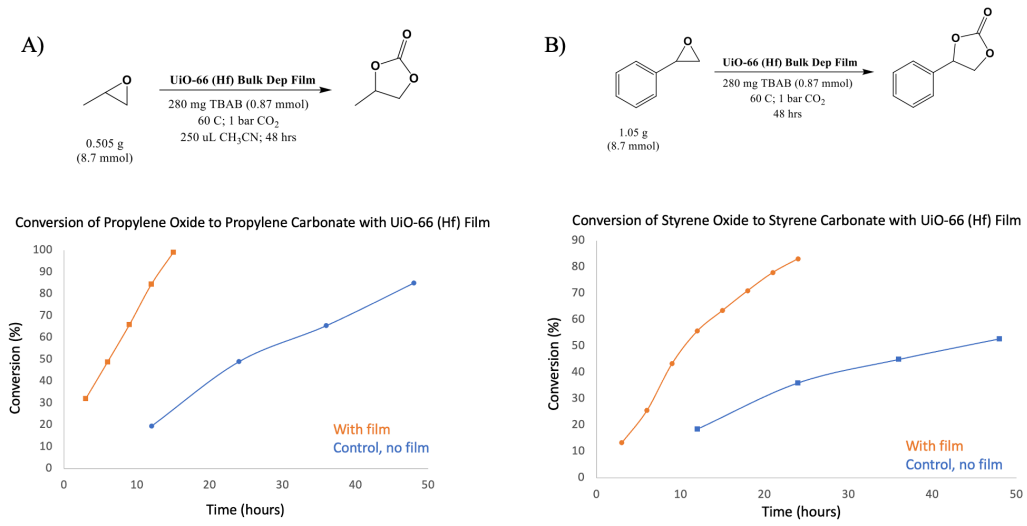

Figure 3.7: Effect of the bulk deposited UiO-66 (Hf) film on the ring expansion of epoxides to cyclic carbonates at 1 bar CO_2. All wafers were 1cm x 2 cm. A) Conversion of propylene oxide to propylene carbonate with film (orange) compared to without film (blue). B) Conversion of styrene oxide to styrene carbonate with film (orange) compared to without film (blue).

styrene oxide molecules is somewhat expected as the pores of the Uio-66 (Hf) inhibit the movement of the styrene oxide to the Lewis acidic metal centers of the MOF.

IV. Experimental Data and Spectra

1. GIWAXS Analysis of Bulk Deposited UiO-66 (Hf) Films

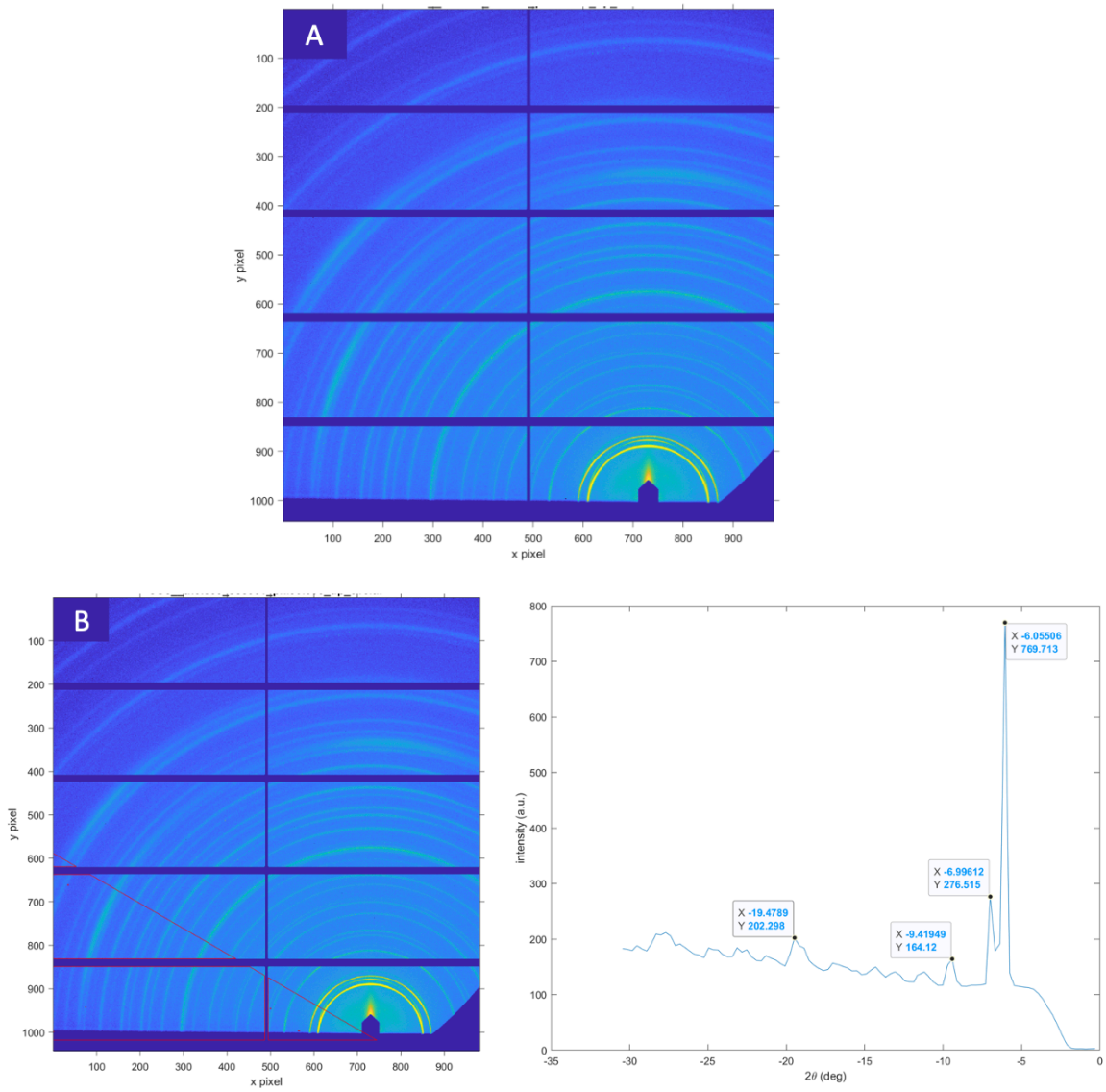

Figure 3.8: GIWAXS analysis of bulk deposited UiO-66 (Hf) on a 2cm x 1cm MHDA-functionalized Au coated Si wafer. A) Image of the 2D diffraction pattern showing the diffraction rings associated with the isotropic growth of a crystallin film on the surface of the wafer. B) Linecut analysis of the film from 180-160° 2Θ showing several diffraction peaks which can be associated with UiO-66 (Hf) structure.

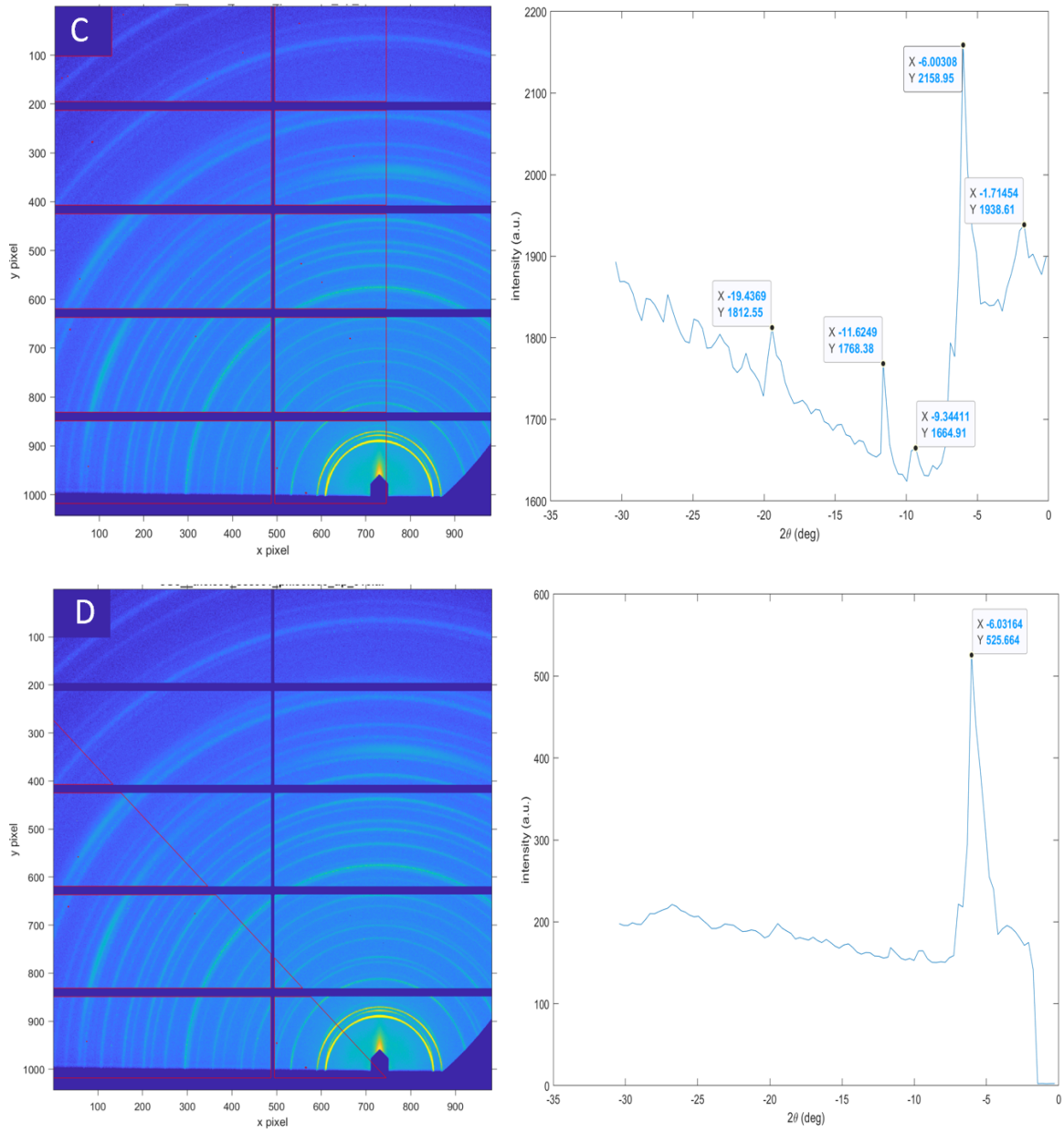

Figure 3.8 Cont.: C) Linecut analysis of the film from 180-90° 2Θ. D) Linecut analysis of the film from 180-135° 2Θ.

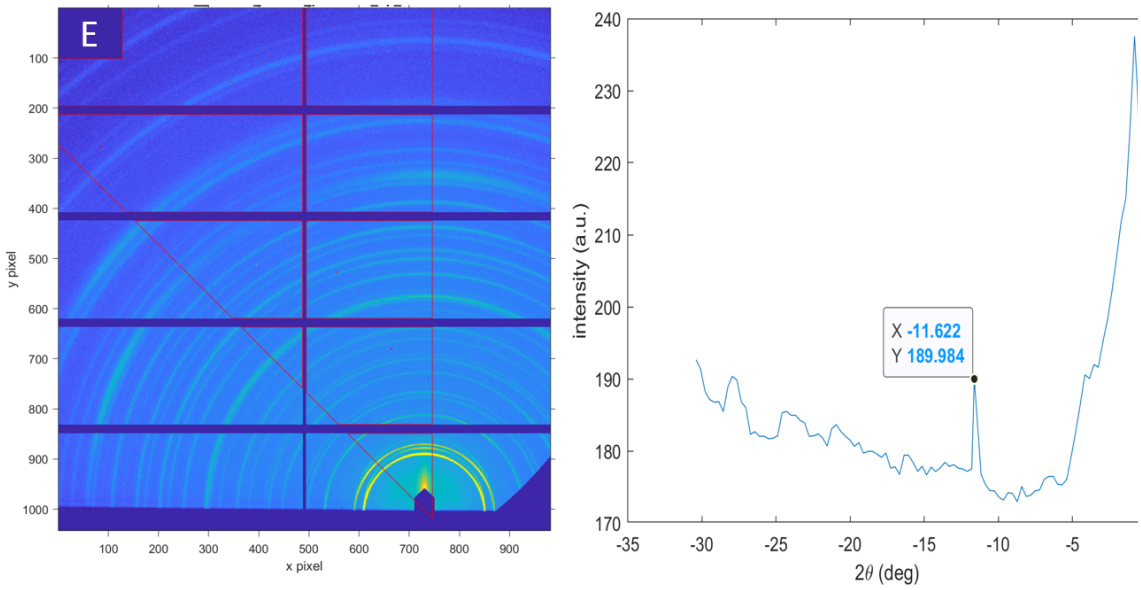

Figure 3.8 Cont.: E) Linecut analysis from 135-90° 2Θ.

Table 3.1 Indexed Peaks and Associated d-Spacings

Entry	Phi Values	Peak Max	d-Spacing (if 1st Order)
	180°-160°		
1		6.05506°	1.07 nm
2		6.99612°	0.93 nm
3		9.41949°	0.69 nm
4		19.4789°	0.34 nm
	180°-90°		
4		1.71454°	3.79 nm
5		6.00308°	1.08 nm
6		9.34411°	0.70 nm
7		11.6249°	0.56 nm
8		19.4369°	0.34 nm
	180°-135°		
9		6.03164°	1.08 nm
	135°-90°		
10		11.622°	0.56 nm

2. NMR Analysis of CO_2 Fixation Reactions

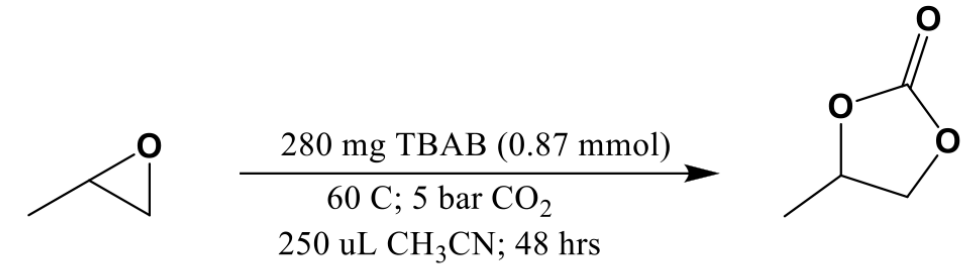

0.505 g
(8.7 mmol)

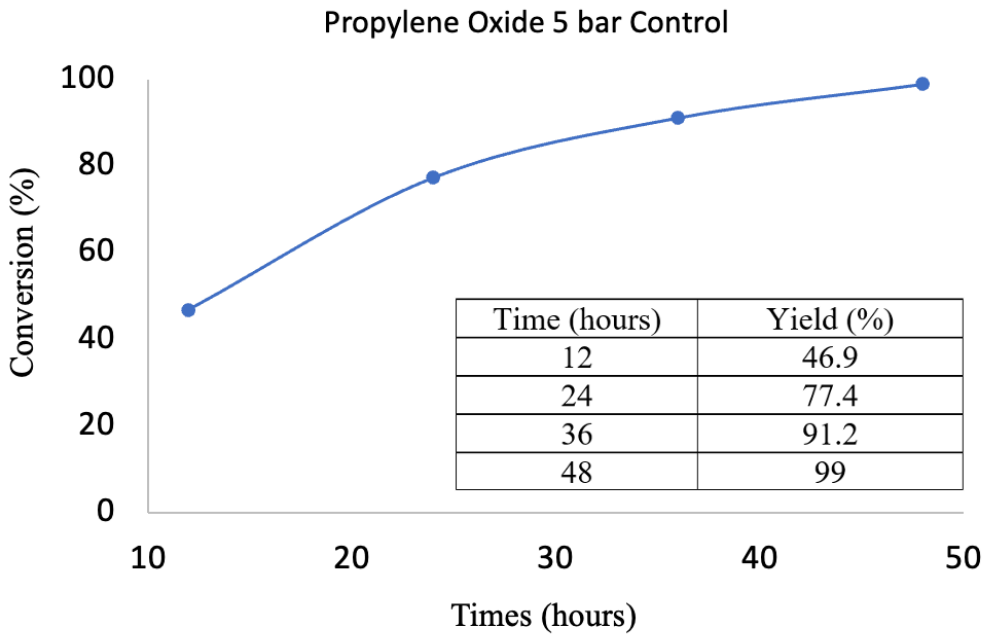

Time (hours)	Yield (%)
12	46.9
24	77.4
36	91.2
48	99

Figure 3.9: Control reaction of propylene oxide held at 5 bar of CO_2 pressure with reaction rate monitored by 1H NMR.

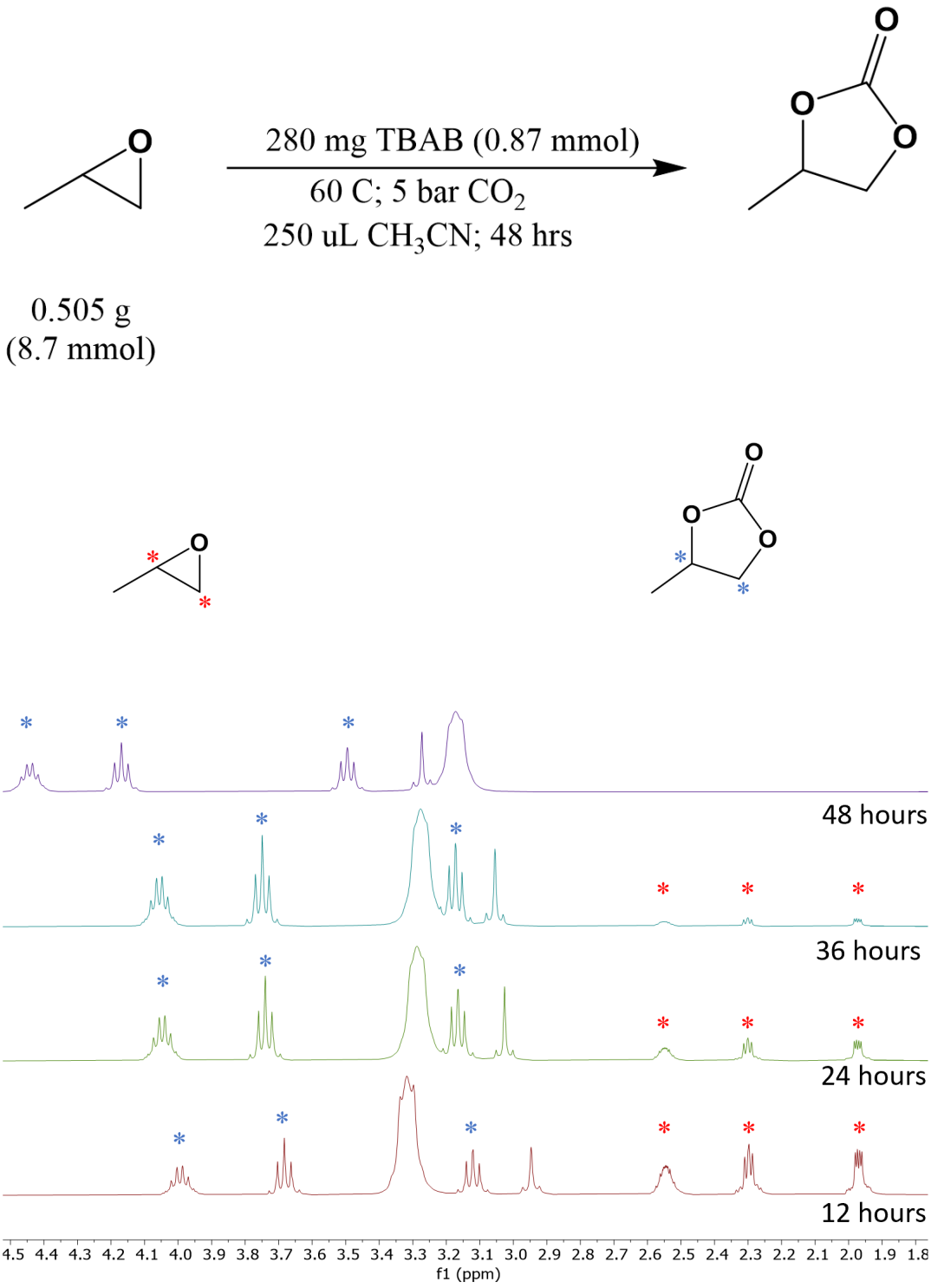

Figure 3.9 Cont.: All NMRs were taken by placing 100 uL of the reaction mixture into 750 uL of CD_3CN. Spectra were collected on a Bruker 400 Mhz NMR with 32 scans.

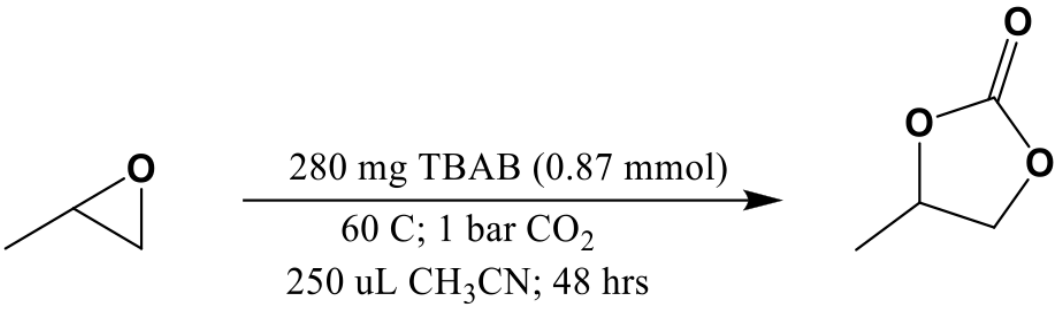

0.505 g
(8.7 mmol)

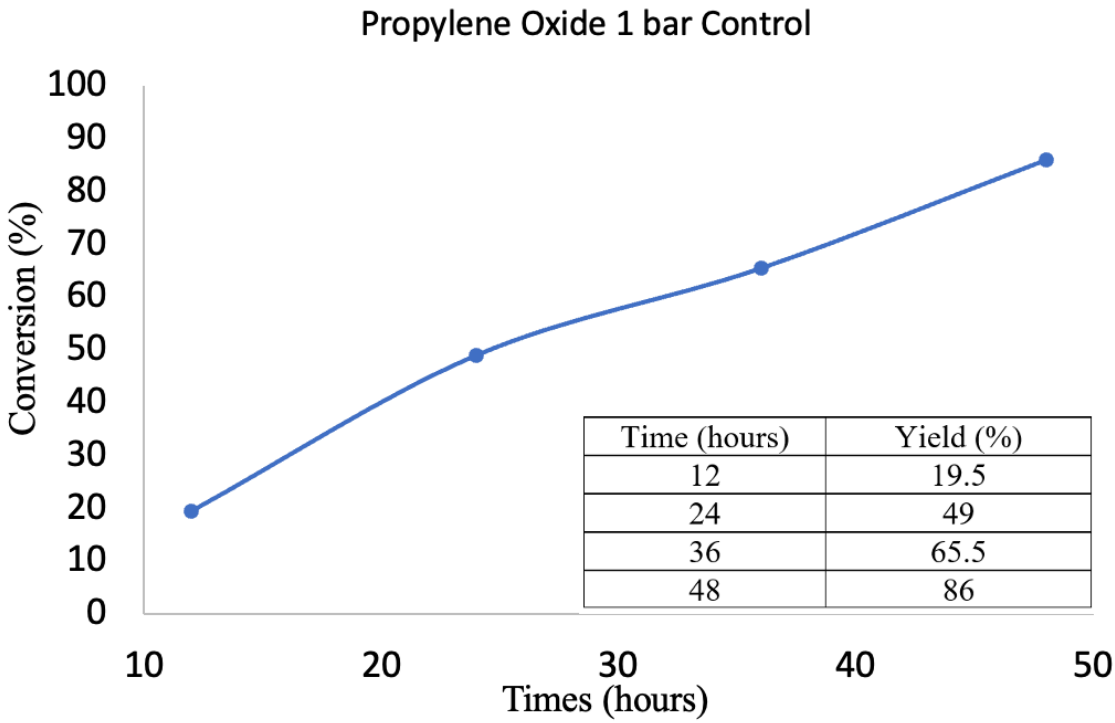

Time (hours)	Yield (%)
12	19.5
24	49
36	65.5
48	86

Figure 3.10: Conversion of propylene oxide to propylene carbonate held at 1 bar of CO_2 pressure with yields determined by 1H NMR.

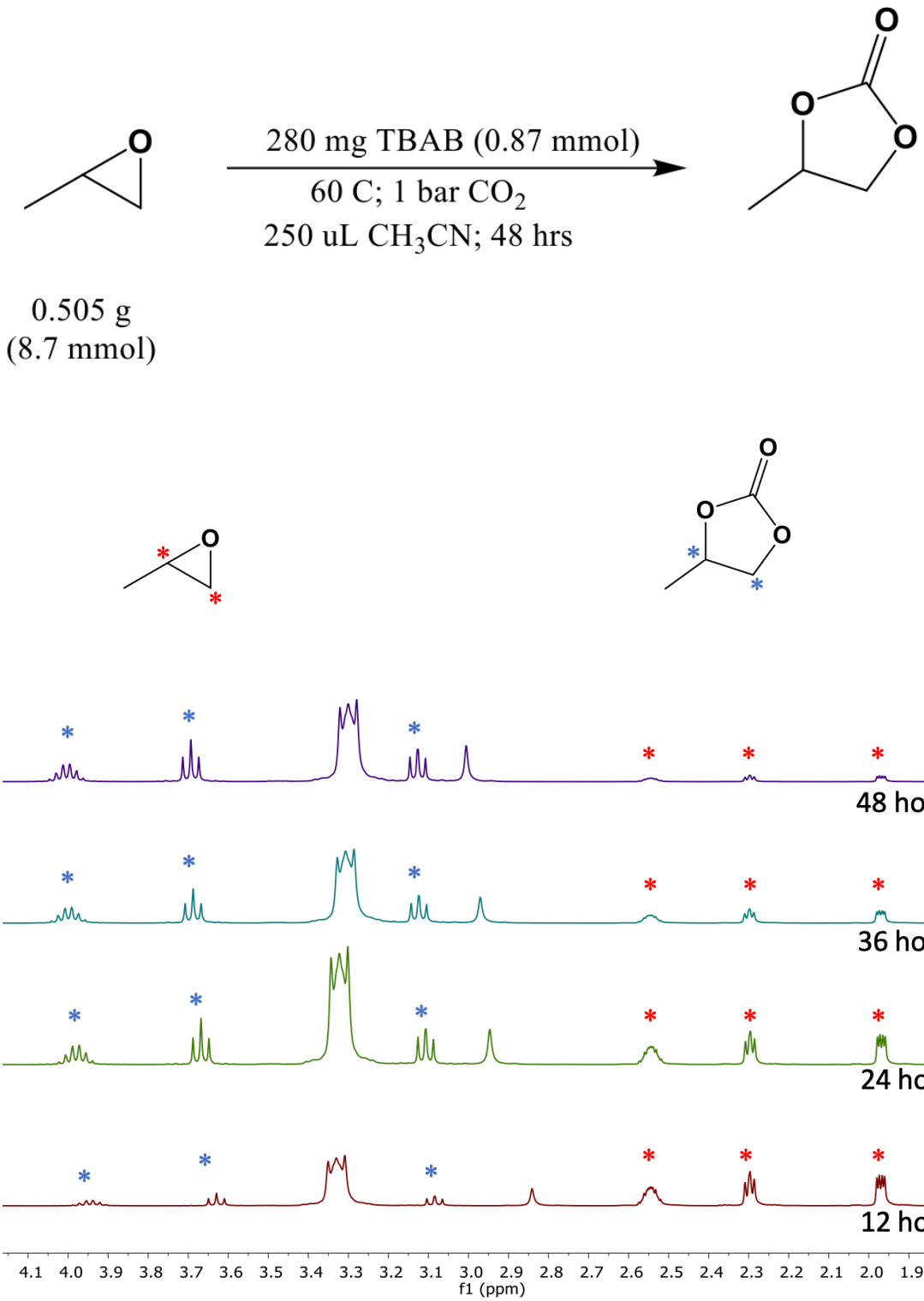

Figure 3.10 Cont.: All NMRs were taken by placing 100 uL of the reaction mixture into 750 uL of CD_3CN. Spectra were collected on a Bruker 400 Mhz NMR.

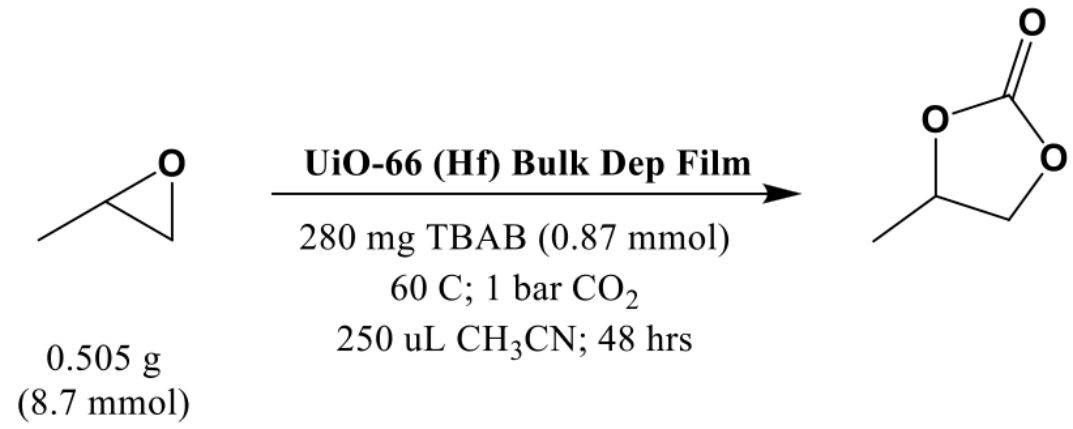

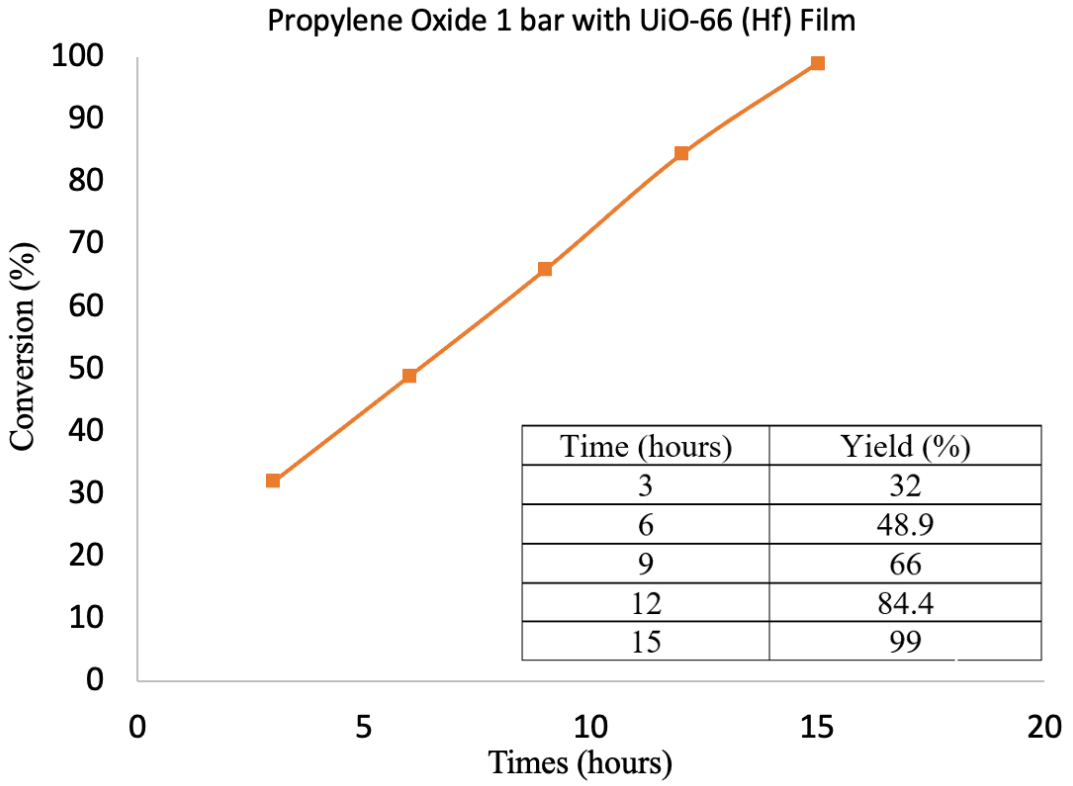

Time (hours)	Yield (%)
3	32
6	48.9
9	66
12	84.4
15	99

Figure 3.11: Conversion of propylene oxide to propylene carbonate catalyzed by the bulk deposited UiO-66 (Hf) film held at 1 bar of CO_2 pressure all yields determined by H1 NMR.

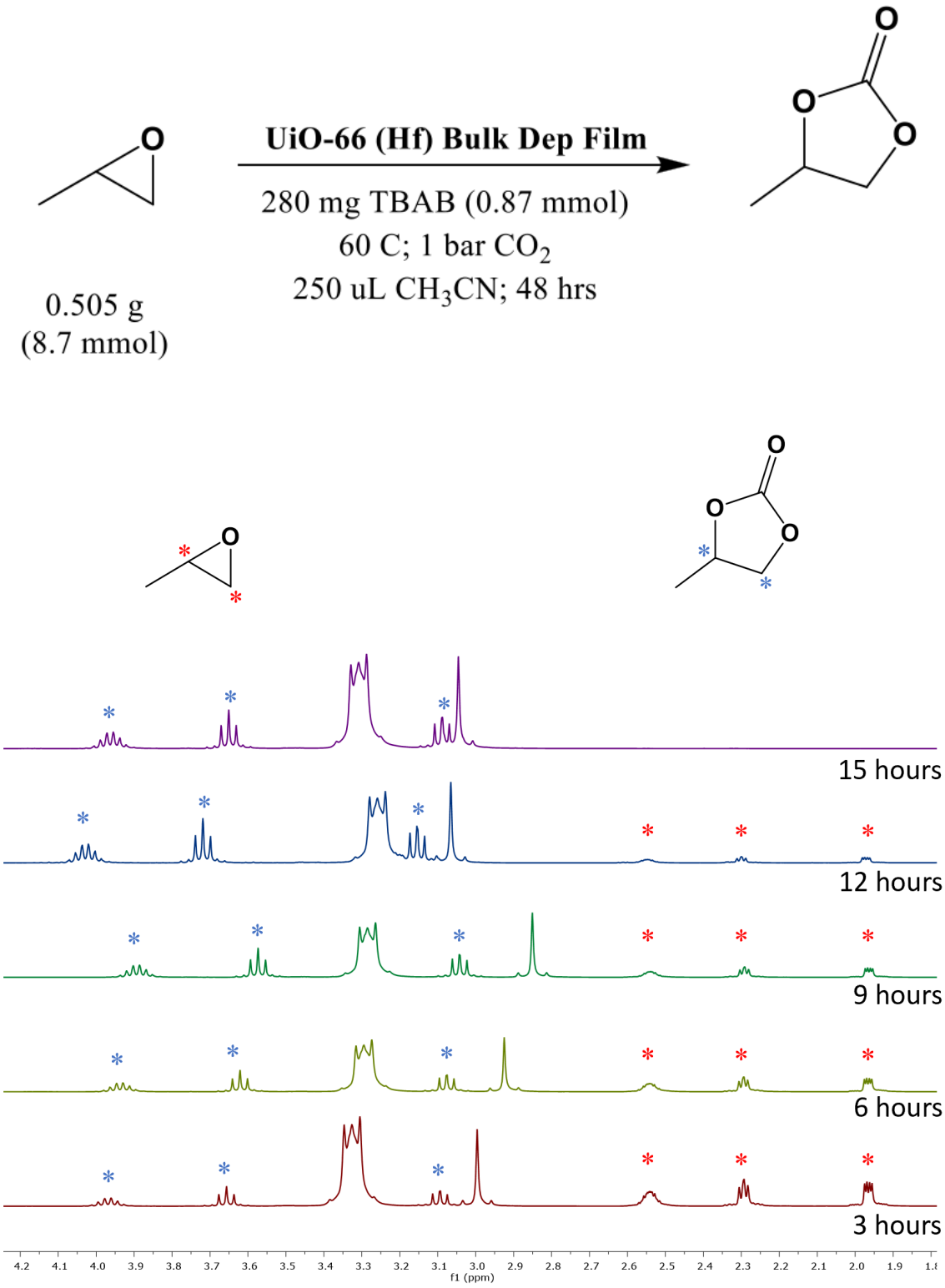

Figure 3.11 Cont.: All NMRs were taken by placing 100 uL of the reaction mixture into 750 uL of CD_3CN. Spectra were collected on a Bruker 400 Mhz NMR.

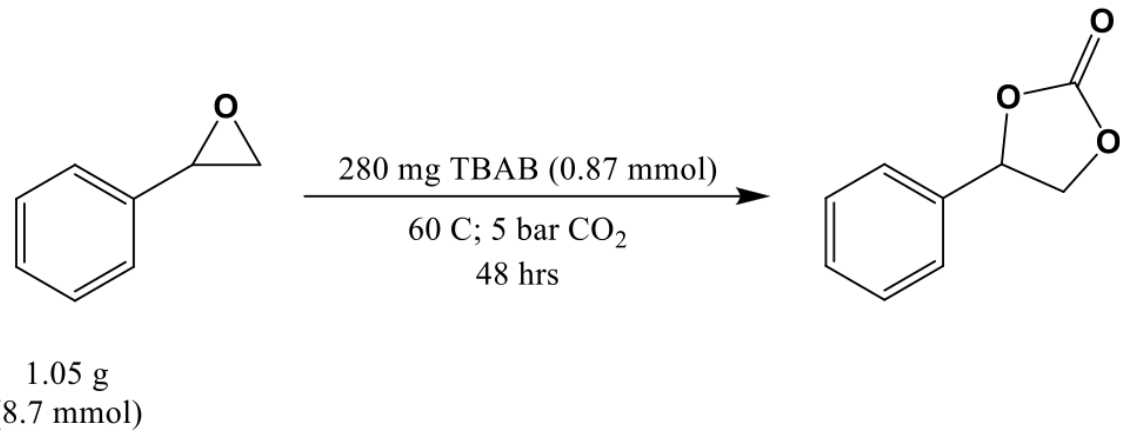

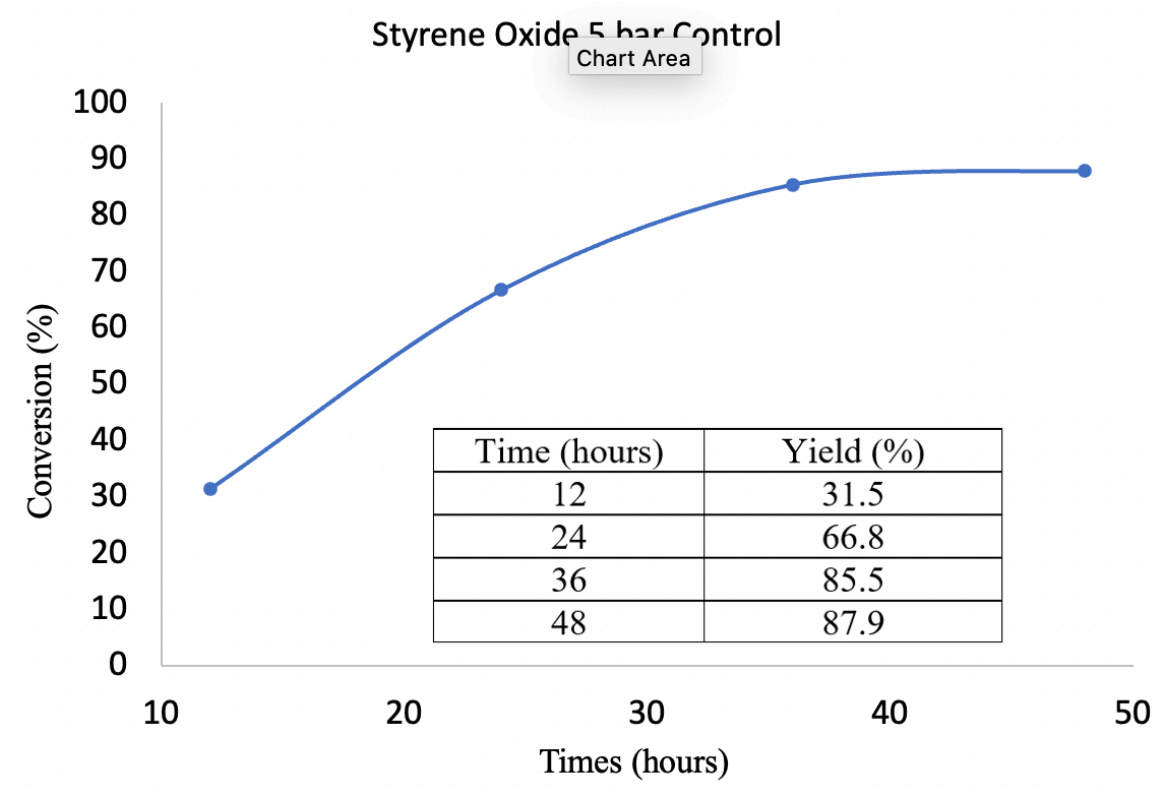

Time (hours)	Yield (%)
12	31.5
24	66.8
36	85.5
48	87.9

Figure 3.12: Conversion of styrene oxide to styrene carbonate under a control condition of 5 bar of CO_2 pressure. All NMRs were taken by placing 100 uL of the reaction mixture into 750 uL of CD_3CN. Spectra were collected on a Bruker 400 Mhz NMR.

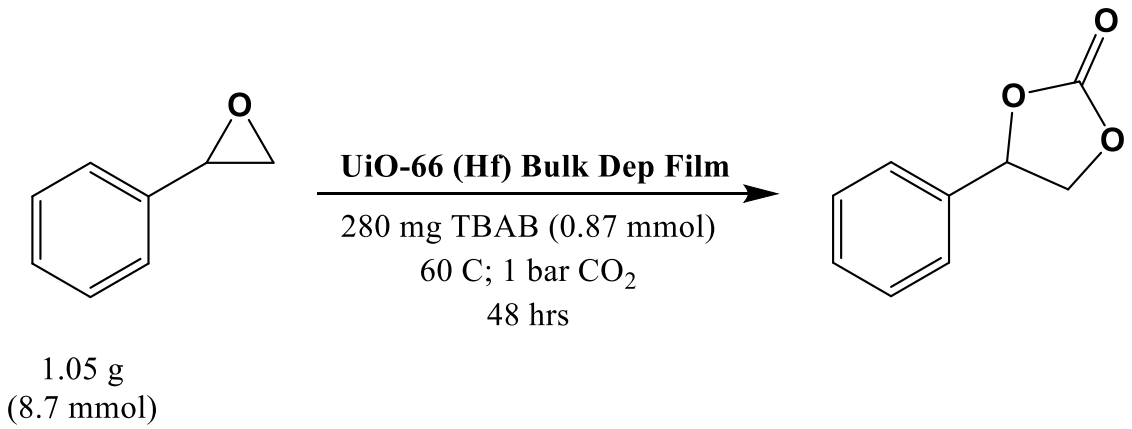

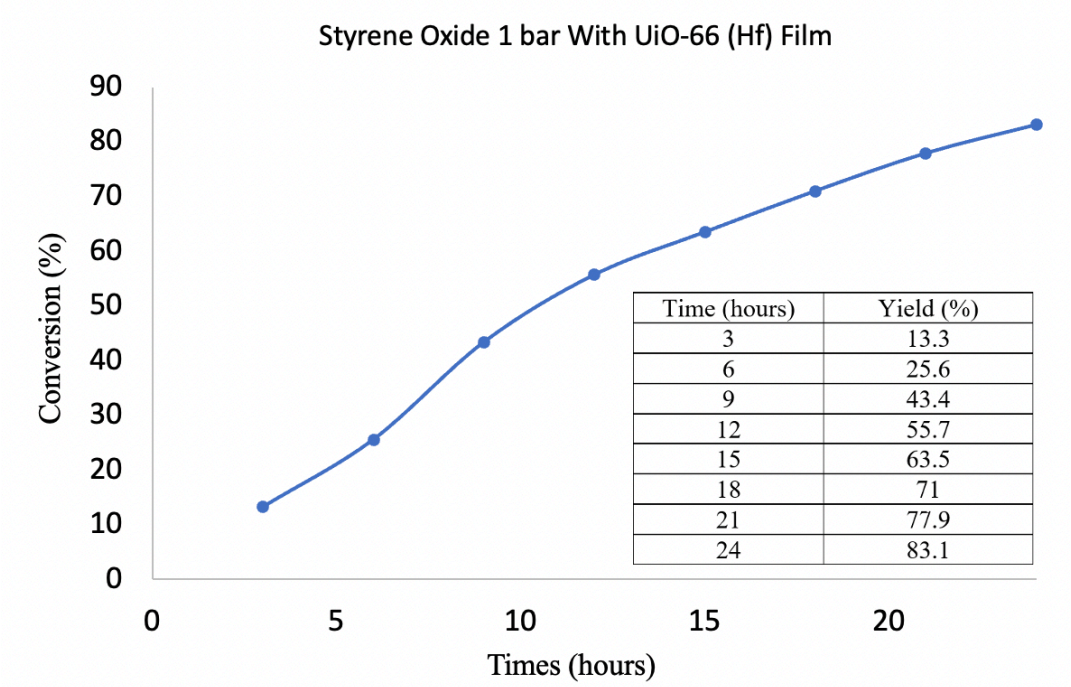

Time (hours)	Yield (%)
3	13.3
6	25.6
9	43.4
12	55.7
15	63.5
18	71
21	77.9
24	83.1

Figure 3.13: Conversion of styrene oxide to styrene carbonate catalyzed by a UiO-66 (Hf) film at 1 bar of CO_2 pressure yields determined by 1H NMR.

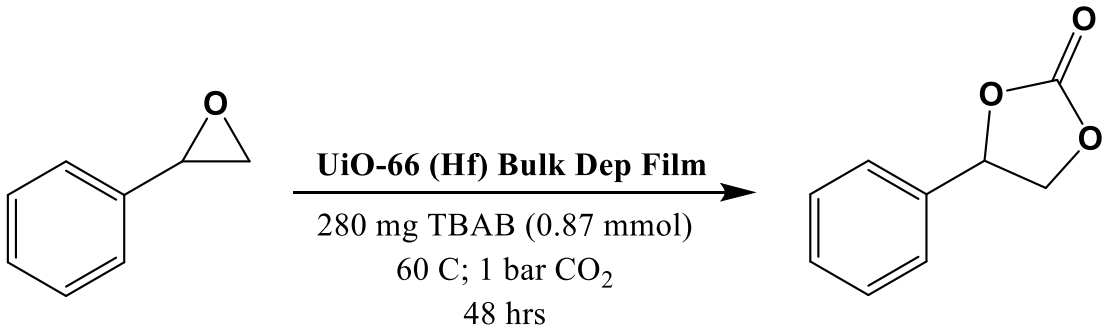

1.05 g
(8.7 mmol)

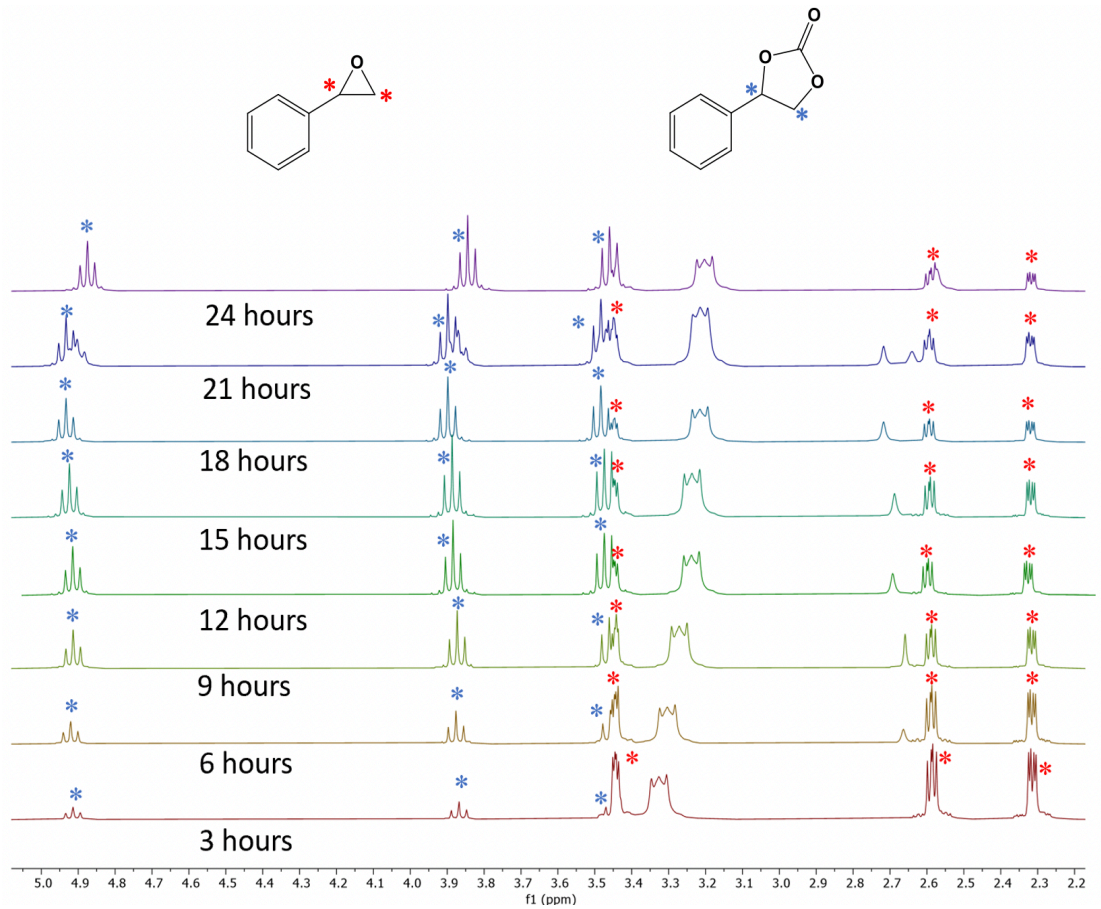

Figure 3.13 Cont.: All NMRs were taken by placing 100 uL of the reaction mixture into 750 uL of CD_3CN. Spectra were collected on a Bruker 400 Mhz NMR.

V. References

1. K., T. A., D., R. C. & A., E. R. Coupling of CO2 and Ice Sheet Stability Over Major Climate Transitions of the Last 20 Million Years. *Science (80-.).* **326**, 1394–1397 (2009).

2. Aresta, M. & Dibenedetto, A. Utilisation of CO2 as a chemical feedstock: opportunities and challenges. *Dalt. Trans.* 2975–2992 (2007) doi:10.1039/B700658F.

3. Ozdemir, J. *et al.* Covalent Organic Frameworks for the Capture, Fixation, or Reduction of CO2 . *Frontiers in Energy Research* vol. 7 77 (2019).

4. Beyzavi, M. H. *et al.* Metal–Organic Framework-Based Catalysts: Chemical Fixation of CO2 with Epoxides Leading to Cyclic Organic Carbonates . *Frontiers in Energy Research* vol. 2 63 (2015).

5. Ji, H. *et al.* Pyridinium-Functionalized Ionic Metal–Organic Frameworks Designed as Bifunctional Catalysts for CO2 Fixation into Cyclic Carbonates. *ACS Appl. Mater. Interfaces* **12**, 24868–24876 (2020).

6. Guo, F. & Zhang, X. Metal–organic frameworks for the energy-related conversion of CO2 into cyclic carbonates. *Dalt. Trans.* **49**, 9935–9947 (2020).

7. Delavari, M. *et al.* Catalytic synthesis of cyclic carbonates from epoxides and carbon dioxide by magnetic UiO-66 under mild conditions. *Appl. Organomet. Chem.* **31**, e3656 (2017).

8. Helal, A., Usman, M., Arafat, M. E. & Abdelnaby, M. M. Allyl functionalized UiO-66 metal-organic framework as a catalyst for the synthesis of cyclic carbonates by CO2 cycloaddition. *J. Ind. Eng. Chem.* **89**, 104–110 (2020).

9. Kim, J., Kim, S.-N., Jang, H.-G., Seo, G. & Ahn, W.-S. CO2 cycloaddition of styrene oxide over MOF catalysts. *Appl. Catal. A Gen.* **453**, 175–180 (2013).

10. Beyzavi, M. H. *et al.* A Hafnium-Based Metal–Organic Framework as an Efficient and Multifunctional Catalyst for Facile CO2 Fixation and Regioselective and Enantioretentive Epoxide Activation. *J. Am. Chem. Soc.* **136**, 15861–15864 (2014).

11. Semrau, A. L. *et al.* Substantial Turnover Frequency Enhancement of MOF Catalysts by Crystallite Downsizing Combined with Surface Anchoring. *ACS Catal.* **10**, 3203–3211 (2020).

12. Semrau, A. L. *et al.* Highly Porous Nanocrystalline UiO-66 Thin Films via Coordination Modulation Controlled Step-by-Step Liquid-Phase Growth. *Cryst. Growth Des.* **19**, 1738–1747 (2019).

13. Lausund, K. B. & Nilsen, O. All-gas-phase synthesis of UiO-66 through modulated

atomic layer deposition. *Nat. Commun.* **7**, 13578 (2016).

14. Ghorbanpour, A., Huelsenbeck, L. D., Smilgies, D.-M. & Giri, G. Oriented UiO-66 thin films through solution shearing. *CrystEngComm* **20**, 294–300 (2018).

15. Hu, Z., Nalaparaju, A., Peng, Y., Jiang, J. & Zhao, D. Modulated Hydrothermal Synthesis of UiO-66(Hf)-Type Metal–Organic Frameworks for Optimal Carbon Dioxide Separation. *Inorg. Chem.* **55**, 1134–1141 (2016).

16. DeStefano, M. R., Islamoglu, T., Garibay, S. J., Hupp, J. T. & Farha, O. K. Room-Temperature Synthesis of UiO-66 and Thermal Modulation of Densities of Defect Sites. *Chem. Mater.* **29**, 1357–1361 (2017).

17. Moghaddam, Z. S., Kaykhaii, M., Khajeh, M. & Oveisi, A. R. Synthesis of UiO-66-OH zirconium metal-organic framework and its application for selective extraction and trace determination of thorium in water samples by spectrophotometry. *Spectrochim. Acta Part A Mol. Biomol. Spectrosc.* **194**, 76–82 (2018).

18. Bunge, M. A., Davis, A. B., West, K. N., West, C. W. & Glover, T. G. Synthesis and Characterization of UiO-66-NH2 Metal–Organic Framework Cotton Composite Textiles. *Ind. Eng. Chem. Res.* **57**, 9151–9161 (2018).

19. Cliffe, M. J. *et al.* Correlated defect nanoregions in a metal–organic framework. *Nat. Commun.* **5**, 4176 (2014).

20. Shearer, G. C. *et al.* Defect Engineering: Tuning the Porosity and Composition of the Metal–Organic Framework UiO-66 via Modulated Synthesis. *Chem. Mater.* **28**, 3749–3761 (2016).

E. Conclusion

MOF thin films of based on the Hf and Zr-oxo clusters provide a reliable platform for tandem catalysis and CO_2 fixation. In this work molecular LbL and bulk deposition have been proven as methods which enable the fabrication of group-IV metal based MOFs, which are sought after due to enhanced stability. The automated epitaxial workstation has been shown to be an essential tool for the molecular LbL deposition of PCN and UiO type Hf MOFs, the deposition of which were undescribed before this work. Porphyrin MOF films have proven to be capable catalytic platforms which lend themselves towards the tandem catalytic action of two distinct porphyrin macrocycles within the same film. In this work UiO-66 (Hf) bulk deposited films have been proven as a useful tool for solving the challenge of rising CO_2 levels in the atmosphere.

Future work on the fabrication of group-IV metal based MOF films should seek to enhance the crystallinity of the films which will aid in structural elucidation. The mechanism of ligand exchange should be further explored so that more effective modulation strategies of the deposition of MOF crystal films can be achieved. There is much room for improvement catalytically for the interchanged metalloporphyrin based films described in this work, specifically achieving the transformation of styrene to styrene carbonate using two gasses, O_2 and CO_2 would be meaningful improvement over the use of hydrogen peroxide and CO_2. In a more general sense, applying the molecular LbL strategy designed in this work for the growth of COF thin films could greatly expand the field of molecular LbL deposition of reticular materials.